
Biological Evaluation of Serine Protease Inhibitors and Inducers of Protein Degradation

Dissertation

zur

Erlangung des Doktorgrades (Dr. rer. nat.)

der

Mathematisch-Naturwissenschaftlichen Fakultät

der

Rheinischen Friedrich-Wilhelms-Universität Bonn

vorgelegt von

Martin Mangold

aus

München

Bonn 2020

Angefertigt mit der Genehmigung der Mathematisch-Naturwissenschaftlichen Fakultät der
Rheinischen Friedrich-Wilhelms-Universität Bonn

1. Gutachter: Prof. Dr. Michael Gütschow
2. Gutachterin: PD Dr. Anke Schiedel

Tag der Promotion: 10.09.2020
Erscheinungsjahr: 2020

Die vorliegende Arbeit wurde im Zeitraum von März 2015 bis Mai 2020 unter der Leitung von Herrn Prof. Dr. Michael Gütschow am Pharmazeutischen Institut der Rheinischen Friedrich-Wilhelms-Universität zu Bonn angefertigt.

Danksagung

Meinen besonderen Dank möchte ich an dieser Stelle Herrn Prof. Dr. Michael Gütschow aussprechen. Dies gilt nicht nur für die Vergabe der interessanten Forschungsprojekte, sondern auch für die sehr gute persönliche wie auch wissenschaftliche Betreuung und das entgegengebrachte Vertrauen bei der Projektplanung und -umsetzung.

Mein Dank gilt auch Frau PD Dr. Anke Schiedel für die freundliche Übernahme des Korreferats.

Weiterhin danke ich dem Maria von Linden-Programm und der Bonn International Graduate School of Drug Sciences (BIGS DrugS) für die finanzielle Unterstützung.

Table of contents

1.	Introduction	1
1.1	Proteases	1
1.2	Serine proteases	2
1.2.1	Type II transmembrane serine proteases	3
1.2.2	Matriptases	5
1.2.3	Matriptase-2	6
1.2.4	Physiological functions of matriptase-2	8
1.2.4.1	Iron homeostasis	8
1.2.4.2	Cancer development and progression	10
1.2.5	Relevance of matriptase-2 as target of enzyme inhibitors	11
1.2.6	Matriptase-2 structure and specificity	12
1.2.7	Ligands of matriptase-2	14
1.2.7.1	Substrates	14
1.2.7.2	Inhibitors	14
1.3	Threonine proteases	18
1.3.1	The proteasome	19
1.3.2	Proteasomal prote in degradation	20
1.3.3	Proteolysis targeting chimeras	22
1.4	Objectives	24
2.	Results and discussion	25
2.1	Evaluation of enzyme inhibitors for matriptase-2 inhibition	25
2.1.1	Peptide inhibitors of matriptase-2	28
2.1.1.1	Sunflower trypsin inhibitors	28
2.1.2	Peptidomimetic inhibitors of matriptase-2	33
2.1.2.1	A chloromethyl ketone as inhibitor of matriptase-2	33
2.1.2.2	Evaluation of a phosphono bis-benzguanidine as inhibitor of matriptase-2	35
2.1.2.3	Synthesis and evaluation of prolineamide inhibitors	37
2.1.3	Chromenone inhibitors	43
2.1.4	Inhibitor library screening for matriptase-2 inhibition	44
2.1.5	Selectivity profiles of established matriptase-2 inhibitors	45
2.1.6	<i>In cellulo</i> matriptase-2 inhibition studies	46
2.1.6.1	Matriptase-2 activity at the cell surface	47
2.1.6.2	Matriptase-2 reporter gene assays	51
2.1.7	Conclusion	53

2.2	Characterization of activity-based probes of matriptase-2	54
2.2.1	Detection of active and inactive matriptase-2	55
2.2.2	Biochemical properties of matriptase-2 activity-based probes	56
2.2.3	The use of activity-based probes in SDS-PAGE and western blot experiments for the detection of matriptase-2	58
2.2.4	Matriptase-2 competition experiments	64
2.2.5	Fluorescence probing of matriptase-2 in confocal microscopy experiments	67
2.2.6	Conclusion	70
2.3	Evaluation of proteolysis targeting chimeras	71
2.3.1	Design of a test system for proteolysis targeting chimeras	71
2.3.2	Establishment of a luciferase-based test system for proteolysis targeting chimeras	73
2.3.3	Influence of proteolysis targeting chimeras on cell viability	74
2.3.4	Application of PROTACs in a luciferase-based test system	77
2.3.5	Detection of Halo-Luc fusion protein by immunoblotting	79
2.3.6	Conclusion	81
3.	Experimental section	82
3.1	Methods	82
3.1.1	Cultivation of cells	82
3.1.2	Counting of cells	82
3.1.3	MTT viability assay	83
3.1.4	Transfection of cells	84
3.1.5	Preparation of cell lysates and culture supernatants	84
3.1.6	Protein determination	85
3.1.7	Enzyme inhibition assays with purified enzymes and cell culture supernatants	85
3.1.8	Matriptase-2 inhibition assay in intact cells	87
3.1.9	Solution-based synthesis of prolineamide inhibitors	87
3.1.10	SDS-PAGE	87
3.1.11	In-gel detection	88
3.1.12	Immunoblotting	88
3.1.13	Confocal microscopy	88
3.1.14	Cloning	89
3.1.15	Proteolysis targeting chimera evaluation assay	90
3.1.16	Transformation of <i>Escherichia coli</i> cells	90
3.1.17	Cultivation of <i>Escherichia coli</i> cells	91
3.1.18	Plasmid isolation from transformed <i>Escherichia coli</i> cells	91
3.1.19	Statistical analysis	92

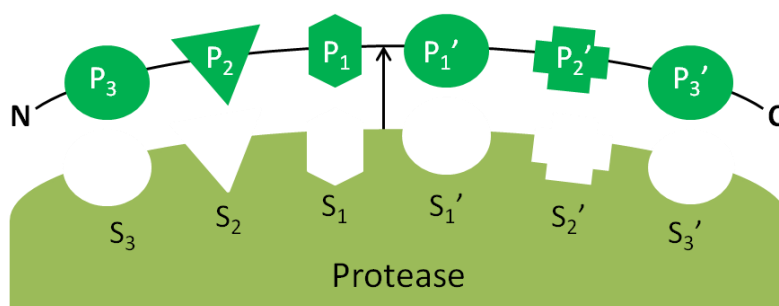
3.2	Devices and Materials	93
3.2.1	Devices	93
3.2.2	Consumables	95
3.2.3	Materials	96
3.2.4	Cell lines	99
3.2.5	Vectors	100
3.2.6	Enzymes	101
3.2.7	Substrates	102
3.2.8	Antibodies, commercially available probes and dyes	103
3.2.9	Buffers and solutions	104
4.	References	107
5.	Registers	126
5.1	List of abbreviations	126
5.2	List of figures	129
5.3	List of tables	131
5.4	List of schemes	132
6.	Summary	133
	Selbstständigkeitserklärung	135
	Danksagung	136
	Curriculum vitae	137

1 Introduction

1.1 Proteases

Proteases are a class of enzymes that catalyze the hydrolysis of peptide bonds and, accordingly, the breakdown of proteins. Depending on the residue that is involved in catalysis, these enzymes are classified as aspartic, cysteine, glutamic, metallo, serine or threonine proteases.^[1,2] Further distinctions can be made between proteases cleaving protein substrates from the C- or N-termini (exopeptidases, carboxypeptidases or aminopeptidases, respectively) and proteases that cleave in the middle of a protein substrate (endopeptidases). Regardless of their type, proteases possess an active site which houses their catalytic group, as well as binding pockets that address corresponding amino acid residues of a substrate. Based on the nomenclature of Schechter and Berger,^[3] binding pockets that depart from the catalytic group in the direction of the N-terminus are termed S, while those directed at the C-terminus are termed S'. Likewise, amino acid residues of a substrate are named P or P', correspondent to their position to the substrate cleavage site (Scheme 1.1).

Scheme 1.1: Schematic depiction of the active site of a protease and its substrate.



The arrow indicates both, the scissile bond of the substrate and the active group of the protease. P and P' represent substrate residues that interact with the corresponding binding pockets S and S' of a protease. P and P' are numbered relative to their position to the scissile bond, while residues departing in the direction of the N-terminus are termed P and those departing in the direction of the C-terminus are termed P'. Numeration rises, the farther away the group is from the cleavage site. S and S' binding pockets are numbered accordingly (modified from Schechter *et al.*^[3]).

Apart from glutamic proteases, that are found only in bacteria and fungi thus far,^[4-6] all protease families are represented in the human degradome. Bioinformatic analysis revealed over 560 genes encoding proteases in the human body which constitutes approximately 2% of the whole human genome.^[7-9] Interestingly, over 40% of all human proteases belong to one of four different families, namely the adamalysins, prolyl oligopeptidases, trypsin-like serine proteases and ubiquitin-specific proteases. Besides the degradation of proteins various physiological functions of proteases have been identified, such as the regulation of protein activation and protein interaction. Due to this involvement in many key physiological processes, abnormal protease activity is often linked to diseases,^[10] thus marking proteases as important targets for the development of drugs.

1.2 Serine proteases

Between all protease families, proteases with a nucleophilic serine (Ser) residue as the catalyst of their enzymatic activities comprise the largest number of proteolytic enzymes in the human degradome.^[11] Nucleophilicity of the active site Ser is typically dependent on a triad of amino acids consisting of aspartic acid (Asp), histidine (His) and Ser.^[12-13] Presently, over a third of all described proteases are categorized as serine proteases,^[14] most of them belonging to the endopeptidase type.

Based on the MEROPS database the serine protease family is divided into 15 clans and over 50 families, of which clan PA represents the largest.^[8] A common feature of clan PA members is their catalytic domain, which shares a similar tertiary structure defined as double β -barrel or trypsin-like folds. Because of this, most clan PA proteases have the trypsin-like primary substrate specificity for arginine (Arg) or lysine (Lys) at P₁ position.^[3] They participate in several important physiological processes such as blood coagulation, food digestion and immune responses.^[15-17] The peptidase S1 family, one of the best described and studied groups of serine proteases, makes up approximately three quarters of all clan PA proteases. While most S1 peptidases are excreted enzymes, some are produced as inactive zymogens and stored in intracellular organelles or on the cell membrane.

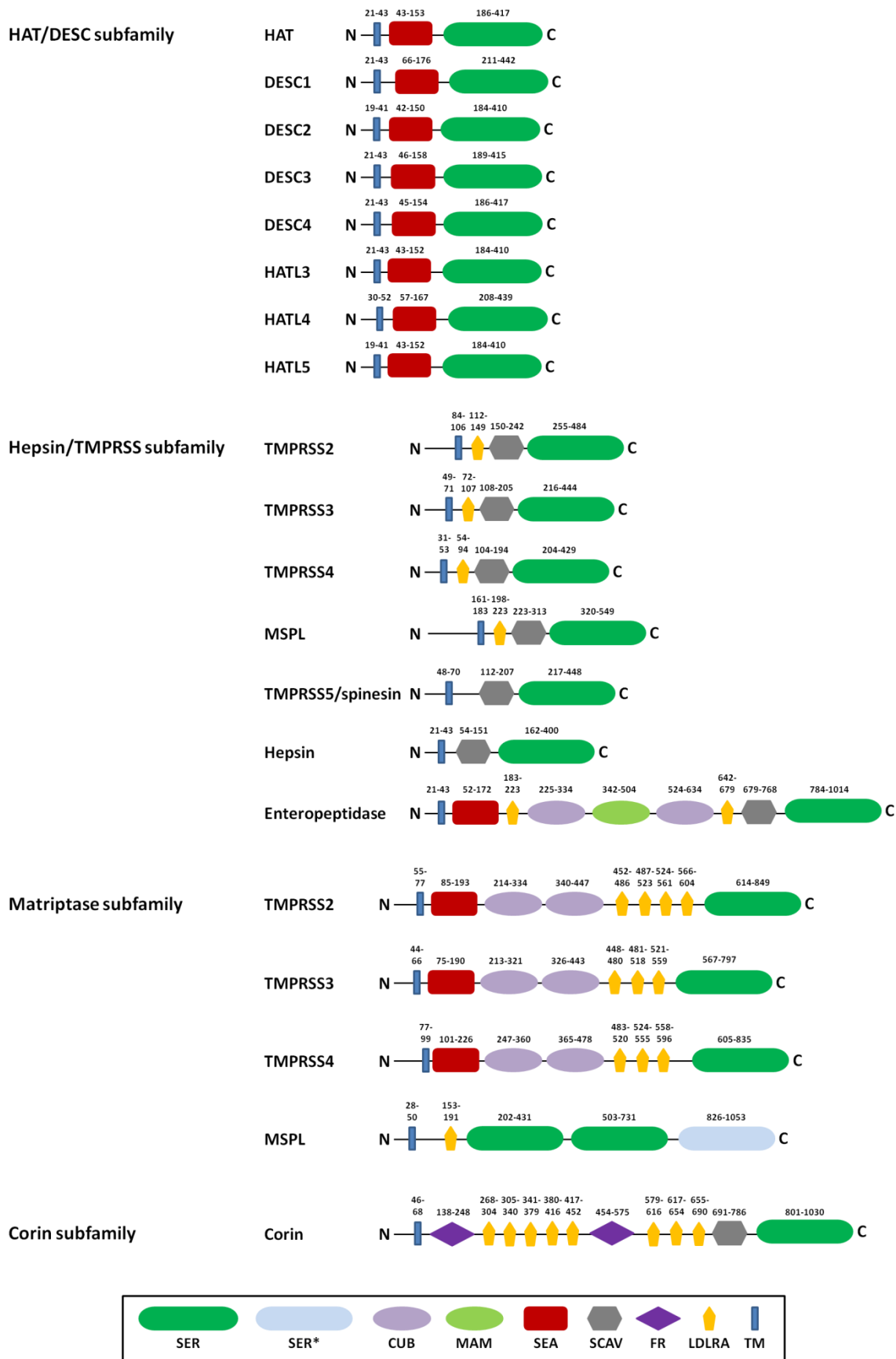
1.2.1 Type II transmembrane serine proteases

The type II transmembrane serine proteases (TTSPs) of the peptidase S1 family represent the largest group of membrane-anchored serine proteases and comprise 20 members (Scheme 1.2). Their location at the cell membrane enables proteases of this family to interact with other cell surface proteins, proteins on neighboring cells, the extracellular matrix and soluble interaction partners, thus allowing the mediation of signal transduction between the cell and its environment.

Even though the first TTSP, enteropeptidase, was discovered over 100 years ago by Pawlow,^[18] it was not until the beginning of the 21st century, that TTSPs were first described and characterized.^[19] Apart from a few exceptions like corin,^[20] enteropeptidase,^[21] matriptase (MT1)^[22] and prostaticin^[23] the physiological function of many TTSPs is not well understood till this day, although the involvement in different pathological conditions like cancer^[24-26] and the activation of the influenza virus^[27-28] brought this protease family into the focus of research. It is indicated that some TTSPs play crucial roles in the development of healthy human tissues.^[20,29-30]

All TTSPs share common structural elements in the form of a short N-terminal cytoplasmatic fragment (20-160 amino acids), a single-pass transmembrane domain and a large extracellular fragment which contains the highly variable stem region, as well as the serine protease catalytic domain of the chymotrypsin-like fold located at the C-terminus.^[31-32] Based on structure similarities in their stem regions TTSPs are categorized into four subfamilies: human airway trypsin-like protease/differentially expressed in squamous cell carcinoma gene (HAT/DESC), hepsin/transmembrane serine protease (hepsin/TMPRSS), matriptase and corin (Scheme 1.2).

Scheme 1.2: The TTSP family and its four subfamilies.



HAT/ DESC, Hepsin/TMPRSS, Matriptase, Corin. The structure of TTSPs is depicted schematically. The localisation of domains is labeled by amino acid position. (modified from Bugge *et al.* [32]).

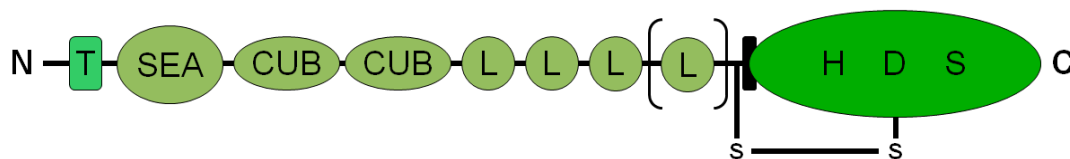
1.2.2 Matriptases

The matriptase family comprises four enzymes, three of which are highly homologous, namely, matriptase (MT1), matriptase-2 (MT2) and matriptase-3 (MT3), and the protease polyserase-1.^[32]

The stem region of polyserase-1 features an atypical mosaic structure composed of one low-density lipoprotein receptor class A (LDLRA) domain and three tandem serine protease catalytic domains, of which only two are catalytically active. Over the past years, two closely related proteases with a similar tandem structure in their stem regions, termed polyserase-2 and polyserase-3, have been described.^[33-34] Due to the lack of a transmembrane domain these polyserases are not categorized as TTSP or matriptase members.

In contrast, the stem regions of MT1, MT2 and MT3 are well conserved and consist of one sea urchin sperm protein, enteropeptidase, agrin (SEA) domain, two complement CIs/Clr, urchin embryonic growth factor and bone morphogenic protein-1 (CUB) domains and three to four LDLRA domains, followed by a serine protease catalytic domain (Scheme 1.3). Despite high structural similarities, members of the matriptase subfamily perform distinct biological functions.^[31,35]

Scheme 1.3: Schematic structure of matriptase proteins.



Domain abbreviations are as follows: T: transmembrane; SEA: sea urchin sperm protein, enteropeptidase, agrin; CUB: CIs/Clr, urchin embryonic growth factor and bone morphogenic protein-1; L: low density lipoprotein receptor class A; HDS: serine protease. S-S represents the disulfide bridge which connects the protease domain to the stem region after autocatalytic cleavage. [L] represents the fourth LDRA domain only present in MT1 (modified from Stimberg *et al.*^[36]).

1.2.3 Matriptase-2

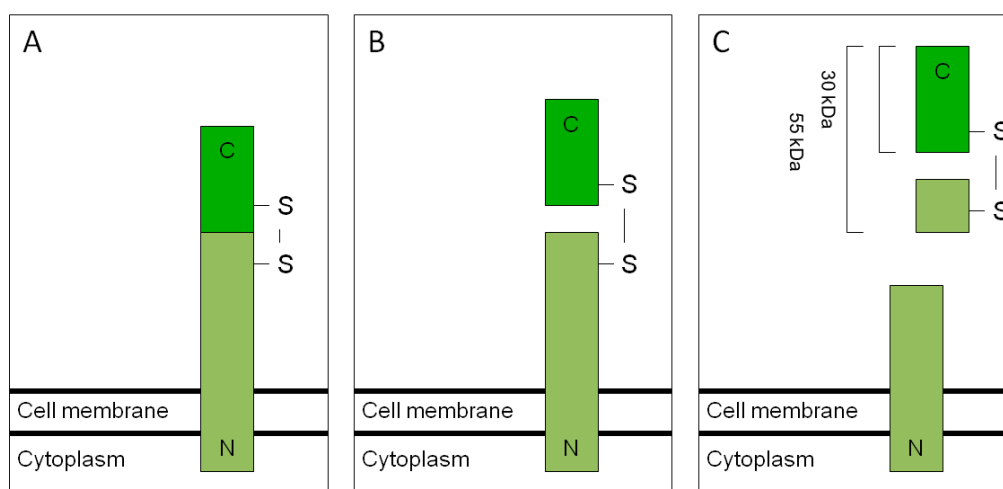
MT2 was first discovered *in silico* by genome databank research and subsequently cloned from fetal liver samples. The protease was described and characterized in 2002 by Velasco *et al.*^[37-38] and named based on its closest structural relative MT1. Mouse MT2 was discovered and characterized independently one year later by another working group.^[39] Based on TTSP nomenclature the mouse gene was named *Tmprss6* (Transmembrane protease serine 6) and the encoded protein Tmprss6, the human gene located on chromosome 22 was named *TMPRSS6*. The *TMPRSS6* gene is highly conserved across the mammalian class and thusly, nowadays the name MT2 is used as a universal term to describe the protein in all species.

In the human body MT2 is expressed as seven different transcripts, of which four are expressed as proteins.^[40] Isoform 2, representing the 802 amino acid form, is studied and used most commonly. Of the other MT2 transcripts, only isoform 1 is catalytically active, but gets internalized into intracellular vesicles. Isoform 3 is expressed as a truncated form, lacking the MT2 catalytic domain, while isoform 4 contains an additional exon in its catalytic domain. Unlike MT1 which is expressed ubiquitously in large amounts in epithelial tissues, MT2 isoforms are mainly expressed in the adult and fetal liver, pituitary glands and testis, but also in the kidney, nasal mucosa, lung, brain and uterus.^[39-41] Isoforms 2 and 4 represent the main transcripts in the liver and pituitary glands, while isoforms 1 and 3 are enriched in the testis. As a side note: The further thesis will focus solely on MT2 isoform 2.

MT2 (Uniprot: Q8IU80, isoform 2) is translated as an 88.9 kDa protein that exhibits typical TTSP structure elements (Scheme 1.3). Although some functionalities of the different domains of MT2 have been described, their full roles for MT2 function remain to be elucidated. Beliveau *et al.* demonstrate that the cytoplasmatic domain of MT2 contains an endocytosis motif that functions as an endogenous regulation mechanism.^[42] While the transmembrane region seems to be essential for the cleavage of substrates at specific sites,^[43] the SEA and LDLRA domains support the transport of the protease to the cell surface.^[44] The whole intact stem region proved to be important for the specificity and efficiency of MT2 substrate cleavage.^[43]

After its synthesis MT2 is transported to the cell surface as an inactive zymogen. The enzyme activates itself by an autocatalytic cleavage in the serine protease domain at the position Arg576 in the activation sequence Arg-Ile-Val-Gly-Gly.^[45] A disulfide bridge connects the cleaved off portion of the protease domain to the stem region (Scheme 1.4). A subsequent second cleavage in the second CUB domain, termed ectodomain shedding, leads to the release of an approximately 55 kDa protein fragment which consists of the three LDLRA domains and the catalytic domain.^[45-46] Both, shedding and release are performed auto-catalytically in a *trans*-mechanism. This could be proven by the employment of a mutated inactive MT2 in which the catalytic Ser762 was switched to an Ala residue.^[45]

Scheme 1.4: MT2 activation mechanism and release.



A: After its expression MT2 is transported to the cell surface as an inactive zymogen. **B:** After the first autocatalytic cleavage, the catalytic domain remains attached to the enzymes stem region by a disulfide bridge. **C:** A second autocatalytic cleavage in the stem region leads to the release of an approximately 55 kDa fragment (modified from Stimberg *et al.*^[36]).

1.2.4 Physiological functions of matriptase-2

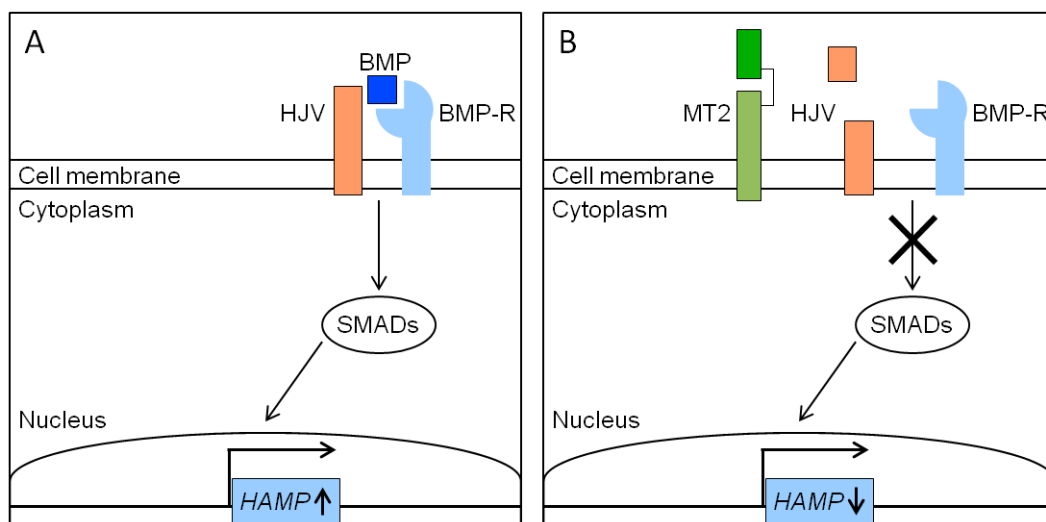
1.2.4.1 Iron homeostasis

Iron is one of the essential trace elements. As component of many sensor, storage and transport molecules, especially due to its role in the transport of oxygen as part of heme, the maintenance of a steady iron level is crucial for a well-functioning human metabolism. An insufficient amount of iron leads to the development of anemia, while iron overload results in accumulation and hemochromatosis.^[47] Thus, the plasma iron level has to be kept in narrow ranges. This is achieved by the precise control of iron absorption, storage and release in the intestine. In 2008, MT2 was identified as an important regulator in the process of iron release.^[48-50]

Two ways of iron transport across intestinal enterocytes are described. The uptake of iron bound in a heme molecule, which is mediated by heme carrier proteins (HCP) like HCP-1,^[51-52] and non-heme iron export, which is performed by ferroportin,^[53] the only known iron exporter. Due to its location on the surface of enterocytes, hepatocytes and macrophages, ferroportin regulates the cellular iron release and plasma iron level. The cellular concentration of the exporter protein is controlled by hepcidin, a 25 amino acid peptide hormone that is produced in the liver and secreted into the blood stream. Binding of the peptide hormone to ferroportin induces the phosphorylation of its tyrosine residues, which leads to its internalization and lysosomal degradation.^[54] Thus chronic excess of hepcidin results in the stop of cellular iron export, decreased supply of plasma iron and in extreme cases the development of iron-restricted anemias.^[55] Hepcidin deficiency on the other hand can cause iron overload, resulting in iron deposits in the liver and heart, as well as the development of hemochromatosis,^[56] although a recent publication describes hepcidin upregulation as a way to suppress obesity-associated conditions, such as hepatic steatosis and insulin resistance.^[57] Hepcidin concentration is regulated at the transcriptional level in hepatocytes, mediated by MT2 and other factors,^[58-60] dependent on changes in iron levels and erythropoietic activity. A high plasma iron level, infections and inflammations promote hepcidin production, thus preventing further iron overload. In the case of iron deficiency and increased erythropoietic activity, hepcidin production is suppressed, to allow an increased uptake of iron.^[56]

The hepcidin gene *Hamp* is expressed under the control of the bone morphogenetic protein/sons of mothers against decapentaplegic (BMP/SMAD) signaling cascade.^[58] Different proteins like the hemochromatosis protein (HFE), hemojuvelin (HJV) and transferrin receptor-2 (TfR2) are involved in this process^[61-62] and seem to promote hepcidin expression, as mutations in these proteins results in the reduction of hepcidin levels.^[61,63] Due to its position at the top of the BMP/SMAD pathway, as the coreceptor of the bone morphogenetic protein receptor (BMPR), HJV plays a prominent role in its regulation (Scheme 1.5). The pathway is activated by the binding of a bone morphogenetic protein (BMP) molecule to the BMPR/HJV complex. MT2 prevents the formation of this complex by the cleavage of HJV.^[50,64-65] HJV degradation in turn leads to a reduction of hepcidin expression.^[64] Although HJV was long considered the only substrate of MT2, new scientific insights indicate that MT2 is involved in the cleavage of different proteins of hepcidin expression pathways.^[66-67] Nonetheless, the importance of BMPR/HJV/MT2 mediated control of *Hamp* expression is supported by the hepcidin insufficiency and iron overload observed only after the combined knockout of HJV and MT2^[58] or BMP and MT2^[68].

Scheme 1.5: Influence of MT2 on hepcidin expression.



A: Expression of the hepcidin gene *HAMP* is regulated by the BMP/SMAD signaling cascade activated by the binding of BMP to the BMPR/HJV complex. **B:** MT2 cleaves HJV, the BMPR/HJV complex cannot form and *HAMP* expression is diminished (modified from Stimberg *et al.*^[36]).

Mutations and the knockout of the MT2 gene lead to the development of iron deficiency anemias,^[50,58] and mutations in the *TMPRSS6* gene are reported in several cases of iron refractory iron deficiency anemia (IRIDA),^[69-71] a disease associated with upregulated hepcidin levels and iron deficiency. Excess MT2 activity on the other hand can result in hepcidin deficiency, iron overload and the development of hereditary hemochromatosis.^[72-73] The symptoms of β -thalassemia, another inherited hematologic disorder resulting in iron overload, could be successfully reduced by the reduction of MT2 levels.^[74-75] This increased the expression of hepcidin, subsequently reducing the plasma iron level and improving erythropoiesis.^[74-75]

1.2.4.2 Cancer development and progression

Based on the abilities to remodel the extracellular matrix and to activate or cleave other enzymes or components of signal pathways, many proteases are associated with the development and progression of cancer.^[76-78] Since MT2 shares a high homology with MT1, which was first discovered due to its gelatinolytic activity in human breast cancer cells,^[79] MT2 was first discussed as a potential mediator of cancer development and metastasis.^[37-38] While increased MT1 levels were verified in several other cancer types, such as prostate^[80], ovarian^[81] and stomach cancer^[82], conversely, MT2 was connected to cancer suppression.^[83] So far, MT2 overexpression was associated with the suppression of tumor growth and progression in breast cancer^[84], prostate cancer^[85] and squamous-cell carcinoma^[86]. In general, high MT2 expression seems to correlate with a better survival prognosis in these types of cancer.^[86-88] Although Webb *et al.* describe a link between MT2 overexpression and a attenuation of new blood vessels formation,^[89] which is crucial for tumor growth and progression, it has to be noted that the exact mechanism of cancer suppression by MT2 remains to be elucidated.

1.2.5 Relevance of matriptase-2 as target of enzyme inhibitors

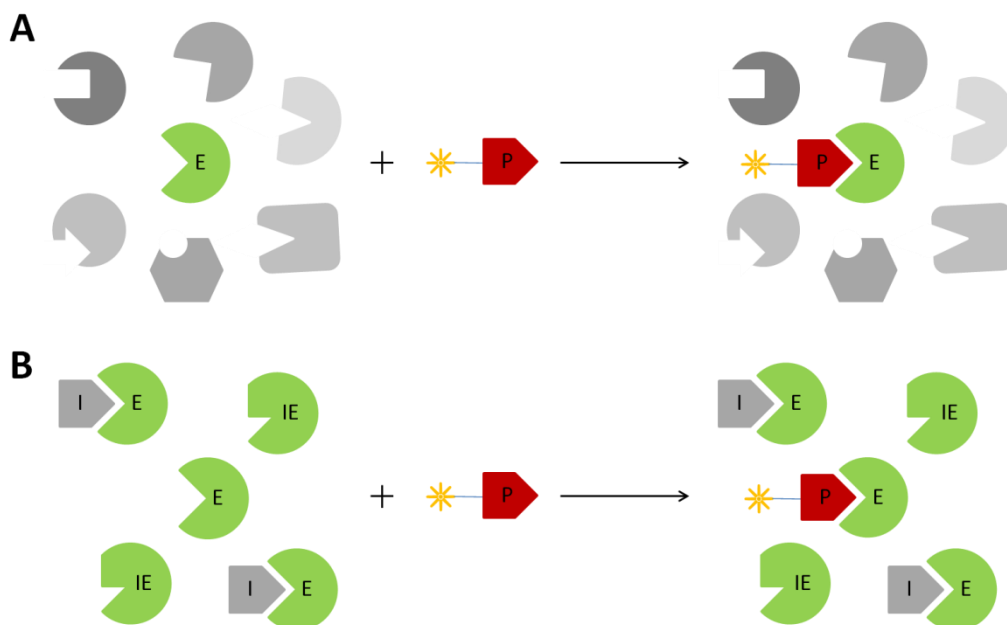
Because of its role in iron homeostasis MT2 presents itself as a promising target for the treatment of diseases linked to hepcidin deficiency, such as iron overload diseases like hereditary hemochromatosis and, especially, β -thalassemia.^[90] β -Thalassemia is caused by mutations in the β -globin gene which lead to an increased but ineffective erythropoiesis and iron-loading anemia.^[91-92] Due to these mutations, non-functional hemoglobin is produced, inducing the apoptosis of erythroid precursors and a disruption of oxygen transport. The metabolism affiliates this to a lack of iron, even though sufficient plasma iron is present, and tries to compensate by increased iron uptake, resulting in iron overload.^[93] The disease is categorized in three orders of severity, β -thalassemia major being the most severe. These patients are in regular need of blood transfusions as a source of functional red blood cells but suffer from a subsequent accumulation of iron and secondary iron overload.^[94] Even though β -thalassemia intermedia patients don't need blood transfusions to maintain a sufficient level of red blood cells, hepcidin expression is still diminished due to the misregulated erythropoiesis which results in an increased iron uptake and iron overload over time.^[95] Lastly, β -thalassemia minor patients display no or only weak symptoms of anemia.

While primary iron overload diseases like hemochromatosis are treated by phlebotomy, this is not an option in secondary iron overload diseases like β -thalassemia since patients suffer from anemia and in some instances require blood transfusions. In these cases patients are often treated with iron chelators, such as deferasirox, deferiprone and deferoxamine, to improve the excretion of excess iron.^[96] MT2 inhibition marks a new therapeutic option with the potential to improve patient compliance and safety compared to chelator treatment or phlebotomy, preventing iron overload before it even manifests. Already, several studies document an improvement of both, β -thalassemia and hemochromatosis symptoms after MT2 knockout or silencing.^[74-75,97-99] Therefore, MT2 inhibitors could provide a new source for potent iron overload drugs.

Apart from the reduction of MT2 activity in the treatment of diseases, MT2 inhibitors could be of great use for the development of ligands that promote MT2 as a prognostic tool. Inhibitors that attack the active site of an enzyme while also bearing detection groups, so called activity-based probes, can be used to selectively detect proteases in complex protein mixtures (Scheme 1.6).^[100-102] In contrast to antibodies, this method provides the advantage to exclusively label active enzymes, which opens up the possibility to compare the level of active to the total enzyme level by using both methods in tandem. Due to its role in various

diseases, selective activity-based probes for MT2 could be promising tools for the detection of MT2 as a prognostic biomarker.

Scheme 1.6: Functionality of activity-based probes.



A: Activity-based probes are able to selectively label an enzyme of interest **B:** Only the active form of an enzyme can be labeled. E: enzyme of interest, P: activity-based probe, I: inhibitor, IE: inactive enzyme of interest.

1.2.6 Matriptase-2 structure and specificity

Regardless the application, the structure of MT2 has to be taken into meticulous account for the design of new selective inhibitors, not only because of the high homology to the closely related MT1.^[37-38] Since no X-ray crystal structure of human MT2 could be obtained as of yet, Sisay *et al.* generated a homology model of the enzymes catalytic domain by fitting the primary structure of MT2 into the available 3D structure of MT1.^[103] A similar model was described by Duchene *et al.*^[104] Due to a high structural similarity of 45% in the catalytic domains of these two enzymes, the resulting models proved to be fitting representations of the MT2 catalytic domain and were successfully employed in various studies.^[100,105-106] Till this day, they remain as useful tools for the search and discovery of novel MT2 substrates, ligands and inhibitors.

The MT2 3D structure displays typical features of the TTSP family. The catalytic activity of the enzyme is mediated by a catalytic triad motif of the chymotrypsin-like fold, composed of His617, Asp668 and Ser762. The MT2 S₁ binding pocket accommodates basic amino acids, preferably Arg over Lys, due to the formation of a direct salt bridge between the guanidinium group of Arg and the carboxylate group of a S₁ Asp residue. This determines the MT2 primary substrate specificity to cleave after Arg residues in P₁ position.^[37-38] Corresponding Arg residues in P₁ position can be found in both autocatalytic cleavage sites of MT2 and cleavage sites of its natural substrate HJV.^[65,107] Further basic amino acids in the P₄-P₂ positions are predicted to improve substrate binding and in a combinatorial approach the preferred sequence Ile-Arg-Ala-Arg was determined,^[108] while Barré *et al.* indicated the importance of the prime side of a peptide to improve cleavage specificity.^[109] Proteomic Identification of Protease Cleavage Sites (PICS) technology revealed that Ala or other hydrophobic residues in P₂' and nonpolar amino acids like Leu or Val in other prime binding pockets are preferred.

The main difficulty in the development of potent and selective inhibitors of MT2 remains the high similarity to MT1. A few key differences between the two enzymes have to be exploited to this end, like the more discriminating substrate specificity of MT1 in contrast to the higher substrate promiscuity of MT2.^[110] In this regard, differences in the S₁ binding pocket are especially important. Due to a replacement of Ala at the bottom of the binding pocket in MT2 for Ser in MT1, the binding pocket of MT2 is more hydrophobic. This exchange determines the preference of MT1 for L-lysine in P₁ position, since a hydrogen bond to the substrate is formed by the Ser hydroxyl group. Furthermore, the lower part of the S₃/S₄ subsite of MT2 is more hydrophobic than that of MT1, which, together with Glu, Asp and Ser residues in the upper part promote the accommodation of positively charged residues in P₃/P₄ position. Lastly, due to a replacement of Ile in MT1 by Gly in MT2, the S₂' binding pocket of MT2 is smaller than that of MT1.

1.2.7 Ligands of matriptase-2

1.2.7.1 Substrates

In the last decades, several interaction partners of MT2, both synthetic and putative, were discovered. Among these, synthetic peptide substrates consisting of three to four amino acid residues are employed to investigate MT2 activity and inhibition. Substrates like Boc-Gln-Ala-Arg or Boc-Gln-Gly-Arg with a C-terminal reporter group like 7-amino-4-methylcoumarine (AMC)^[111] or *para*-nitroaniline (pNA)^[103] are frequently used to monitor MT2 activity, even though they are not specific for MT2 and can be cleaved by many other enzymes with trypsin-like substrate specificity.^[36] Combinatorial approaches by Béliveau *et al.*^[110] and Wysocka *et al.*^[108] revealed a series of seven to eight amino acid substrates of MT2, of which Abz-Arg-Arg-Ala-Arg-Val-Val-Gly-Gly-Y(3-NO₂) was the most potent with a K_m value of 3.3 μ M for MT2. Still, other trypsin-like enzymes like MT1, hepsin and DESC1 were able to cleave these newly developed compounds. While synthetic substrates are of great use for the analysis of enzyme activity, putative substrates of MT2 are essential to further the understanding of its physiological role and functions. Natural substrates of MT2 comprise HJV,^[65,107,112] fetuin-A,^[113] meprin β ^[114] and MT2 itself.^[45]

1.2.7.2 Inhibitors

In recent years, a number of inhibitors of MT2 activity were identified, first among these, the natural peptides aprotinin^[37-38] and leupeptin^[110]. Established MT2 inhibitors mostly comprise peptidomimetic but also some non-peptidomimetic molecules.^[115]

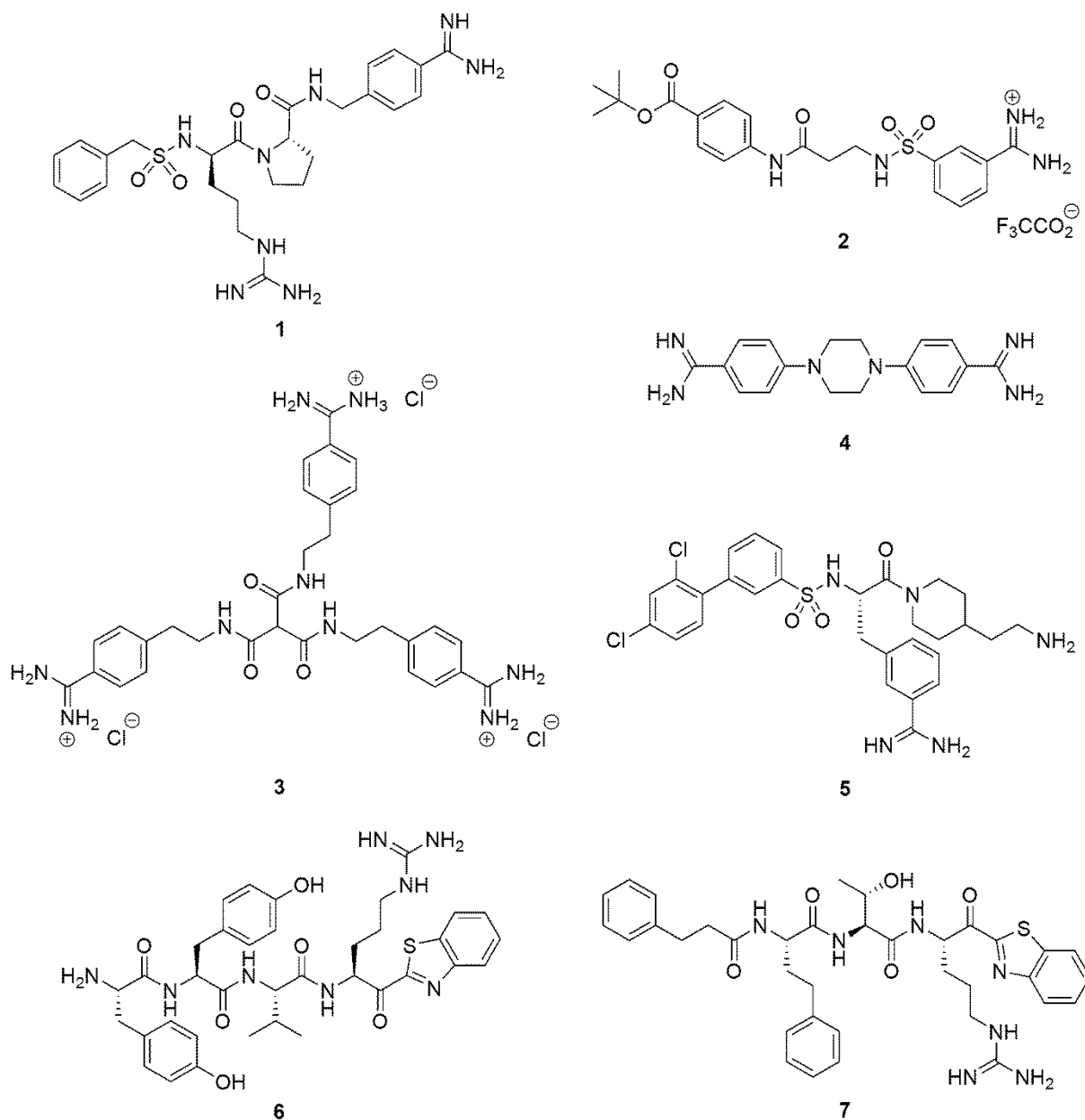


Figure 1.1: Chemical structures of synthetic MT2 inhibitors. **1** ($K_i = 0.19 \mu\text{M}$)^[103], **2** ($K_i = 7.6 \mu\text{M}$)^[111], **3** ($K_i = 1.46 \mu\text{M}$)^[116], **4** ($K_i = 1.16 \mu\text{M}$)^[117], **5** ($K_i = 0.11 \mu\text{M}$)^[118], **6** ($K_i = 2.56 \text{nM}$)^[104], **7** ($K_i = 3.1 \text{nM}$)^[106].

The first synthetic peptidomimetic low-molecular-weight inhibitors of MT2 were designed and synthesized based on the MT2 homology model.^[103] Out of the series of presented compounds, **1** (Figure 1.1), bearing two basic residues, was the most potent MT2 inhibitor with a K_i value of $0.19 \mu\text{M}$. While the benzamidine group of the compound is probably directed to the S_1 pocket, the D-configured Arg most likely targets the S_3/S_4 binding pockets.^[119] Replacement of the benzamidine moiety led to an extreme loss in inhibitory potency towards MT2 ($K_i > 10 \mu\text{M}$) further promoting its accommodation in the P_1 site of MT2. Dosa *et al.* developed another series of compounds with a sulfamoyl benzamidine moiety

connected to a second aromatic ring as a defining feature.^[111] Study of linker length, orientation of the amidine group, as well as substitutions of the second aromatic ring revealed bisbenzamidines as the most potent inhibitors of MT2. Compound **2** (Figure 1.1) with a K_i value of 7.6 μM represents the inhibitor with the highest inhibitory activity against MT2 out of this approach, but still displayed potency against other proteases like trypsin and thrombin. The addition of a third branch to the linker substructure didn't result in improved selectivity or potency against MT2 until the introduction of symmetry into the trifunctional scaffold.^[116] For this purpose, a small library of symmetrical and nonsymmetrical bis and trisbenzamidines was designed and synthesized. Among these the trifunctional compound **3** was the most potent MT2 inhibitor with a K_i of 1.46 μM (Figure 1.1). Beckmann *et al.* presented another series of symmetric, achiral bisbenzamidines with **4** as the compound with the highest overall activity against MT2 with a K_i of 1.16 μM (Figure 1.1),^[117] but unfortunately exhibited even more potency against MT1 ($K_i = 0.719 \mu\text{M}$). A similar relationship was described 2012 by Hammami *et al.*^[118] Different substitution patterns in a series of L-3-amidinophenylalanine derivatives resulted in nanomolar (K_i between 110 and 750 nM) inhibitors of MT2 activity which were even more active against MT1. Compound **5** (Figure 1.1), bearing a terminal 2,4-dichlorophenyl group expressed the highest inhibition rates for both, MT1 and MT2, with K_i values of 2 nM and 110 nM respectively.

Peptidomimetics with different amino acid substitutions were designed and tested by a combinatorial approach for their inhibitory activity and selectivity towards MT2.^[104] These compounds contain an electrophilic bezothiazole ketone warhead next to an Arg residue in P_1 position used to mimic the P_1 - P_1' scissile bond. By modification of the amino acids in P_2 - P_4 position MT2 selectivity over MT1 could be achieved. A Tyr-Tyr-Val-Arg-ketobenzothiazole (**6**, Figure 1.1) was discovered as potent inhibitor of MT2 activity with a K_i value of 2.56 nM for MT2 and a K_i value of 31.54 for MT1. By the employment of unnatural amino acids selectivity for MT2 could be improved even further.^[106] This approach yielded compound **7** (Figure 1.1) with L-allo-Thr in P_2 , homo-Phe in P_3 and desamino-Phe in P_4 position as the most potent MT2 inhibitor with a K_i value of 3.1 nM. Compared to MT1 (K_i value of 200 nM) this compound was approximately 65-fold selective for MT2.

In recent years, compounds based on the sunflower trypsin inhibitor 1 (SFTI-1) of the Bowman Birk inhibitor (BBI) class (**8**, Figure 1.2) emerged as potent inhibitors of both MT1 and MT2.^[120-122] SFTI-1 consists of 14 amino acids that are connected in a cyclic structure.^[123] A disulfide bridge between two cysteine (Cys) residues of the peptide backbone divides the peptide into two loops. The larger loop, which consists of a nine amino acid

sequence (Thr-Lys-Ser-Ile-Pro-Pro) typical for the BBI class, functions as the binding site that interacts with the target enzyme. Over 40 sun flower trypsin inhibitor (SFTI) analogs were synthesized and examined for their inhibitory activity against MT2 by Gitlin *et al.*^[122,124] While monocyclic analogs in general displayed weaker MT2 inhibition, high potency and even selectivity toward MT2 over MT1 could be achieved by the introduction of Arg in P₁ and D-Arg in P₄ position of the bicyclic peptide. Out of this series, compound **9** (Figure 1.2) was the most selective inhibitor with a 228-fold lower K_i value towards MT2 compared to MT1 (278 nM vs. 63400 nM, respectively). Compound **10** (Figure 1.2) exhibited the strongest inhibition of MT2 activity ($K_i = 15$ nM) but was even more active against MT1 ($K_i = 5$ nM).

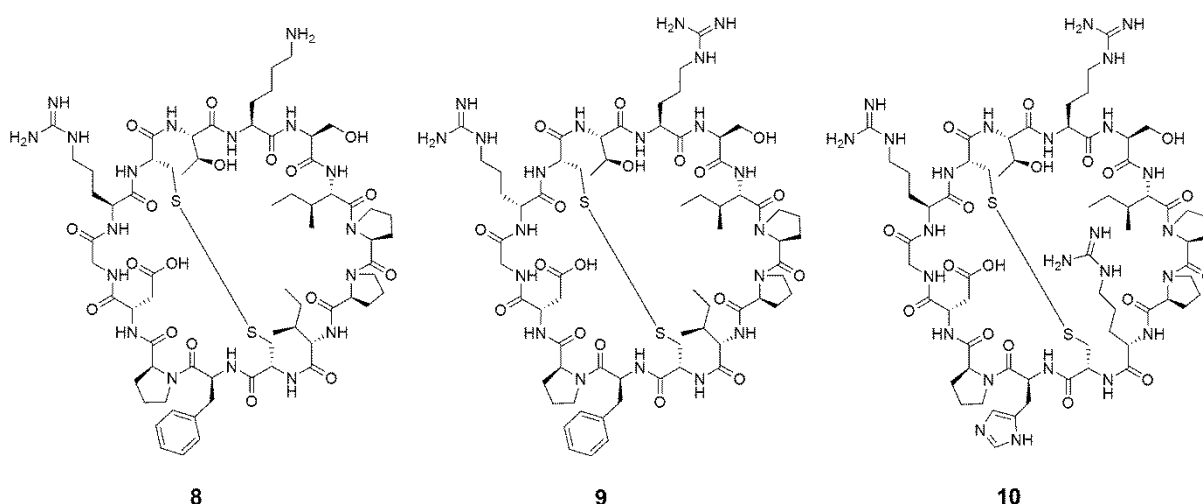


Figure 1.2: Chemical structures of sunflower trypsin inhibitors. Compounds **8** ($K_i = 218$ nM)^[122], **9** ($K_i = 278$ nM)^[122] and **10** ($K_i = 15$ nM)^[124].

In conclusion, structural similarities between MT1 and MT2 remain to be the biggest obstacles for the development of MT2 inhibitors. Potency and selectivity towards MT2 were achieved in various studies, but mostly independent from each another. Thus, the need for inhibitors that are both potent and selective for MT2 is still apparent.

1.3 Threonine proteases

Threonine proteases are a relatively small group of enzymes which comprises a total of 3 clans and 6 families according to MEROPS database.^[8] They are prevalent in all kingdoms of life. The prototype of this enzyme group, the β -subunit of the proteasome is highly conserved in eukaryotes, archaea and several species of bacteria.^[125] Threonine proteases are mainly involved in protein degradation and recycling processes.^[125-127]

Like serine proteases, this enzyme group uses an amino acid residue in the enzymes active site to perform its catalytic actions. In this case, the secondary alcohol of a threonine (Thr) residue, organized in a catalytic triad, serves as the means for a nucleophilic attack at the target molecule.^[125] This process is analogous to the use of the primary alcohol in the active site Ser of serine proteases, but in contrast, the active site Thr is always located at the N-terminus of the protein.^[128] In this constellation the N-terminal amide group can function as a base to circumvent the steric interference by the γ -methyl group of Thr. This leads to the polarization of a water molecule and, subsequently, to the deprotonation of the hydroxyl group of Thr, thereby improving its reactivity.^[129] Substitution of active site amino acid residues that are not positioned at the N-terminus with a Thr residue results in an attenuation of enzymatic activity,^[130-131] further supporting the importance of this structural composition for Thr mediated activity.

Given these narrow structural limitations, it is not surprising that serine proteases permeated and constitute an evolutionary more diverse group compared to threonine proteases. Buller *et al.* proved this principle by comparing the structural constraints of different catalytic residues and their influence on the convergent evolution of enzyme structure.^[132] Analysis of possible rotamers and the geometry of the oxyanion hole revealed Thr as the catalytic residue as unsuitable in serine protease scaffolds due to the interference of the γ -methyl residue or incompetent catalytic conformation.^[132] Nonetheless, threonine proteases provide a conserved scaffold for proteolytic reactions that relies on the unique confirmation of their catalytic Thr. Consistent with these findings the exchange of the N-terminal Thr in the β -subunit of the proteasome for Ser resulted in a reduction of catalytic activity.^[133]

1.3.1 The proteasome

Until the late 1930s proteins were believed to remain in a state of nearly constant stability. The concept of protein turnover was first described by Schoenheimer *et al.* after the application of ^{15}N -labeled amino acids in metabolic studies.^[134-135] The results of Simpson *et al.* established that this process is energy dependent.^[136] Discovery of the lysosome as a cellular compartment that houses a plethora of enzymes with different specificities^[137-138] provided a secluded space inside the cell to support this form of protein metabolism. Nonetheless, the fact that the process of protein turnover is energy dependent remained, contradictory to the known mode of action of proteases that function energy independent under the appropriate physiological conditions. At first, this was contributed to the energy requirement of H^+ ion pumps,^[139] that maintain the acidic conditions in the lysosome, and the active transport of proteins into the lysosomal compartment.^[140] However, it became apparent, that a second intracellular protein degradation system had to exist.^[141] Subsequently, a small heat-stable protein that gets covalently conjugated to proteins designated for degradation,^[142-143] termed ATP-dependent proteolysis factor-1, later identified as ubiquitin,^[144] and other components of non-lysosomal protein degradation were described,^[145] explaining the energy requirement of this process. Finally, the protease responsible for the degradation of ubiquitin-protein-complexes was discovered by Hough *et al.* and Waxman *et al.*^[146-147]

The so called proteasome is a multicatalytic protein complex existent in both, eukaryotic and prokaryotic cells. The eukaryotic proteasome, also termed 26S proteasome, consists of a central 20S core particle (CP) and one or two 19S regulatory particles (RP).^[148] The 20S CP is formed by two identical inner rings, made up of seven distinct β subunits, and two identical outer rings, consisting of seven distinct α subunits.^[149] While proteolytic activity is mediated by Thr residues in the β subunits in the inner compartment of the proteasome,^[150] the N-terminal tails of α subunits form the α -ring gate that regulates substrate entry into the CP.^[151] The 19S RP is exclusive and highly conserved among eukaryotic proteasomes which comprises the lid and base sub complexes. It regulates substrate recognition through Rpn ubiquitin binding domains,^[152] as well as the unfolding and entry of peptide substrates by multiple Rpt ATPase subunits.^[153] Two isoforms of the proteasome, the immunoproteasome and the thymoproteasome, responsible for antigen processing and killer T cell generation have been discovered.^[154]

An intact and active proteasome is important for the maintenance of protein homeostasis. Accordingly, the ubiquitin proteasome system (UPS) is involved in many physiological processes such as apoptosis, metabolic regulation, cell proliferation and the immune response^[155-157] and the deregulation of proteasomal activity often leads to the development of disease. Upregulation of UPS activity can cause an attenuation of apoptosis and increase in cell proliferation in cancer types like multiple myeloma and is also observed in sepsis patients, increasing the breakdown of skeletal muscle proteins,^[158-159] while the formation of protein plaques in neurodegenerative diseases like Alzheimer's and Parkinson's,^[160-161] as well as the development of HIV and hepatitis B infections^[162-163] is furthered by a decrease in UPS activity. Taken together, these findings promoted the proteasome as a possible new drug target. Several studies investigating the potential of proteasome ligands were conducted, resulting in the discovery of drugs like Bortezomib and PR-957 for the treatment of cancer and autoimmune diseases.^[164-165] In recent years, a new class of drugs acting as inducers of targeted protein degradation was described.^[166] These compounds, named proteolysis targeting chimeras, use the mechanism of proteasomal proteolysis to mark and degrade a target protein, providing potential new treatment options for various diseases.

1.3.2 Proteasomal protein degradation

Targeted protein degradation by the proteasome is an intricate cellular pathway that undergoes tight regulation to assure the maintenance of protein homeostasis. First, a protein designated for degradation is marked with a poly-ubiquitin chain in a multi-step process.^[167] For this purpose, ubiquitin is activated by an E1 ubiquitin-activating enzyme and conjugated to this enzyme by a thiolester bond.^[168] The activated ubiquitin is then transferred to the sulfhydryl group of a cysteine residue in an E2 ubiquitin carrier protein.^[169] While there is generally only one type of E1 ubiquitin activator in a cell, several different E2 ubiquitin carriers contribute to the specificity of the ubiquitin tagging system.^[170] The final transfer of the ubiquitin molecule from the E2 ubiquitin carrier to a lysine residue of the target protein is catalyzed by an E3 ubiquitin ligase.^[171] Molecules with E3 activity comprise either a single protein or a multi-protein complex that interacts with the target protein and an E2 ubiquitin carrier. With over 1000 members the E3 ubiquitin ligases are the main factor for the specificity of the UPS.^[172] However, ubiquitination is a dynamic process. Depending on the pattern, conjugation with ubiquitin molecules can designate a protein for degradation or

translocation and is even used for the regulation of protein transcription.^[173-174] Similarly, a host of deubiquitination enzymes counteracts these functions and reverses ubiquitin tagging, allowing the tight control of protein homeostasis.^[175]

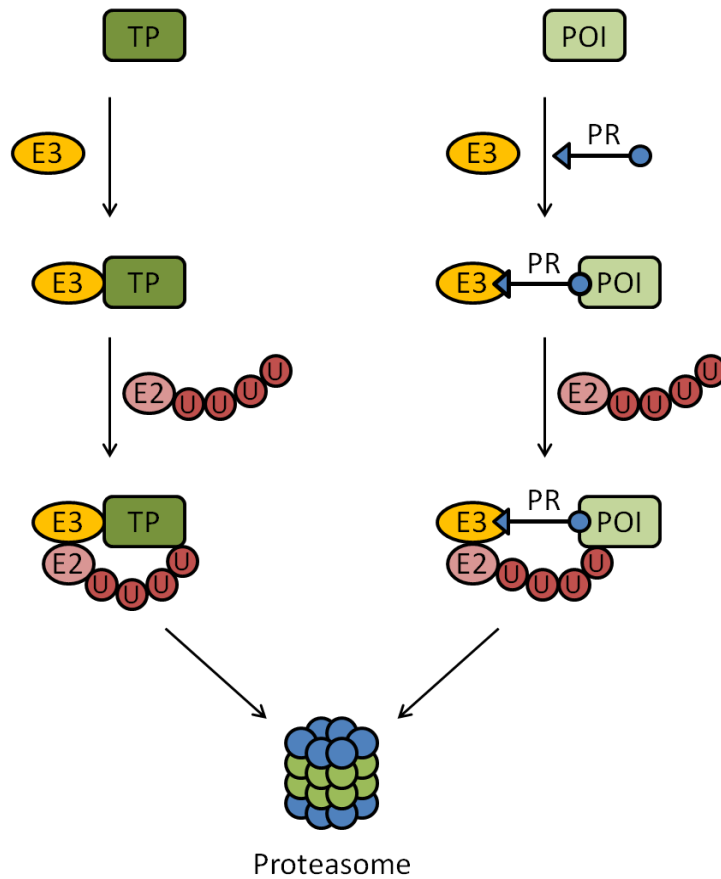
Appropriately ubiquitinated proteins are transported to the proteasome where substrate recognition and entry is conducted by the 19S subunit.^[153] Here, multiple Rpn non-ATPase subunits serve as ubiquitin and ubiquitin receptor binding domains that facilitate substrate attachment.^[176] Subsequently, the ubiquitin tags on the bound target protein are removed by deubiquitinases in the lid subcomplex, while six Rpt ATPase subunits in the 19S RP linearize the protein and translocate it to the 20S CP.^[177] For this purpose, each Rpt possesses an ATPases associated with various cellular activities (AAA+) domain which, taken together, form a heterohexameric ring structure that engages the protein substrate.^[178] Upon ATP binding and hydrolysis the AAA+ domains undergo a conformational change that translates into mechanical energy used to unfold and pull the linearized protein into the 20S CP.^[179] After entry into the inner compartment the target polypeptide is cleaved consecutively by the proteasomal catalytic groups resulting in peptide fragments of 3 to 25 amino acids.^[180] These fragments are released and rapidly digested into single amino acids by cytosolic peptidases, ready to be incorporated in the synthesis of new proteins.^[181] Differing from the common proteasomal pathway of complete protein breakdown the proteasome is able to selectively process and partially degrade target proteins, as is the case in the activation of the transcription factor NF- κ B.^[182]

1.3.3 Proteolysis targeting chimeras

Advancements in the understanding of the proteasome and its mode of action promoted the idea to use its activity for the treatment of disease. The past 20 years saw the development of the proteolysis targeting chimera (PROTAC) technology as means to exploit this system.^[166,183] PROTAC molecules (PROTACs) are commonly characterized by a heterofunctional scaffold that comprises two distinct moieties connected by a linker structure.^[184] While one moiety is able to engage an E3 ubiquitin ligase, the second is directed towards a target protein of interest, bringing both binding partners into close proximity with each other.^[166] If the right structural conditions are met a ternary complex made up of E3 ligase, E2 ubiquitin carrier and the target protein is formed, leading to the ubiquitination of the latter (Scheme 1.7). After ubiquitination the target protein is directed to the proteasome and subsequently degraded. In principle, this use of controlled targeted protein degradation could provide new and selective means for the treatment of diseases associated with protein overexpression or malregulation.^[185] In this context, PROTACs could open up treatment strategies for targets that were previously considered undruggable, such as scaffolding proteins and transcription factors.^[186]

In the recent years the design of PROTACs strongly focused on ligands of two well described E3 ligases, cereblon (CRBN)^[187] and von Hippel-Lindau (VHL).^[188] These ligands were typically based on the immunomodulatory imide drug (IMiD) scaffold, represented by thalidomide and its analogues in the case of CRBN,^[189] or compounds that mimic the binding mode of the HIF-1 α protein, a substrate of the VHL ligase,^[190] respectively. Presently, the emerging field of PROTAC research continues to develop successful new scaffolds and ligands for the recruitment of other E3 ligases such as cIAP1^[191] and DCAF15^[192]. A plethora of studies for PROTAC function and activity were conducted by various working groups, ranging from heterofunctional PROTACs that could induce degradation of a protein of interest (POI),^[184] to homobifunctional PROTACs for the self-ubiquitination and degradation of CRBN and VHL.^[193-194] As of august 2019, two PROTACs for the treatment of prostate^[195] and breast cancer^[196], respectively, entered clinical phase I trials. As the field of PROTAC research keeps growing, so is the need for new assay systems and methods to assess and evaluate the activity of this emerging drug class.

Scheme 1.7: Schematic depiction of endogenous *versus* targeted protein degradation induced by PROTACs.



In both cases an E3 ubiquitin ligase attaches a poly-ubiquitin chain to a protein. PROTACs can artificially induce complex formation of a protein of interest with the E3 ligase. Subsequently, the protein is designated for degradation by the proteasome. TP: target protein, E3: E3 ubiquitin ligase, E2: E2 ubiquitin carrier, U: ubiquitin, POI: protein of interest, PR: PROTAC molecule.

1.4 Objectives

The aim of this study was twofold. On one hand novel ligands and interaction partners of the regulator of iron homeostasis, the type II transmembrane serine protease MT2, should be identified and characterized. There is a strong need for advancements in this field that could help to further the development of potent and selective inhibitors and tool compounds, as well as the knowledge of the enzyme's physiological role (chapter 1.2.4). On the other hand, novel proteolysis targeting chimera molecules should be evaluated and characterized in biological systems. This emerging field of research continues to grow and develop and thus new ways and systems to measure PROTAC activity could prove helpful for its advancement.

The first project (chapter 2.1) dealt with the analysis and evaluation of different series of potential inhibitors of MT2 activity. These series comprised sunflower trypsin inhibitors, peptidomimetics and a small substance library containing various compounds with basic subgroups. Additionally, successful inhibitors were evaluated for MT2 inhibition in a living cell system, as well as against other serine proteases like MT1 and thrombin to obtain a selectivity profile. *In cellulo* evaluation of successful MT2 inhibitors concluded this project.

In the second project (chapter 2.2), those inhibitors with a detection group were further characterized for their labeling abilities. For this purpose, these so called activity-based probes were tested in SDS-PAGE/Western blot, microscopy and cell viability assays.

In the final project (chapter 2.3) the biochemical parameters of proteolysis targeting chimera molecules were investigated in cell systems. Compounds were tested for cytotoxicity, as well as cellular uptake. Furthermore, fusion protein systems for the analysis of PROTAC activity *in vitro* were conceptualized and developed. These systems were evaluated with the use of a small library of PROTAC compounds.

2 Results and discussion

2.1 Evaluation of enzyme inhibitors for matriptase-2 inhibition

As indicated in previous studies, the reduction of MT2 activity can be used to counteract the increased iron uptake associated with iron overload diseases, such as β -thalassemia and hemochromatosis.^[74-75] Yet, to date, iron excess is treated by continuous phlebotomy due to the lack of sufficient alternatives. The discovery of new and potent MT2 inhibitors could provide new treatment options for these disorders while simultaneously improving patient compliance.

In this part of the work a series of synthetic compounds was evaluated for their inhibitory potency towards the type II transmembrane serine protease MT2, a key regulator of iron homeostasis. MT2 activity derived from the culture supernatant of stably transfected human embryonic kidney (HEK) cells (Figure 2.1) was used to evaluate the potency and binding type of potential inhibitors. Tested compounds comprised several classes of chemical scaffolds such as peptide inhibitors, peptidomimetics and chromenones. A small library screen with 50 compounds chosen for their basic substructures concluded the inhibitor screening approach. Finally, established inhibitors were evaluated in additional *in cellulo* experiments for their inhibitory activity towards MT2.

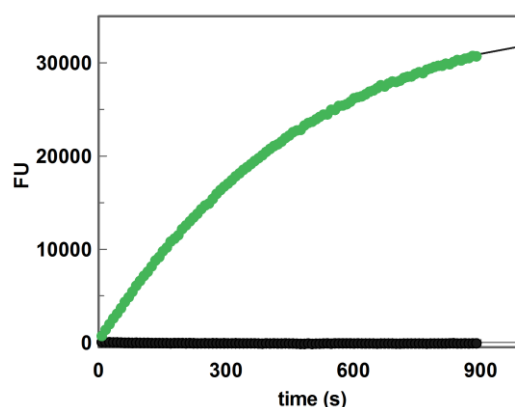
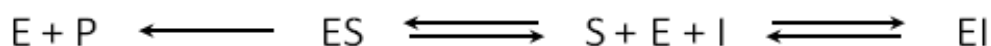


Figure 2.1: Matriptase-2 activity in the supernatant of transfected HEK cells. Black: HEK wild type activity; green: HEK MT2 activity. 5 μ g of either HEK wild type or HEK MT2 cell culture supernatant were measured in the presence of the fluorogenic substrate Boc-Gln-Ala-Arg-AMC. The generated fluorescence units (FU) are plotted against time.

In general, inhibitors can be categorized in two groups, those that chemically target an enzyme and form a covalent bond with it and those that interact by non-covalent means such as hydrophobic interactions and hydrogen bond formation. Further distinctions can be made in regard of an inhibitors binding behavior. Reversible inhibitors attach only temporary to a target enzyme and an equilibrium of substrate-bound, free and inhibitor-bound enzyme is developed (Scheme 2.1). In inhibition measurements this can be observed in activity curves, which exhibit a steady inhibition rate that does not change over time.

Scheme 2.1: Schematic depiction of the general mechanism of competitive reversible inhibition.



The enzyme (E) interacts with substrate (S) and inhibitor (I) in a competitive manner. An equilibrium of free enzyme, enzyme-inhibitor complex (EI) and enzyme-substrate complex (ES) is formed. The enzyme catalyzed reaction of ES to E and product (P) is performed at a steady rate.

The potency of reversible inhibitors was evaluated by the determination of IC_{50} and K_i values. The inhibitory constant K_i and the inhibitor concentration of half maximal enzyme inhibition IC_{50} are reflective of the binding affinity and of the functional strength of an inhibitor, respectively. Fluorogenic assays were used to measure the reaction rate of the enzyme catalyzed reaction in the presence of different inhibitor concentrations (minimum of four different concentrations). IC_{50} values were obtained by nonlinear regression of data points using equation (Scheme 2.2A). Values K_i were calculated using equation (Scheme 2.2B).

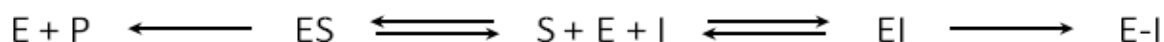
Scheme 2.2: Equations used for the determination of IC_{50} and K_i values.

$$\text{A} \quad v_i = v_0 / \left(1 + \left(\frac{[I]}{IC_{50}} \right) \right) \quad \text{B} \quad K_i = \frac{IC_{50}}{\left(1 + \frac{[S]}{K_m} \right)}$$

(A) Inhibitor concentrations of half maximal enzyme activity, IC_{50} , were estimated by nonlinear regression of data points in absence and presence of different inhibitor concentrations. v_i : reaction rate in the presence of inhibitor, v_0 : initial reaction rate, $[I]$: inhibitor concentration. (B) The inhibitory constant K_i was calculated by plotting IC_{50} values against a correction factor $(1+[S]/K_m)$. $[S]$: substrate concentration, K_m : Michaelis-Menten constant.

Irreversible inhibitors chemically interact with a target enzyme and form a covalent-bound enzyme-inhibitor complex (Scheme 2.3). This reaction is performed in a time-dependent manner. In the presence of an irreversible inhibitor enzyme activity is decreased over time, until all target enzymes are bound in complex with an inhibitor molecule and no more substrate is converted.

Scheme 2.3: Schematic depiction of the general mechanism of competitive irreversible inhibition.



The enzyme (E) interacts with inhibitor (I) in a time-dependent manner to form enzyme-inhibitor complex (EI) and irreversible enzyme-inhibitor complex (E-I). Since E-I are formed at a constant rate, the equilibrium of the depicted reaction is shifted to the right side. Consequently, less enzyme-substrate complex (ES) and product (P) is formed, the reaction rate k_{cat} is reduced over time.

The potency of irreversible inhibitors was not determined by conventional IC_{50} measurement since the time dependency of the reaction results in varying IC_{50} values subordinate to the used measurement period. Hence, the observed rate constant for inhibition k_{obs} and second order rate constants k_{inac}/K_i of inactivation were calculated. Fluorogenic assays were used to measure the reaction rate of the enzyme catalyzed reaction in the presence of different inhibitor concentrations (minimum of four different concentrations). The exponential rate equation (Scheme 2.4A) was applied to the kinetic data to obtain values k_{obs} from non-linear regression. Under conditions of linear dependency of k_{obs} on $[I]$, the second order rate constant of inactivation, k_{inac}/K_i , was calculated using the equation (Scheme 2.4B).

Scheme 2.4: Equations used for the determination of k_{obs} and k_{inac}/K_i values.

$$\mathbf{A} \quad [P] = v_0 \times \frac{(1 - e^{-k_{obs}t})}{k_{obs}} + d \quad \mathbf{B} \quad \frac{k_{inac}}{K_i} = \left(\frac{k_{obs}}{[I]} \right) \times \left(1 + \frac{[S]}{K_m} \right)$$

(A) First order rate constants k_{obs} were estimated by non-linear regression. [P]: product concentration at time t, d: offset. (B) Second order rate constants k_{inac}/K_i were determined by multiplying $k_{obs}/[I]$ with the correction factor $(1+[S]/K_m)$.

2.1.1 Peptide inhibitors of matrilysin-2

The past century saw the identification and characterization of chemical structures and modes of action of an abundance of natural products.^[197-198] Peptide inhibitors, derived from the structure motifs of natural enzyme inhibitors and substrates, emerged as prominent tools for the design and synthesis of new modulators of enzymatic activity.^[199] Herein, four inhibitors with a cyclic peptide structure, derived from the prototype of sunflower trypsin inhibitors (SFTI-1) were analyzed for their inhibitory potency towards MT2.

2.1.1.1 Sunflower trypsin inhibitors

Compounds **11** to **14** are presented in figure 2.2. They all possess the 14 amino acid backbone structure and intra-molecular disulfide bridge shared as a common feature by SFTI.^[123] In the past, these smallest members of the BBI family emerged as viable inhibitors of serine proteases and promising tools for the development of new pharmaceutical agents.^[200] SFTI interact with enzymes in a substrate-like fashion via a conserved binding loop made up of the canonical sequence Thr-Lys-Ser-Ile-Pro-Pro with the P₁-P₁' reactive site located between Lys5 and Ser6.^[123]

Compound **11** was established previously as a potent inhibitor of MT2 activity with a K_i value of 19 nM for the purified enzyme^[122] and represents the second most active MT2 inhibitor out of a series of molecules based on SFTI-1.^[201] By exchange of Lys5 in wild type SFTI-1 for an Arg residue in **11**, a 10-fold increase in inhibitory potency towards MT2 could be achieved (K_i values of 218 nM *versus* 19 nM, respectively). In addition **11** displayed a 10-fold selectivity for MT2 over MT1 in contrast to SFTI-1 which was 2-fold selective for MT1 (K_i values MT1 269 nM *versus* 102 nM; K_i values MT2 19 nM *versus* 218 nM, respectively).^[122] Out of the series of SFTI-1 analogs **11** was the most selective for MT2.^[201]

In the course of this work, **11** was re-evaluated in comparison to three fluorescently labeled analogs **12**, **13** and **14** (Figure 2.2). These compounds feature the typical SFTI-1 scaffold with a disulfide bridge formed between two Cys residues which comprise the BBI binding loop. The native BBI domain^[202] was modified by the replacement of Lys5 by Arg to address the primary substrate specificity of MT2 for basic amino acids, and Arg in particular, in P₁ position.^[37-38] Additionally, compound **12** saw the introduction of a Lys residue, labeled with a 5(6)-carboxyfluorescein fluorophore, as substitute for Asp14 of the bicyclic scaffold. In

contrast to **11** and **12** the bicyclic structure of analogs **13** and **14** was disrupted due to a ring-opening between Gly1 and Asp14. In these molecules the 5(6)-carboxyfluorescein group was attached to the free Gly1 residue by either a 8-amino-3,6-dioxaoctanoic acid (PEG) linker in case of **13**, or a β -alanine linker in case of **14**.

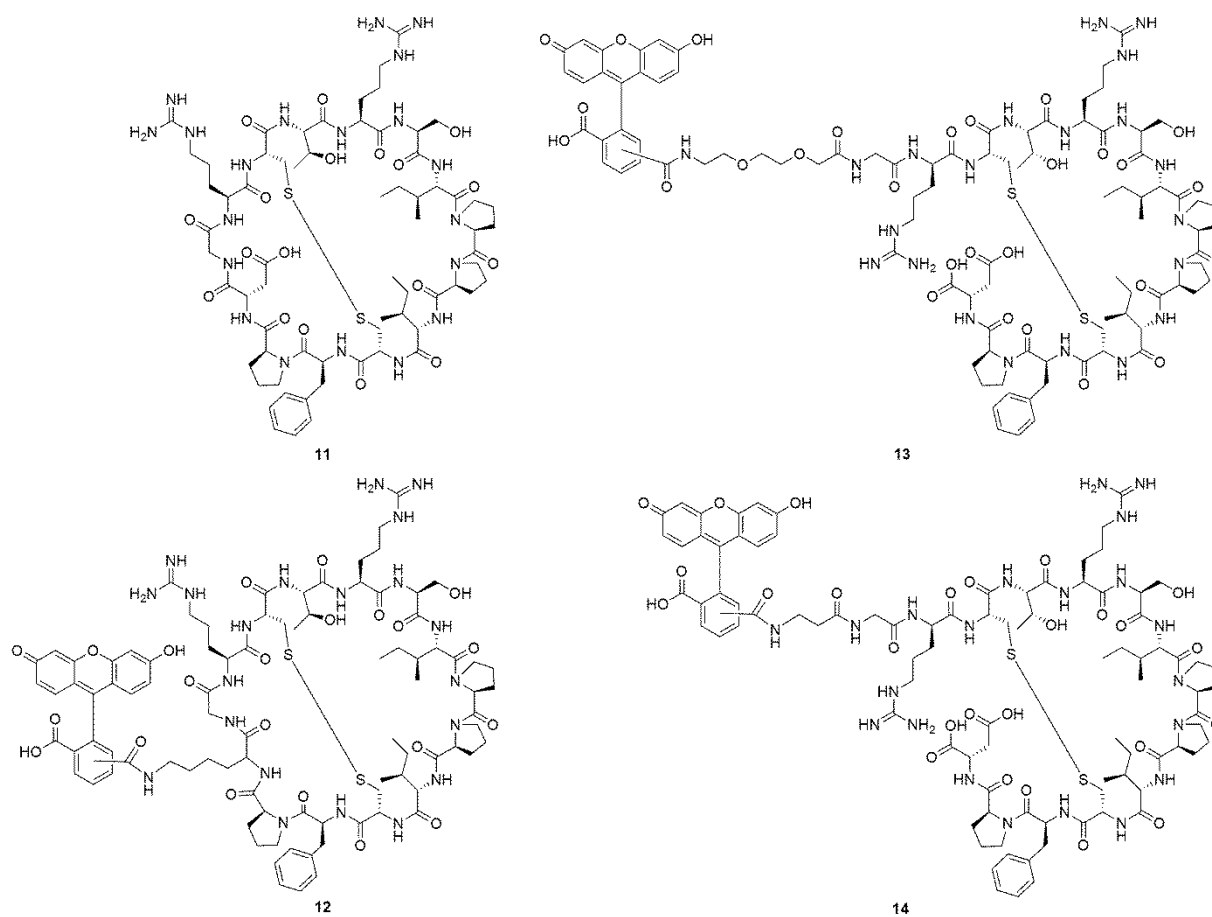


Figure 22: Chemical structures of SFTI-1 analogs. Compounds **11** ^[122] to **14** were provided by the group of Prof. Dr. K. Rolka, Faculty of Chemistry, University of Gdansk, Gdansk, Poland. Stock solutions were prepared in DMSO at a concentration of 10 mM.

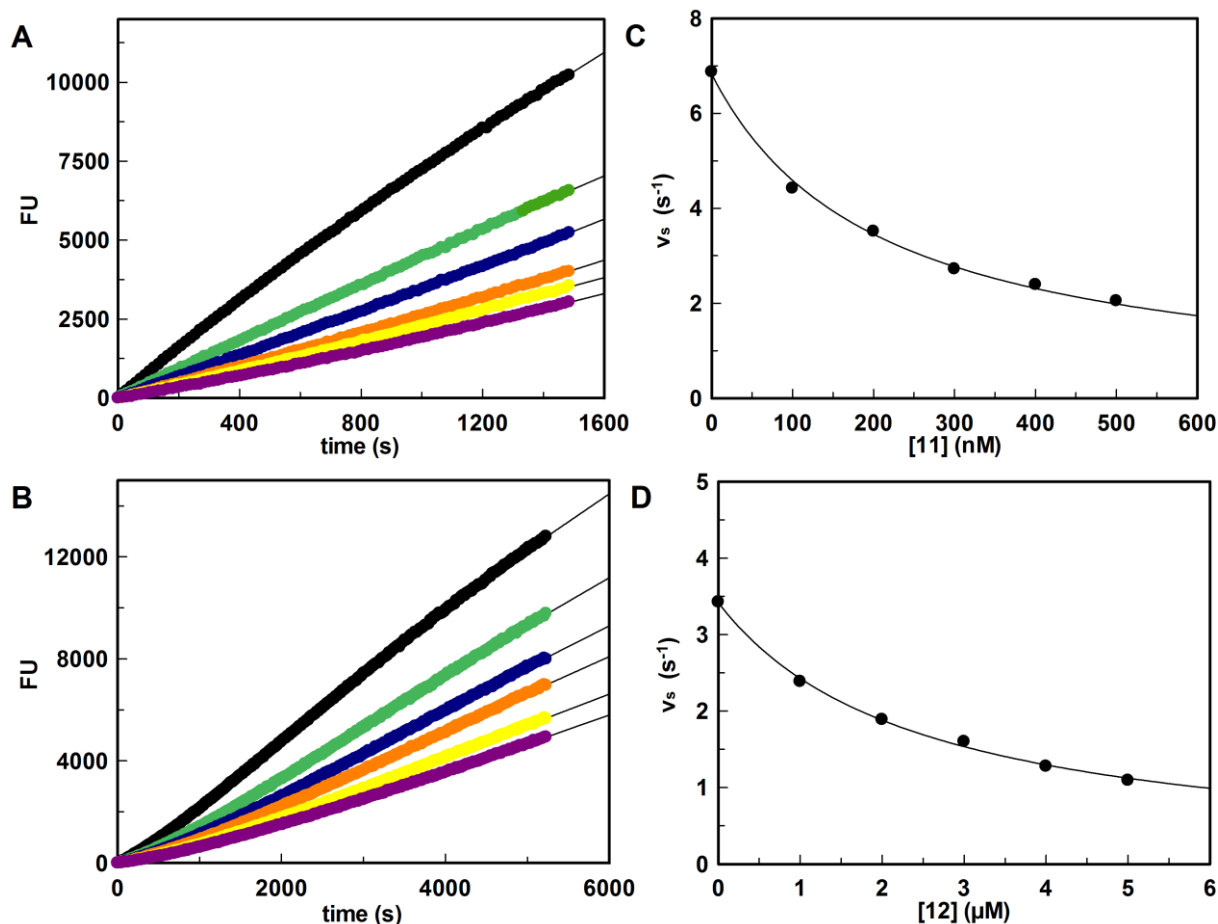


Figure 23: MT2 activity in the supernatant of transfected HEK cells in the presence of increasing concentrations of SFTI inhibitors 11 and 12. (A-B) Fluorescence units (FU) plotted versus time. (C-D) Corresponding values v_s plotted versus probe concentrations. Colored progress curves represent reactions in the presence of different inhibitor concentrations (A: ● uninhibited reaction, ● 100 nM, ● 200 nM, ● 300 nM, ● 400 nM, ● 500 nM of compound 11; B: uninhibited reaction, ● 1 μM, ● 2 μM, ● 3 μM, ● 4 μM, ● 5 μM of compound 12). Depicted binding curves are generated from duplicate measurements.

Compounds 11 to 14 were kinetically characterized for MT2 inhibition. For this purpose the MT2 activities in the supernatant of transfected HEK cells were measured at increasing inhibitor concentrations (Figures 2.3 A/B and 2.4 A/B). Dose-dependent inhibition of MT2 was observed in the presence of all SFTI analogs. Since activity curves in the presence of the tested compounds exhibited a linear course they were evaluated for reversible inhibition as described in chapter 2.1. Accordingly, values K_i were determined by non-linear regression of the progress curves. Compound 11 emerged as the most potent MT2 inhibitor out of the tested series with a value K_i in the nanomolar range (Figure 2.3 C). However, it is noteworthy, that it displayed an about 4.8-fold higher K_i value in comparison to literature data (91.1 nM versus 19 nM).^[122] Analog 12 bearing a 5(6)-carboxyfluorescein labeled Lys instead of the Asp14

residue in **11** exhibited approximately 12-fold lower inhibition with a K_i value of 1.1 μM (Figure 2.3 D). Application of compounds **13** and **14** led to a decrease in MT2 activity to a similar degree resulting in values K_i of 1 μM for **13** and 1.3 μM for **14**, respectively (Figure 2.4 C/D).

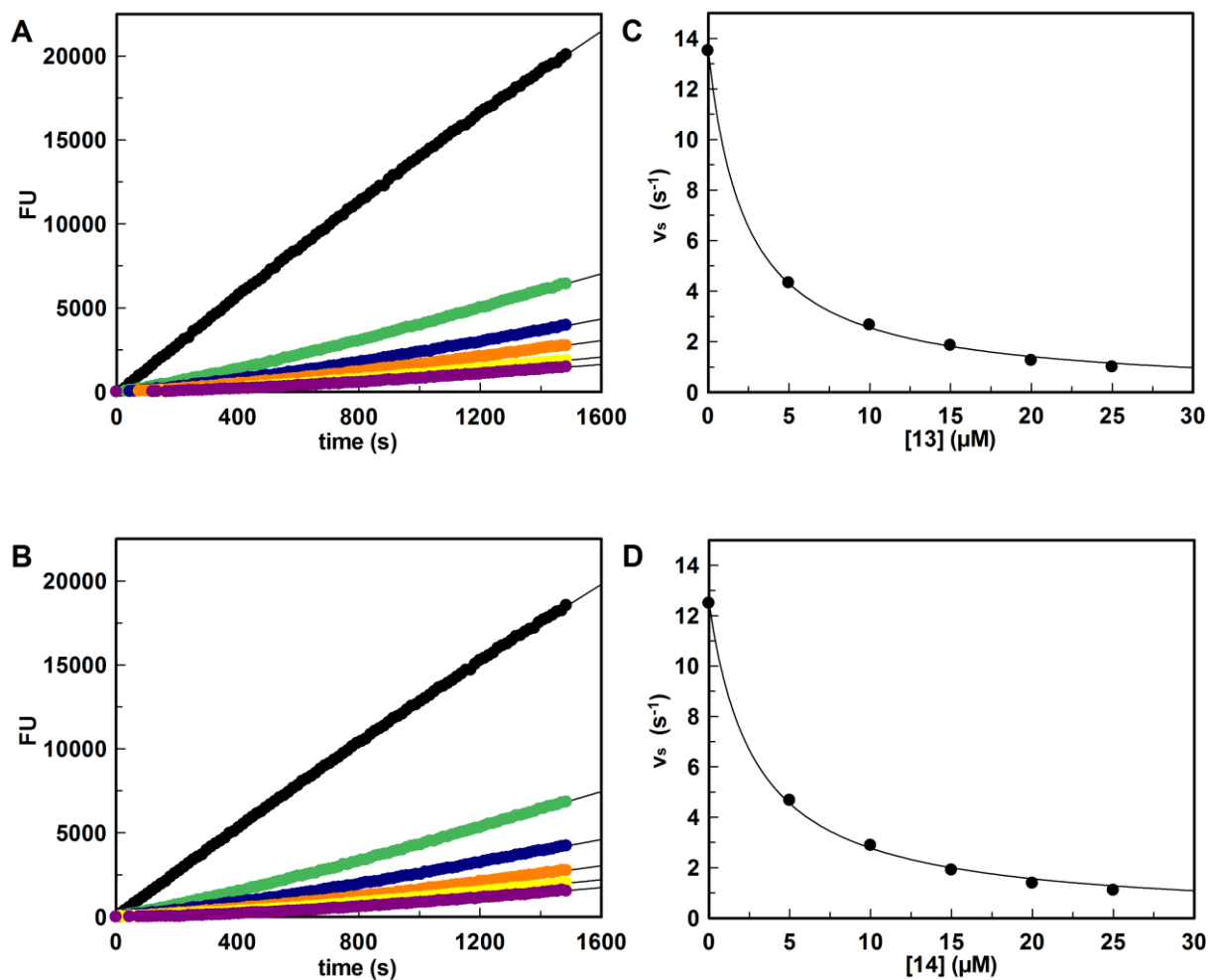


Figure 2.4: MT2 activity in the supernatant of transfected HEK cells in the presence of increasing concentrations of SFTI inhibitors 13 and 14. (A-B) Fluorescence units (FU) plotted versus time. (C-D) Corresponding values v_s plotted versus probe concentrations. Colored progress curves represent reactions in the presence of different inhibitor concentrations (A: ● uninhibited reaction, ● 5 μM , ● 10 μM , ● 15 μM , ● 20 μM , ● 25 μM of compound **13**; B: uninhibited reaction, ● 5 μM , ● 10 μM , ● 15 μM , ● 20 μM , ● 25 μM of compound **14**). Depicted binding curves are generated from duplicate measurements.

Taken together, these findings are in coherence with previous research.^[122] The modified BBI domain present in all analogs has proven to be essential for the inhibition of MT2. The substitution of Lys5 for Arg in compounds **11** to **14** led to excellent inhibitors of MT2 in the nano- to low micromolar range. The importance for Arg in P₁ position was highlighted by compound **11** in particular, since this substitution marks its only difference to native SFTI-1, resulting in an approximately 10-fold increase in inhibitory activity and a 10-fold selectivity for MT2 over MT1.^[201] The addition of further modifications to the general structure of **11** led to an overall loss of inhibitory activity against MT2. Interestingly, all three analogs **12** to **14** displayed a similar, approximately 10-fold drop to K_i values of 1 to 1.3 μM . This could possibly be contributed to the introduction of the 5(6)-carboxyfluorescein group present in **12** to **14**. But, noteworthy and contrary to previous reports,^[201] the ring opening of bicyclic SFTI-1, as is the case in compounds **13** and **14**, did not lead to further decrease in inhibitory potency towards MT2. Gitlin *et al.*^[122] demonstrated that the disruption of the bicyclic structure of SFTI-1 always results in a significant, approximately 10-fold drop in K_i values, which is in coherence with the observations made in this work, if monocyclic **13** and **14** are compared with the bicyclic molecule **11**. In consequence, bicyclic compound **12** should display a lower K_i value than **13** and **14**. Yet, this was not the case, as **12** exhibited inhibitory potency towards MT2 to a similar extent. To explain this similarity the structural differences between the three analogs should be taken into account. Other than its bicyclic nature, **12** possesses another key difference that sets it apart from the other tested analogs. While **13** and **14**, as well as **11**, share the modified peptide structure of native SFTI-1 with the substitution of Lys5 by Arg, compound **12** features an additional substitution of the Asp14 residue by Lys to serve as an attachment site for the 5(6)-carboxyfluorescein moiety. Since the ring opening in **13** and **14** which was executed between the Gly1 and Asp14 residues resulted in a similar loss of inhibitory activity it could be concluded that Asp14 in the bicyclic peptide facilitates MT2 inhibition. A previous publication by Hilpert *et al.* investigated the influence of different SFTI moieties on the enzyme-inhibitor-interaction with trypsin and found that Asp14 may contribute to a favorable conformation by the formation of H-bonds.^[203] This effect could also contribute to the inhibition of MT2 and to continue with this hypothesis, analogs with different substitution patterns of the fluorophore group should be investigated.

2.1.2 Peptidomimetic inhibitors of matriptase-2

In addition to polypeptides **11** to **14** several peptidomimetic molecules were chosen for evaluation as inhibitors of MT2 activity. Peptidomimetics are compounds whose modified structures mimic the 3D structures of natural peptides or proteins, thereby retaining the ability to interact with their biological targets.^[204] Such structural modifications offer the opportunity to improve stability and bioavailability of therapeutics while maintaining their pharmacological properties at the same time. Over the course of this thesis, a chloromethyl ketone inhibitor, a phosphono bisbenzguanidine and a library of prolineamides were tested towards MT2.

Results of this chapter (chapter 2.1.2) are included in the following publication: Martin Mangold, Michael Gütschow and Marit Stirnberg, A Short Peptide Inhibitor as an Activity-Based Probe for Matriptase-2, *Pharmaceuticals*. **2018**, 11, pii: E49. doi: 10.3390/ph11020049.^[205]

2.1.2.1 A chloromethyl ketone as inhibitor of matriptase-2

The short biotinylated peptide **15** was designed based on the preferred substrate sequence of MT1^[110] and consists of an N-terminal biotin moiety, a tetrapeptide (Arg-Gln-Arg-Arg) and a C-terminal chloromethyl ketone (CMK) group (Figure 2.5). Previously, this compound was established as an activity-based probe for both, MT1^[206] and MT2^[207] in independent studies. Since **15** was first developed and described as an inhibitor of MT1 activity^[206] and only characterized as an activity-based probe for MT2^[207] further kinetic characterization was conducted to determine its potency towards this enzyme.

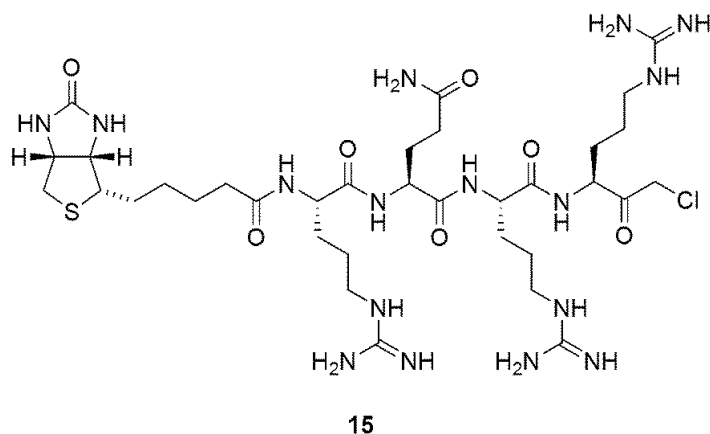


Figure 2.5: Chemical structure of biotinylated CMK peptide probe 15. Compound **15** (biotin-Arg-Gln-Arg-Arg-CMK)^[206] was acquired from the American peptide company. Stock solutions were prepared in DMSO at a concentration of 10 mM.

MT2 activity was reduced in the presence of increasing amounts of **15** (Figure 2.6 A), activity curves exhibited a non-linear course. The inhibition of MT2 activity was time-dependent and reached steady-state after approximately 1 hour, dependent on the concentration of **15**, reflecting an irreversible binding behavior. Subsequently, values k_{obs} were determined by non-linear regression and plotted *versus* inhibitor concentrations (Figure 2.6 B). Since $k_{\text{obs}}/[I]$ displayed linear dependency the corresponding second-order rate constant of inactivation was calculated, yielding a k_{inac}/K_i value of $10,800 \text{ M}^{-1} \text{ s}^{-1}$.

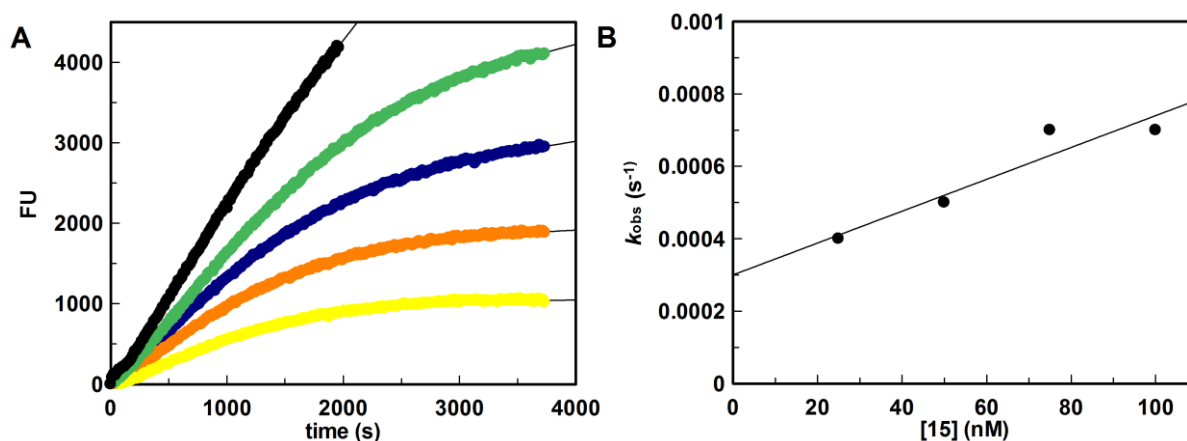


Figure 2.6: MT2 activity in the supernatant of transfected HEK cells in the presence of increasing concentrations of CMK probe 15. (A) Fluorescence units (FU) plotted versus time. (B) The observed rate constant for inhibition k_{obs} plotted versus probe concentrations. Colored progress curves represent reactions in the presence of different inhibitor concentrations (● uninhibited reaction, ● 25 nM, ● 50 nM, ● 75 nM, ● 100 nM of compound **15**). Depicted binding curves are generated from duplicate measurements.

These results highlight CMK probe **15** as a very potent inhibitor of MT2 activity in the nanomolar range. With a k_{inac}/K_i value of $10,800 \text{ M}^{-1} \text{ s}^{-1}$, **15** represents the most potent irreversible inhibitor of MT2 known so far. Due to its three Arg residues the compound most likely occupies the P₁, P₂ and P₃/P₄ binding pockets of the enzyme,^[36,110] in coherence with the general MT2 substrate specificity for basic amino acids in these positions.^[108] In turn, the chloromethyl ketone warhead is subjected to a nucleophilic attack by the active site Ser of MT2 and acts as a serine trap that forms an irreversible bond, thereby inhibiting the enzyme.

2.1.2.2 Evaluation of a phosphono bisbenzguanidine as inhibitor of matriptase-2

In the past, bisbenzamidines and bisbenzguanidines have proven as an excellent scaffold for the development of potent inhibitors of MT2 activity.^[100,116] Activity-based probe **16** features this dipeptidomimetic scaffold bearing two benzguanidine moieties (Figure 2.7) which facilitate accommodation in the S₁ and S₃/S₄ binding sites of MT2. In addition, the compound bears a phosphonate warhead and a 7-diethylamino-coumarin moiety attached to the peptide backbone which serves as fluorophore for detection.

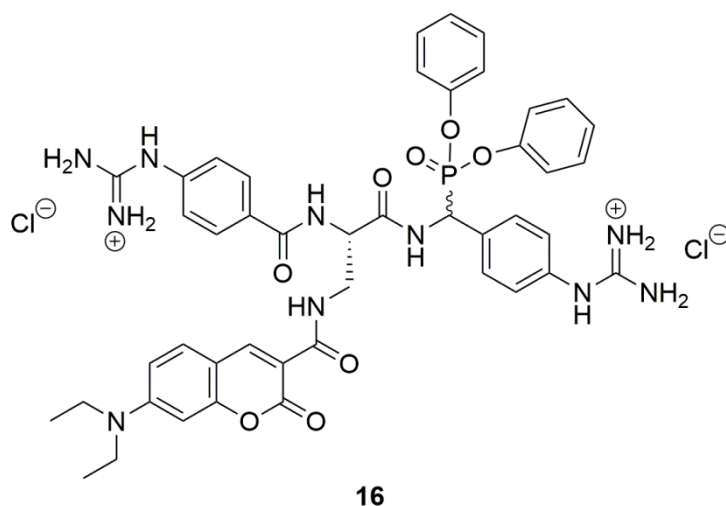


Figure 2.7: Chemical structure of activity-based probe 16. Phosphono bisbenzguanidine **16** was provided by Dr. Daniela Häußler.^[100] Stock solutions were prepared in DMSO at a concentration of 10 mM.

Previously, this compound was discovered as an irreversible inhibitor of MT2 and could be successfully employed as an activity-based probe of this enzyme.^[100] Here, the inhibitory activity of **16** towards MT2 was to be re-evaluated for reasons of comparison with additional kinetic experiments that were carried out over the course of this thesis.

Activity curves in the presence of increasing inhibitor concentrations indicated an irreversible binding mode of **16** (Figure 2.8 A) and thus, values k_{obs} were determined by non-linear regression. Since plotting of k_{obs} values *versus* inhibitor concentrations revealed a linear dependency (Figure 2.8 B), the second-order rate constant of inhibition was calculated as described in chapter 2.1, yielding a k_{inac}/K_i value of $68 \text{ M}^{-1} \text{ s}^{-1}$. The minor 1.3-fold increase in comparison to the originally determined k_{inac}/K_i value^[100] ($68 \text{ M}^{-1} \text{ s}^{-1}$ versus $50 \text{ M}^{-1} \text{ s}^{-1}$) can be contributed to experimental deviations. Overall, these findings are in coherence with the original publication, which established **16** as an irreversible inhibitor of MT2 activity in the micromolar range.

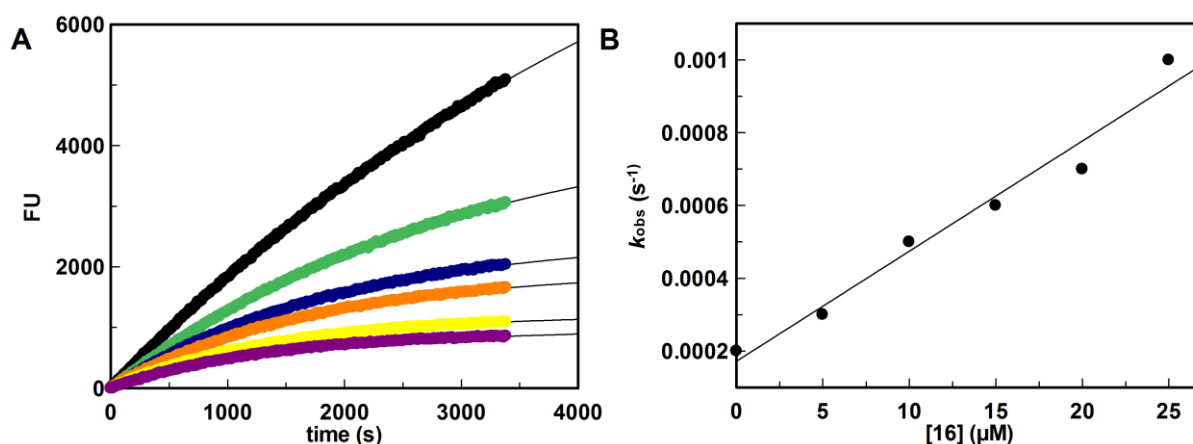
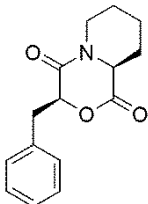
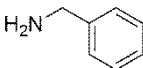
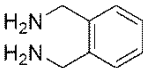
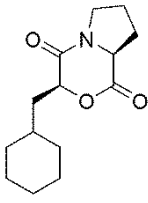
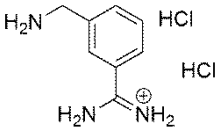
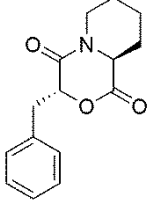
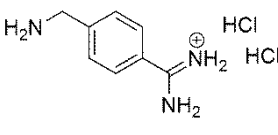
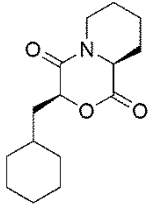
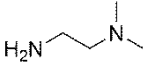
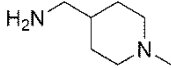


Figure 2.8: MT2 activity in the supernatant of transfected HEK cells in the presence of increasing concentrations of phosphono bisbenzguanidine 16. (A) Fluorescence units (FU) plotted versus time. (B) The observed rate constant for inhibition k_{obs} plotted versus probe concentrations. Colored progress curves represent reactions in the presence of different inhibitor concentrations (● uninhibited reaction, ● 5 μM , ● 10 μM , ● 15 μM , ● 20 μM , ● 25 μM of compound **16**). Depicted binding curves are generated from duplicate measurements.

2.1.2.3 Synthesis and evaluation of prolineamide inhibitors

A series of twenty-four prolineamide inhibitors was synthesized in a solution-based approach and tested for MT2 inhibition, as well as inhibition of other serine proteases. For this purpose a two component library of four lactone and six amine or amide molecules was prepared (Table 2.1). Lactones **17** to **20** were synthesized by Lan Phuong Vu in a solid phase approach, while amines **A**, **B**, **E** and **F**, as well as amidines **C** and **D** were purchased.

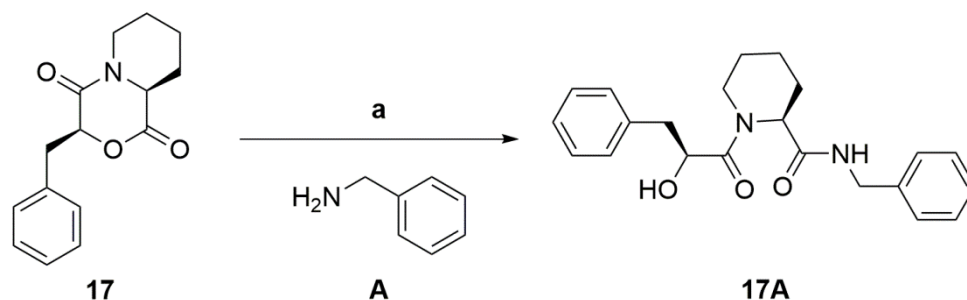
Table 2.1: Chemical structures of lactone and amine/amidine molecules.

	Lactone	Amine/Amidine	
17			A
			B
18			C
19			D
20			E
			F

Lactones **17** to **20** were provided by Lan Phuong Vu, while amines **A**, **B**, **E** and **F**, as well as amidines **C** and **D** were purchased from ABCR, Sigma Aldrich and TCI. Stock solutions were prepared in acetonitrile at a concentration of 4 mM. Stock solutions of **C** and **D** were additionally supplemented with 1 or 2 equivalents of triethylamine.

The NH₂ group of the nucleophiles **A** to **F** should attack the carbonyl carbon of the lactone ring resulting in a ring opening and the formation of a covalent bond between the lactone carbonyl carbon and the amino group (Scheme 2.5). These prolineamide inhibitors possess a peptidic backbone structure for accommodation in the binding pockets of a target enzyme, while the basic substructures provided by some of the nucleophiles could promote inhibition of MT2 activity. Inhibitor solutions were prepared prior to measurements by combining one lactone and one amine component in stoichiometric amounts in a reaction tube. Incubation for 24 hours at 45 °C yielded inhibitors **17A** to **20F** and subsequently, reaction mixtures were applied in kinetic assays. For the purpose of applicability, inhibitor solutions were considered to contain 100% of formed inhibitor and no adducts.

Scheme 2.5: Synthesis of prolineamide inhibitors based on the example of 17A.



Reagents and conditions: (a) Acetonitrile, 24 hours, 45 °C.

Inhibitor solutions of **17A** to **20F** were prepared in a concentration of 2 mM and screened for MT2 inhibition in a final concentration of 50 μM. Since none of the tested compounds displayed inhibitory activity towards MT2 (Table 2.2), thrombin was employed as an additional test enzyme. The kinetic evaluation of test results revealed several prolineamides as inhibitors of thrombin activity. It is noteworthy, that none of the tested lactones **17** to **20** and amines **A** to **F** exhibited inhibitory activity towards the tested enzymes. Overall, combinations with amine **B** proved to be beneficial for thrombin inhibition as all compounds featuring its aminomethylbenzene moiety were active towards the enzyme although in different degrees. Inhibitor **19B** with a nearly complete reduction of enzymatic activity at the tested concentration emerged as the most active thrombin inhibitor of the series. These findings correlate well with the thrombin substrate specificity for arginine in P₁, proline in P₂ and hydrophobic amino acids in P₃ position.^[208]

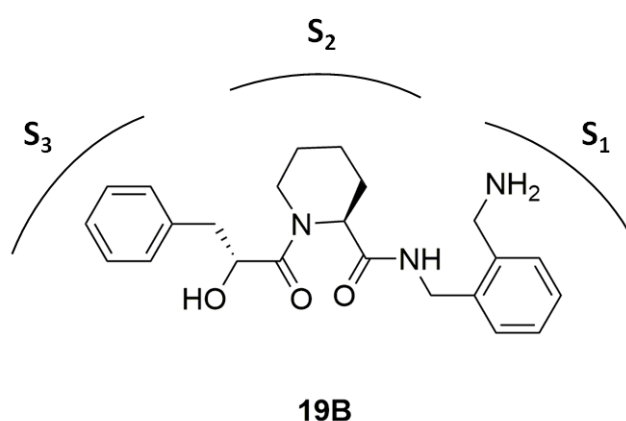
Table 2.2: Inhibition of MT2 and thrombin by prolineamides 17A to 20F, as well as lactones 17 to 20 and amines A to F.

Inhibitory activity @ 50 μ M (%)					
Compound	MT2 (%)	Thrombin (%)	Compound	MT2 (%)	Thrombin (%)
17A	n.i. ^a	n.i.	19F	n.i.	11%
17B	n.i.	22%	20A	n.i.	n.i.
17C	n.i.	n.i.	20B	n.i.	12%
17D	n.i.	n.i.	20C	n.i.	11%
17E	n.i.	n.i.	20D	n.i.	n.i.
17F	n.i.	n.i.	20E	n.i.	n.i.
18A	n.i.	n.i.	20F	n.i.	n.i.
18B	n.i.	60%	17	n.i.	n.i.
18C	n.i.	12%	18	n.i.	n.i.
18D	n.i.	n.i.	19	n.i.	n.i.
18E	n.i.	n.i.	20	n.i.	n.i.
18F	n.i.	n.i.	A	n.i.	n.i.
19A	n.i.	n.i.	B	n.i.	n.i.
19B	n.i.	98%	C	n.i.	n.i.
19C	n.i.	n.i.	D	n.i.	n.i.
19D	n.i.	n.i.	E	n.i.	n.i.
19E	n.i.	n.i.	F	n.i.	n.i.

^a n.i.: no inhibition refers to <10% inhibitory activity @ 50 μ M. Determined from duplicate measurements.

Thus, a binding mode of **19B** with aminomethylbenzene in S_1 , homoproline in S_2 and benzyl in S_3 could be proposed (Scheme 2.6). Differences in inhibitory potencies between compounds **19B** and **17B**, which only differ in the configuration of the phenylalanine-analogous P_3 component, indicate an importance of the distinct configurations at positions P_2 (S) and P_3 (R). Interestingly, the S -configured methylcyclohexane group provided by the lactones **18** and **20** was accepted in P_3 position, but only in the presence of proline in P_2 position in prolineamide **18B**. This could be due to the more rigid nature of proline in comparison to homoproline and the resulting change of the dihedral angle which could be favourable for the interaction of the methylcyclohexane group with thrombin.

Scheme 2.6: Proposed binding mode of 19B in the thrombin active site.



Binding pockets of thrombin are depicted schematically and numbered from S_1 to S_3 .

Since amidines **C** and **D** displayed poor solubility under the employed reaction conditions, prolineamides containing these moieties were examined separately by Lan Phuong Vu. Unfortunately, thin layer chromatography results confirmed, that in these combinations no or only small amounts of prolineamides were formed. Nonetheless, compounds **18C** and **20C** displayed weak inhibitory activity against thrombin and thus, could represent potent thrombin inhibitors. As neither **C** and **D** nor lactones **18** and **20** alone exhibited inhibitory potency towards thrombin, this activity possibly stems from small amounts of formed prolineamide inhibitor. The benzamidine moieties present in both amides **C** and **D** proved to be efficient arginine mimetics in the past^[116] and should be beneficial for the inhibition of both, MT2 and thrombin.^[37-38,209] To be able to investigate this hypothesis, further optimization of reaction conditions is needed to allow the sufficient formation of inhibitors.

The most potent inhibitor of thrombin activity **19B** was evaluated in additional kinetic experiments (Figure 2.9). Activity curves in the presence of rising inhibitor concentrations displayed concentration-dependent, but no time-dependent inhibition and thus, data was analyzed by linear regression yielding values IC_{50} of 2.8 μM and K_i of 5.6 μM for the selected compound. Since the total concentration of **19B** in the prepared solution is unknown, calculations were based on the supposition that 100% of inhibitor was formed during incubation time.

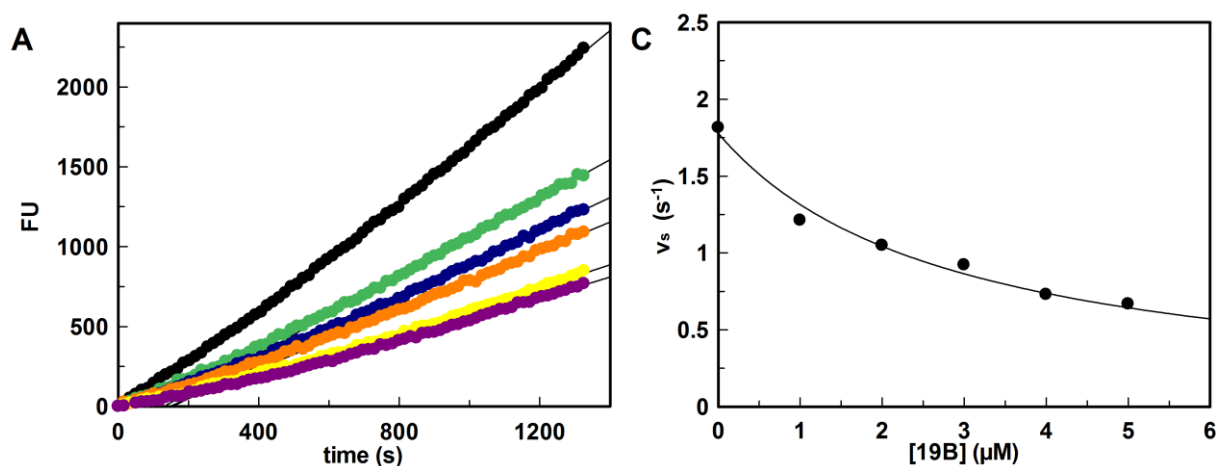


Figure 2.9: Inhibition of human thrombin by prolineamide 19B. (A) Fluorescence units (FU) plotted versus time. (B) The observed rate constant for inhibition k_{obs} plotted versus probe concentrations. (C) Corresponding values v_s plotted versus probe concentrations. Colored progress curves represent reactions in the presence of different inhibitor concentrations (● uninhibited reaction, ● 1 μM , ● 2 μM , ● 3 μM , ● 4 μM , ● 5 μM of compound **19B**). Depicted binding curves are generated from duplicate measurements.

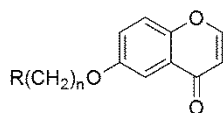
With these experiments the prolineamide synthesis and screening was concluded. Evaluation of the most active compound **19B** towards thrombin demonstrated the applicability of the chosen experimental approach. Still, **19B** remains to be synthesized and evaluated by conventional routes to confirm these findings. Since the total amount of formed inhibitor in reaction mixtures is unknown this could well influence and even improve the kinetic parameters determined over the course of these experiments. Nonetheless, the herein presented system is highlighted as a powerful tool and could be used in a large scale synthesis approach for the quick and cost effective evaluation of additional prolineamide molecules.

2.1.3 Chromenone inhibitors

As members of the flavonoid family, chromenones offer an interesting and versatile scaffold for the generation of bioactive compounds.^[210] Apart from their pharmacological use, as anti-inflammatory and anti-oxidative drugs or as enzyme inhibitors,^[211-213] many chromenone-derivatives are used as reporter groups due to their fluorescence properties.^[214]

Results of this chapter (chapter 2.1.3) are included in the following publication: Carina Lemke, Joscha Christmann, Jiafei Yin, José M. Alonso, Estefanía Serrano, Mourad Chioua, Lhassane Ismaili, María Angeles Martínez-Grau, Christopher D. Beadle, Tatiana Vetman, Florian M. Dato, Ulrike Bartz, Paul W. Elsinghorst, Markus Pietsch, Christa E. Müller, Isabel Iriepa, Timo Wille, José Marco-Contelles and Michael Gütschow, Chromenones as Multineurotargeting Inhibitors of Human Enzymes, *ACS Omega*. **2019**, 4(26), 22161–22168. doi: 10.1021/acsomega.9b03409.^[215]

A series of 28 chromenone derivatives **21** to **48** was evaluated for inhibition of MT2 and other enzymes such as humane monoamine oxidases (MAO) and cholesterol esterase. These compounds share a common chromen-4-one moiety which was substituted with different sized cyclic (or acyclic) tertiary amine moieties attached by methylene linkers of various lengths (Table 2.3). This library of compounds has been evaluated as inhibitors of MT2 activity derived from the conditioned medium of transfected HEK cells. Kinetic experiments were performed by Jiafei Yin. Out of the series of compounds, no MT2 inhibitors have been identified. While basic structures, represented by the tertiary amine moieties of chromenone derivatives, might interact in a beneficial manner with the S₁ specificity pocket of MT2, only weak inhibitory activity was observed in the case of nearly all tested compounds. However, this activity did not surpass 20% inhibition and was thus regarded as negligible. Contrary to MT2, multiple compounds out of the tested series exhibited excellent inhibitory activity towards other enzyme targets such as MAO-B and acetylcholinesterase.^[215]

Table 2.3: Chemical structures of chromenone derivatives and inhibition of MT2.

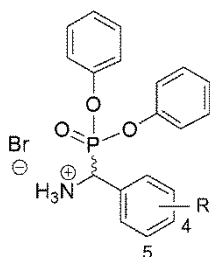
Compound	R	n	MT2 (%)	Compound	R	n	MT2 (%)
21		2	5	35		4	11
22		3	9	36		5	n.i.
23		4	12	37		2	n.i.
24		5	14	38		3	12
25		2	9	39		4	n.i.
26		3	8	40		5	5
27		4	12	41		2	n.i.
28		5	11	42		3	10
29		2	n.i. ^a	43		4	13
30		3	10	44		5	13
31		4	n.i.	45		2	20
32		5	n.i.	46		3	n.i.
33		2	6	47		4	10
34		3	5	48		5	14

^a n.i.: no inhibition refers to <5% inhibitory activity @ 10 μ M. (%)MT2 refers to the relative inhibition of MT2 activity in comparison to uninhibited control samples. Determined from duplicate measurements. Stock solutions were prepared in DMSO at a concentration of 10 mM.

2.1.4 Inhibitor library screening for matriptase-2 inhibition

A screening for inhibition of MT2 for 50 compounds out of the substance library of our group has been performed by Leyla Kathep. These compounds were chosen due to basic structural elements that could be beneficial for MT2 inhibition. In this screening approach one active compound, phosphonate **49** was identified (Table 2.4).

Table 2.4: Inhibition of MT2 by phosphonates 49 to 53.



Compound	R	MT2 (%)
49	4-I	n.i. ^a
50	4-SMe	n.i.
51	5-NO ₂	n.i.
52	4-NO ₂	n.i.
53	4-CN	n.i.

^a n.i.: no inhibition refers to <5% inhibitory activity @ 10 μM. Determined from duplicate measurements. Phosphonates were chosen from the substance library of our working group and synthesized by Dr. Daniela Häußler. Stock solutions were prepared in DMSO at a concentration of 10 mM.

Accordingly, over the course of this thesis, compound **49** together with analogs **50** to **53** were evaluated as inhibitors of MT2 activity. However, in contrast to the screening experiments, no concentrations dependent inhibition for **49** was found. The analogs **50** to **53** did not exhibit inhibitory activity towards MT2 either. While the phosphonate moiety was evaluated as an excellent warhead for the inhibition of MT2,^[100] addressing only one binding pocket of MT2 seems to be insufficient for the accommodation of such inhibitors in the enzymes binding pockets.

2.1.5 Selectivity profiles of established matriptase-2 inhibitors

Besides inhibitory potency the selectivity towards a chosen target is the main focus in the development of modern drugs and tool compounds.^[216] Poor selectivity often coincides with unwanted pharmacological side effects and should be circumvented.^[217] Therefore, the in chapters 2.1.1 and 2.1.2 established inhibitors **11** to **16** were evaluated for their selectivity towards MT2. For this purpose, these compounds were also tested at the related trypsin-like serine proteases MT1 and thrombin and an inhibition profile was compiled (Table 2.5).

Table 2.5: Selectivity profiles of inhibitors 11 to 16.

Compound	Inhibitory parameters K_i or k_{inac}/K_i		
	MT2	MT1	Thrombin
11	91.1 ± 3.6 nM	1.7 ± 0.2 μ M	3.99 ± 0.22 μ M
12	1.09 ± 0.04 μ M	n.i. ^a (19%)	17.2 ± 2.5 μ M
13	1.04 ± 0.04 μ M	n.i. (19%)	15.9 ± 2.1 μ M
14	1.27 ± 0.04 μ M	n.i. (17%)	18.5 ± 3.6 μ M
15	10800 ± 1580 $\text{M}^{-1} \text{s}^{-1}$	89950 ± 11550 $\text{M}^{-1} \text{s}^{-1}$	n.i. (10%)
16	68.1 ± 6.3 $\text{M}^{-1} \text{s}^{-1}$	58.5 ± 12.4 $\text{M}^{-1} \text{s}^{-1}$	n.i. (15%)

^a n.i.: no inhibition refers to <5% inhibitory activity @ 10 μ M. Inhibitory parameters represent values K_i in case of **11** to **14** or values k_{inac}/K_i in case of **15** to **16**. Determined from duplicate measurements. Phosphonates were chosen from the substance library of our group and synthesized by Dr. Daniela Häußler. Stock solutions were prepared in DMSO at a concentration of 10 mM.

As expected, the recorded progress curves in the presence of inhibitors **11** to **14** were linear reflecting the proposed reversible interaction mechanism between the trypsin-like proteases and the SFTIs. Progress curves in the presence of inhibitors **15** to **16** on the other hand displayed the irreversible binding behavior determined earlier. Remarkably, SFTIs **11** to **14** exhibited a greater inhibitory potential towards MT2 than towards the other tested serine proteases. The about 20 fold selectivity for MT2 over MT1 in particular further emphasizes the importance of Arg in P₁ position which is strongly favored by MT2.^[201] However, these compounds also inhibited thrombin to a certain degree and in the case of **12** to **14** were even more potent towards thrombin than MT1. This finding seems to indicate that thrombin is more tolerable towards variation in the backbone structure of SFTIs and is able to accommodate **12** to **14** regardless, in contrast to MT1 which only accepts **11**. Activity-based probe **15** was the

overall most potent inhibitor of MT2 activity but was even more active towards MT1. Since this compound was designed based on the preferred substrate specificity of MT1 this is not surprising.^[206] **16** on the other hand inhibited MT1 nearly to the same degree as MT2. Both activity-based probes displayed no inhibitory activity towards thrombin probably due to differences in substrate specificity such as the preference for proline residues in P₂ position by thrombin.^[209]

2.1.6 *In cellulo* matriptase-2 inhibition studies

Inhibitors **11** to **16** were chosen for further characterization and evaluation by assessing their *in cellulo* inhibitory activity towards MT2 in living HEK cells. Since catalytic activity can be displayed by both, the soluble shed and the membrane-anchored enzyme,^[45] the inhibitory behavior of a compound towards MT2 could very well change in this context. Not only due to differences in protein size, but also due to the complex environment on the cell surface, inhibition of full-length MT2 could differ in comparison to inhibition of the shed catalytic domain. To investigate this possibility, a new assay method for the monitoring of cell surface MT2 activity was conceptualized and established. In addition, MT2 inhibitors were applied in reporter gene assays to investigate their effect on the expression of down-stream interaction partners of MT2 such as HJV and, subsequently, hepcidin.

Results of this chapter (chapter 2.1.6) are included in the following publication: Martin Mangold, Michael Gütschow and Marit Stirnberg, A Short Peptide Inhibitor as an Activity-Based Probe for Matriptase-2, *Pharmaceuticals*. **2018**, 11, pii: E49. doi: 10.3390/ph11020049.^[205]

2.1.6.1 Matriptase-2 activity at the cell surface

To measure the activity of surface-bound MT2 in the presence of enzyme inhibitors a microwell culture plate approach was chosen. For this, a set amount of HEK cells, stably transfected with either MT2 expression plasmid or the empty expression vector were seeded into 96-well plates. Preliminary tests indicated cell-detachment after subsequent PBS buffer washing steps to remove the soluble form of the enzyme. Thus, well plates were coated with poly-D-lysine prior to the addition of cells for optimal attachment of cell cultures.

After two days the culture supernatants were removed and cells were washed several times with PBS buffer to remove any residual shed MT2. The activity measurements in presence of different inhibitor concentrations were carried out immediately afterwards by the addition of prepared solutions containing enzyme buffer, substrate and inhibitors at the desired concentrations at 37 °C. This way it was ensured that only the activity of membrane-bound and of newly shed MT2 was monitored. After the successful establishment of this new test method inhibitors **11** to **16** were applied for kinetic evaluation.

Interestingly, all progress curves of MT2 surface activity displayed a linear course after an initial exponential rise in enzymatic activity (Figures 2.10 and 2.11). This was also the case for **15** and **16** which exhibited a time-dependent inhibitory behavior towards MT2 in supernatant measurements. This could be explained by the fact that living cells were used for these measurements. Since MT2 is expressed as an inactive zymogen at the cell surface this finding could reflect the opportunity that living cells can produce and activate new enzyme, thereby generating a continuous flow of MT2 activity and counteracting inhibition. Additionally, it is conceivable that enzymes in complex with inhibitors get internalized and degraded.

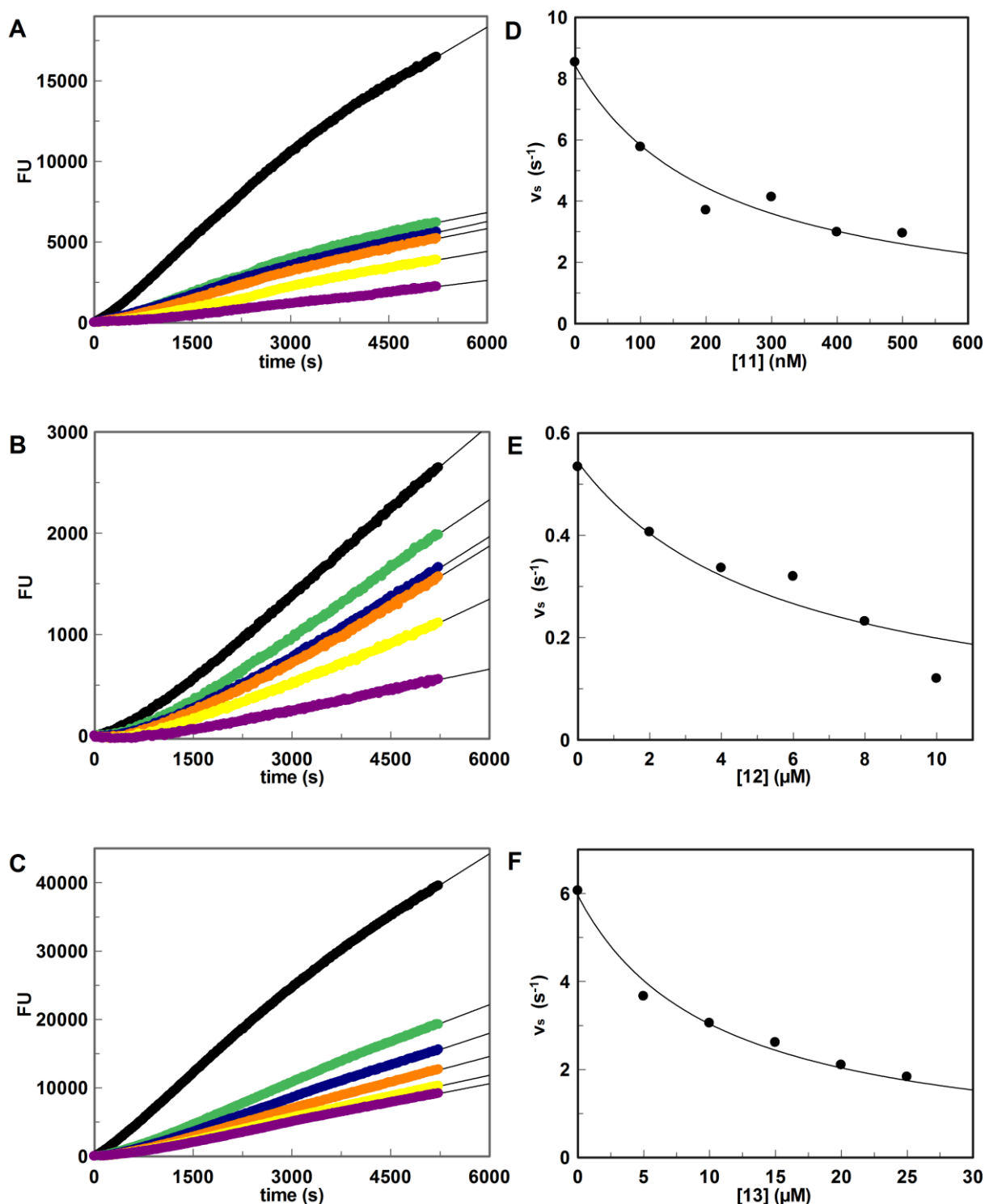


Figure 2.10: MT2 activity at the surface of transfected HEK cells in the presence of increasing concentrations of SFTI inhibitors 11 to 13. (A-C) Fluorescence units (FU) plotted versus time. (D-F) Corresponding values v_s plotted versus probe concentrations. Colored progress curves represent reactions in the presence of different inhibitor concentrations (A: ● uninhibited reaction, ● 100 nM, ● 200 nM, ● 300 nM, ● 400 nM, ● 500 nM of compound **11**; B: ● uninhibited reaction, ● 2 μ M, ● 4 μ M, ● 6 μ M, ● 8 μ M, ● 10 μ M of compound **12**; C: ● uninhibited reaction, ● 5 μ M, ● 10 μ M, ● 15 μ M, ● 20 μ M, ● 25 μ M of compound **13**). Depicted binding curves are generated from duplicate measurements.

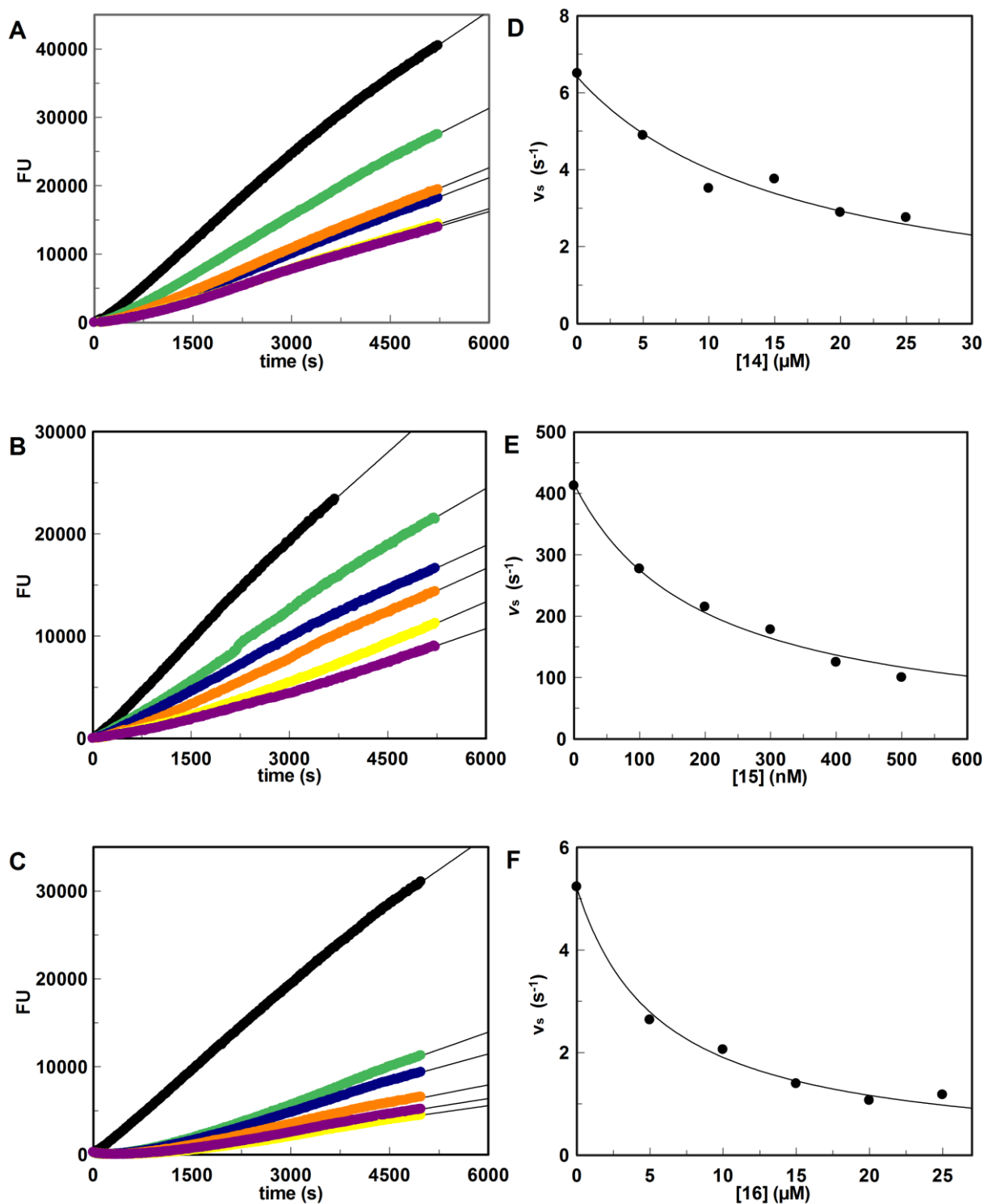


Figure 2.11: MT2 activity at the surface of transfected HEK cells in the presence of increasing concentrations of inhibitors 14 to 16. (A-C) Fluorescence units (FU) plotted versus time. (D-F) Corresponding values v_s plotted versus probe concentrations. Colored progress curves represent reactions in the presence of different inhibitor concentrations (A: ● uninhibited reaction, ● 5 μM , ● 10 μM , ● 15 μM , ● 20 μM , ● 25 μM of compound 14; B: ● uninhibited reaction, ● 100 nM, ● 200 nM, ● 300 nM, ● 400 nM, ● 500 nM of compound 15; C: ● uninhibited reaction, ● 5 μM , ● 10 μM , ● 15 μM , ● 20 μM , ● 25 μM of compound 16). Depicted binding curves are generated from duplicate measurements.

Nonetheless, a concentration-dependent decrease of MT2 activity was observed, but slightly higher concentrations of **11** to **16** were needed to achieve inhibition. Due to the linear course of these activity curves values K_i were obtained by linear regression (Table 2.6). The values K_i out of cell surface MT2 measurements turned out to be in coherence with those out of the traditional *in vitro* approach. Compounds **11** and **15** emerged as the most potent MT2 inhibitors in the nanomolar range in both experimental setups. Even though the potencies out of the cell-based measurements were lower they are comparable to those determined by supernatant measurements and only deviated by a negligible amount which can be easily contributed to the difference of the experimental approaches. Overall, the conceptualized and established *in cellulo* measurement method for MT2 activity proved as sufficient for the determination of basic kinetic parameters such as IC_{50} and K_i . However, since progress curves did not display time-dependent courses, even in the presence of irreversible inhibitors **15** and **16**, this experimental approach seems to be unsuitable for the determination of inhibitor binding modes.

Table 2.6: Inhibition of soluble MT2 and MT2 at the cell surface by compounds 11 to 16.

Inhibitory parameters K_i or k_{inac}/K_i		
Compound	MT2 supernatant	MT2 cell surface
11	91.1 ± 3.6 nM	99.3 ± 15.8 nM
12	1.09 ± 0.04 μM	3.6 ± 1.5 μM
13	1.04 ± 0.04 μM	4.6 ± 0.4 μM
14	1.27 ± 0.04 μM	7.5 ± 1.1 μM
15	10800 ± 1580 M ⁻¹ s ⁻¹	87.1 ± 7.6 nM
16	68.1 ± 6.3 M ⁻¹ s ⁻¹	2.6 ± 0.2 μM

Inhibitory parameters represent values K_i in case of supernatant measurements of **11** to **14** and cell surface measurements of **11** to **16** or values k_{inac}/K_i in case supernatant measurements of **15** to **16**. Determined from duplicate measurements. Phosphonates were chosen from the substance library of our working group and synthesized by Dr. Daniela Häußler. Stock solutions were prepared in DMSO at a concentration of 10 mM.

2.1.6.2 Matriptase-2 reporter gene assays

Due to its physiological role as regulator of hepcidin expression, MT2 plays an important part in the regulation of iron uptake from the intestine.^[48-50] The enzyme achieves this by the cleavage of HJV, thereby influencing the BMP-SMAD signaling cascade.^[48-50] Inhibitors **11** and **13** to **16** were applied in a reporter gene assay to assess their ability to influence this system. In this approach, the reporter enzyme firefly luciferase was expressed under the control of the promoter of the hepcidin gene *Hamp*. Test compounds were added at a concentration of 5 μ M 16 hours prior to measurements. Naturally, co-expression with HJV led to increased luciferase activity, while MT2 activity reduced the expression of hepcidin by the cleavage of HJV to below control levels (Figure 2.12). This influence of MT2 could be successfully counteracted by the application of test compounds. While compounds **11** and **16** only achieved a slight increase of luciferase expression levels, application of SFTIs **13** and **14**, as well as peptide inhibitor **15**, resulted in an approximately 50% recovery of luciferase activity relative to cell samples stimulated with HJV.

Differences in the inhibitory potency could possibly be assigned to the degradation of such compounds over the application period. To test this hypothesis, stability studies should be conducted, especially for **11** and **16** which exhibited only slight activity in these experiments. Additionally, the fact that luciferase activity could only be recovered by about 50% by inhibitors **13** to **15**, could be further proof to the chance that cell cultures generate newly activated enzyme to counteract inhibition. Either way, these findings showcase the ability of MT2 inhibitors to influence MT2 activity *in cellulo* and the degradation of its endogenous targets. This can be considered as a first step towards a possible *in vivo* application of these compounds.

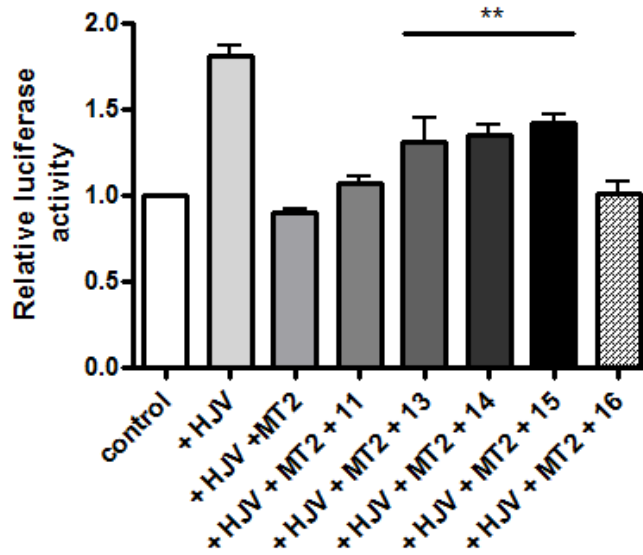


Figure 2.12: Modulation of hepcidin expression by inhibitors 11 and 13 to 16. Luciferase activities of Huh-7 cells transiently transfected with pGL2-HAMP, pcDNA4-HJVstop or pcDNA4-MT2-Myc-His were measured. The histogram shows the mean luciferase activity derived from transfection of pGL2-HAMP. Activity ratios are normalized to a control mean value of 1 derived from cells transfected with pGL2-HAMP alone. All data points are averages of at least three independent biological replicates and are expressed as means \pm standard deviation. *** indicate $P < 0.0001$.

2.1.7 Conclusion

Due to its role in iron homeostasis, the inhibition of the type II transmembrane serine protease MT2 is a promising prospect for the treatment of diseases related to hepcidin deficiency and secondary iron overload, such as β -thalassemia.^[90] Several studies indicate the positive influence of MT2 silencing and knockout on such pathologies.^[74-75,97]

Over the course of the presented thesis a total of 73 compounds were evaluated as possible inhibitors of MT2 activity. Out of these series of peptide inhibitors and peptidomimetics, the most promising candidates were characterized kinetically. This way, six compounds, **11** to **16**, exhibiting MT2 inhibition in the low micromolar to nanomolar range were identified. The applicability of **11** to **16** was further emphasized in additional cell-based experiments established to assess MT2 activity *in cellulo*. Compounds **11** and **15** emerged as the most potent MT2 inhibitors with a K_i value of 91.1 ± 3.6 nM and a k_{inac}/K_i value of 10800 ± 1575 $\text{M}^{-1} \text{s}^{-1}$, respectively. While **15** was the overall most potent inhibitor of MT2 activity, **11** expressed the better selectivity towards MT2 over the related serine proteases MT1 and thrombin. Additional experiments saw the design and establishment of a novel solution-based synthesis and screening approach for the preparation of a prolineamide inhibitor library. While prolineamide inhibitors tested over the course of this thesis did not exhibit inhibitory activity towards MT2 they emerged as inhibitors of the related serine protease thrombin, thereby proving the applicability of the proposed experimental setup.

2.2 Characterization of activity-based probes of matriptase-2

While **12** to **16** were characterized as excellent inhibitors of MT2 activity in chapter 2.1, all five compounds possess an additional feature that sets them apart from conventional inhibitors. Detection groups in the form of 5(6)-carboxyfluorescein in **12** to **14**, biotin in **15** and 7-diethylamino-coumarin in **16** (Figure 2.13), define them as so called activity-based probes. This type of molecules allows for the visualization of a target protein in a wide array of biological applications.^[218] Over the course of this work **13** to **16** were to be evaluated for their applicability as activity-based probes of MT2.

Results of this chapter (chapter 2.2) are included in the following publications: Martin Mangold, Michael Gütschow and Marit Stirnberg, A Short Peptide Inhibitor as an Activity-Based Probe for Matriptase-2, *Pharmaceuticals*. **2018**, 11, pii: E49. doi: 10.3390/ph11020049.^[205] Daniela Häußler, Martin Mangold, Norbert Furtmann, Anette Braune, Michael Blaut, Jürgen Bajorath, Marit Stirnberg and Michael Gütschow, Phosphono Bisbenzguanidines as Irreversible Dipeptidomimetic Inhibitors and Activity-Based Probes of Matriptase-2. *Chemistry* **2016**, 22, 8525-8535. doi: 10.1002/chem.201600206.^[100]

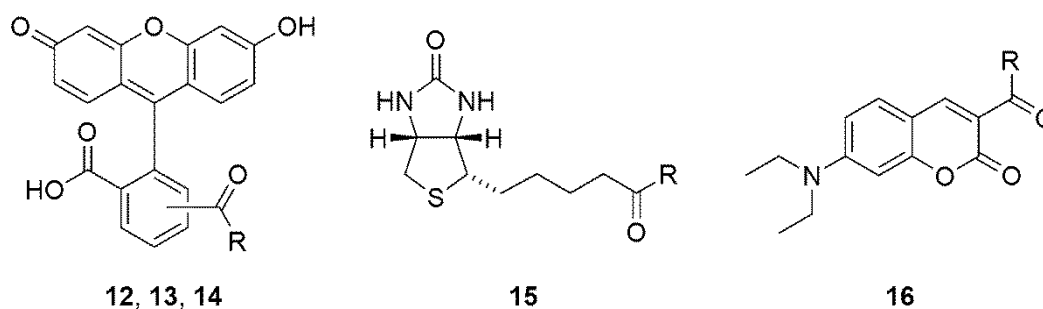


Figure 2.13: Chemical structure of detection groups of activity-based probe 12 to 16.

2.2.1 Detection of active and inactive matriptase-2

To evaluate activity-based probes **12** to **16** towards MT2, first-off a sufficient biological test system was needed that would allow the distinction of active and in-active enzyme. For this purpose, a cell culture expressing a mutated form of MT2 was established by stable transfection. This mutation was introduced in the enzymes active site by the exchange of the active site serine at position 753 for an alanine residue.^[45] This mutated form of MT2, MT2-S753A, was expressed in the same manner as the native enzyme and transported to the cell surface but lacked the enzymatic activity of native MT2 (Figure 2.14). Since MT2 undergoes auto-catalization, the mutation influenced its release from the cell surface and thus the localization of the enzyme. While native MT2 can be found both in the supernatant and in membrane fractions of transfected HEK cells, MT2-S753A was only found in the cell supernatant (Figure 2.15). Since the enzyme displays no catalytic activity, auto-catalization and the subsequent release from the cell surface is prevented. Because of these attributes MT2-S753A was deemed as sufficient and chosen as negative control for the purpose of subsequent evaluation experiments.

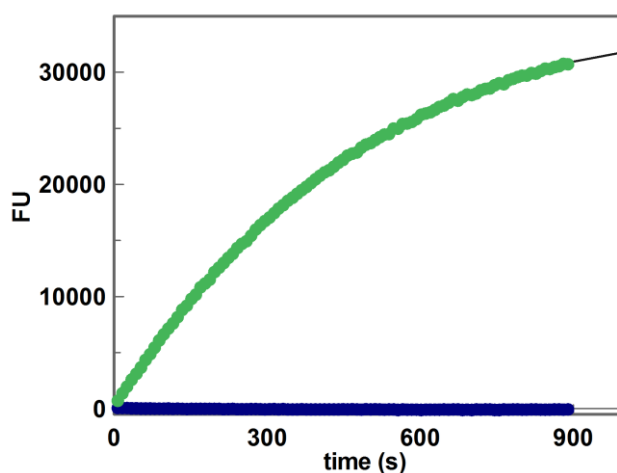


Figure 2.14: Enzymatic activity of native MT2 and mutated MT2-S753A. Colored progress curves represent the substrate conversion of ● MT2, or ● MT2-S753A, respectively. Depicted binding curves are generated from duplicate measurements.

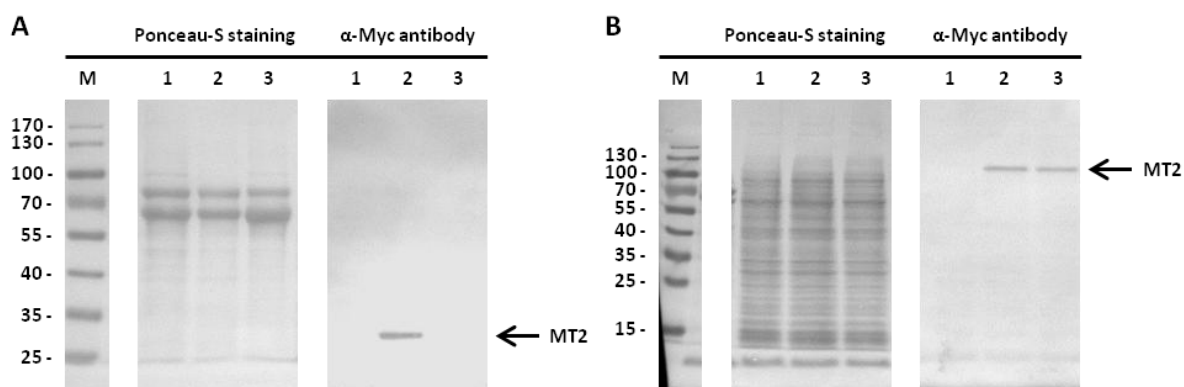


Figure 2.15: Detection of MT2 in the supernatant and membrane fractions of transfected HEK cells. (A) Detection of Myc-tagged MT2 in supernatant samples derived from transfected HEK cell cultures. (B) Detection of Myc-tagged MT2 in membrane fraction samples derived from transfected HEK cell cultures. 30 μ g of cell supernatant or membrane samples were loaded onto a 10% SDS gel. A Ponceau staining and the corresponding antibody detection is depicted. Detected MT2 is indicated by arrows at approximately 30 kDa in the case of supernatant or at approximately 110 kDa in the case of membrane fraction samples. 1: HEK-mock; 2: HEK-MT2-MycHis; 3: HEK-MT2-S753A-MycHis.

2.2.2 Biochemical properties of matriptase-2 activity-based probes

Spectrophotometric properties of **12** to **16** were obtained by the recording of absorbance and fluorescence spectra (Figure 2.16) to determine appropriate detection windows for their usage as activity-based probes. Spectra were recorded in PBS, as well as OptiMEM solutions to ensure their applicability. This approach yielded identical spectrophotometric properties for the tested activity-based probes in both buffer systems. Carboxyfluorescein probes **12** to **14** displayed absorption maxima at 498 nm and fluorescence maxima at 534 nm with a Stokes shift of 36 nm, while the coumarin-probe **16** displayed an absorption maximum at 434 nm and a fluorescence maximum at 476 nm with a Stokes shift of 42 nm, respectively. These parameters were deemed sufficient for the purpose of the experiments presented herein. While **15** does not possess a classical fluorescence detection group, the attached biotin moiety can be used to label the probe with detection groups as needed.

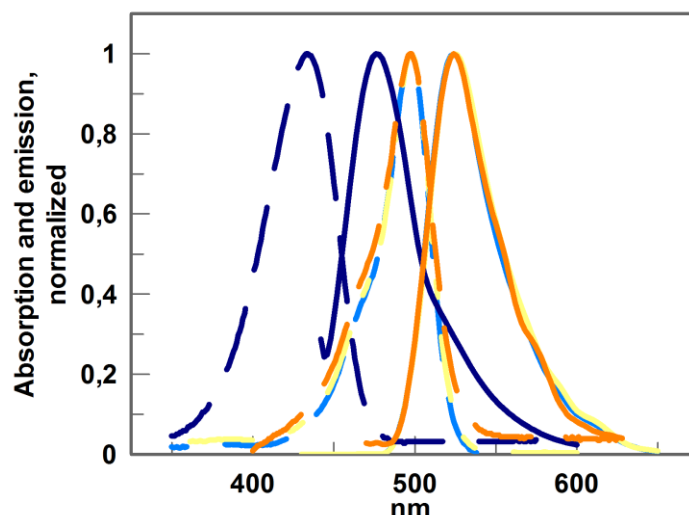


Figure 2.16: Normalized absorption and emission spectra of fluorescent activity-based probes. Absorption spectra, recorded at a concentration of 10 μM and 1% DMSO, are depicted in dashed lines. Emission spectra, recorded at a concentration of 1 μM and 1% DMSO, are depicted as continuous lines. Maxima are as follows: **12** (light blue, UV λ_{max} 498 nm, F λ_{max} 534 nm), **13** (yellow, UV λ_{max} 498 nm, F λ_{max} 534 nm), **14** (orange, UV λ_{max} 498 nm, F λ_{max} 534 nm), **16** (dark blue, UV λ_{max} 434 nm, F λ_{max} 476 nm).

To assess suitable concentrations for the application of activity-based probes in cell-based experiments 3-(4,5-dimethylthiazol-2-yl)-2,5-diphenyltetrazolium bromide (MTT) viability assays were performed (Figure 2.17). Test results indicated that concentrations of up to 1 μM were applicable for all tested probes in the chosen time frame of 24 hours and did not impair cell viability in comparison to control samples. While cell viability was only diminished slightly in the presence of probes **15** and **16** in concentrations of up to 10 μM , cell viability was reduced by approximately 25% upon treatment with 10 μM **13** and **14**. These results were taken into account for the design of further experiments and 10 μM was specified as the highest probe concentration which would be applied on living cell cultures.

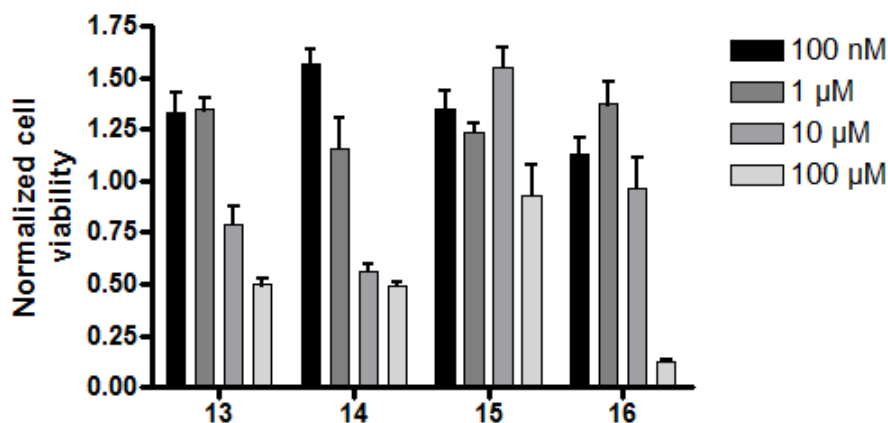


Figure 2.17: Normalized cell viability of activity-based probes 13 to 16. HEK cells were treated with 100 nM to 100 μM of activity-based probes 13 to 16 for 24 h at 37 °C. After MTT treatment and lysis the formation of formazan was monitored at 595 nm. Test values were normalized relative to positive controls of untreated cells and negative controls of cells treated with 100% DMSO. Bars were generated from test values of three independent experiments and depicted as means \pm standard deviation.

2.2.3 The use of activity-based probes in SDS-PAGE and western blot experiments for the detection of matriptase-2

A SDS-PAGE and western blot experimental setup was used as basic means to assess the ability of activity-based probes 12 to 16 to label active MT2. Supernatant samples derived from HEK cell cultures were chosen as a source of the enzyme. For reasons of comparison, cell cultures expressing MT2, mutated MT2-S753A, as well as the empty plasmid vector mock were employed. Samples were incubated with activity-based probes at different concentrations for up to 1 h at 37 °C prior to SDS-PAGE application. Subsequently, labeled MT2 was visualized under UV light or by western blot. Below, the evaluation of MT2 labeling by SFTI probes 12 to 14, CMK probe 15 and phosphono bisbenzguanidine probe 16 is depicted and described successively.

MT2 labeling by **13** and **14** was tested by the application of 1 to 100 μM activity-based probe to 30 μg of HEK-MT2-MycHis supernatant to assess the optimal probe concentration for detection (Figure 2.18A). Previously established activity-based probes were able to label the marginal portion of active MT2 contained in this amount of supernatant sample.^[100] While a single, approximately 30 kDa protein band, representing the catalytic domain of MT2, was detected by antibody staining (Figure 2.18B), in case of **13** and **14** no MT2 protein bands could be identified. Thus, subsequently, an even higher total protein amount of 100 μg of supernatant samples was chosen for the further evaluation of probes **12** to **14**. In addition, non-reducing conditions were applied in the following SDS-PAGE experiments. Without the addition of reducing agents like β -mercaptoethanol, which disperse protein disulfide bridges, MT2 persists as an approximately 50 kDa fragment in the supernatant consisting of the enzyme catalytic and a part of the stem region. Both, the intact 50 kDa shed form of the enzyme, as well as the overall milder incubation conditions could be beneficial for the formation of the enzyme-probe complex.

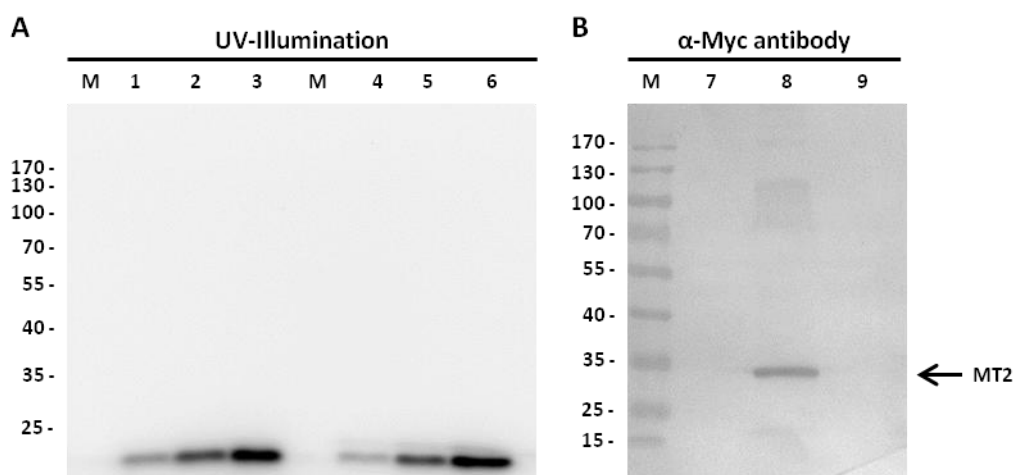


Figure 2.18: Screening for detection of active MT2 in HEK cell supernatants by activity-based probes **13 and **14**.** (A) UV-illumination after SDS-PAGE. (B) Detection of Myc-tagged MT2 in membrane supernatant samples. Equivalents of 30 μg of HEK-MT2-MycHis cell supernatant were incubated with different concentrations of **13** or **14** for 1 hour at 37 $^{\circ}\text{C}$ and loaded onto a 10% SDS gel. DMSO content was standardized to a concentration of 10% in all samples. After SDS-PAGE UV light was applied to the gel to detect the activity-based probes. A western blot of the used supernatant was performed as a positive control for MT2 expression. Detected MT2 is indicated by the arrow at approximately 30 kDa. 1: 1 μM **13**; 2: 10 μM **13**; 3: 100 μM **13**; 4: 1 μM **14**; 5: 10 μM **14**; 6: 100 μM **14**; 7: HEK-mock supernatant; 8: HEK-MT2-MycHis supernatant; 9: HEK-MT2-S753A-MycHis supernatant.

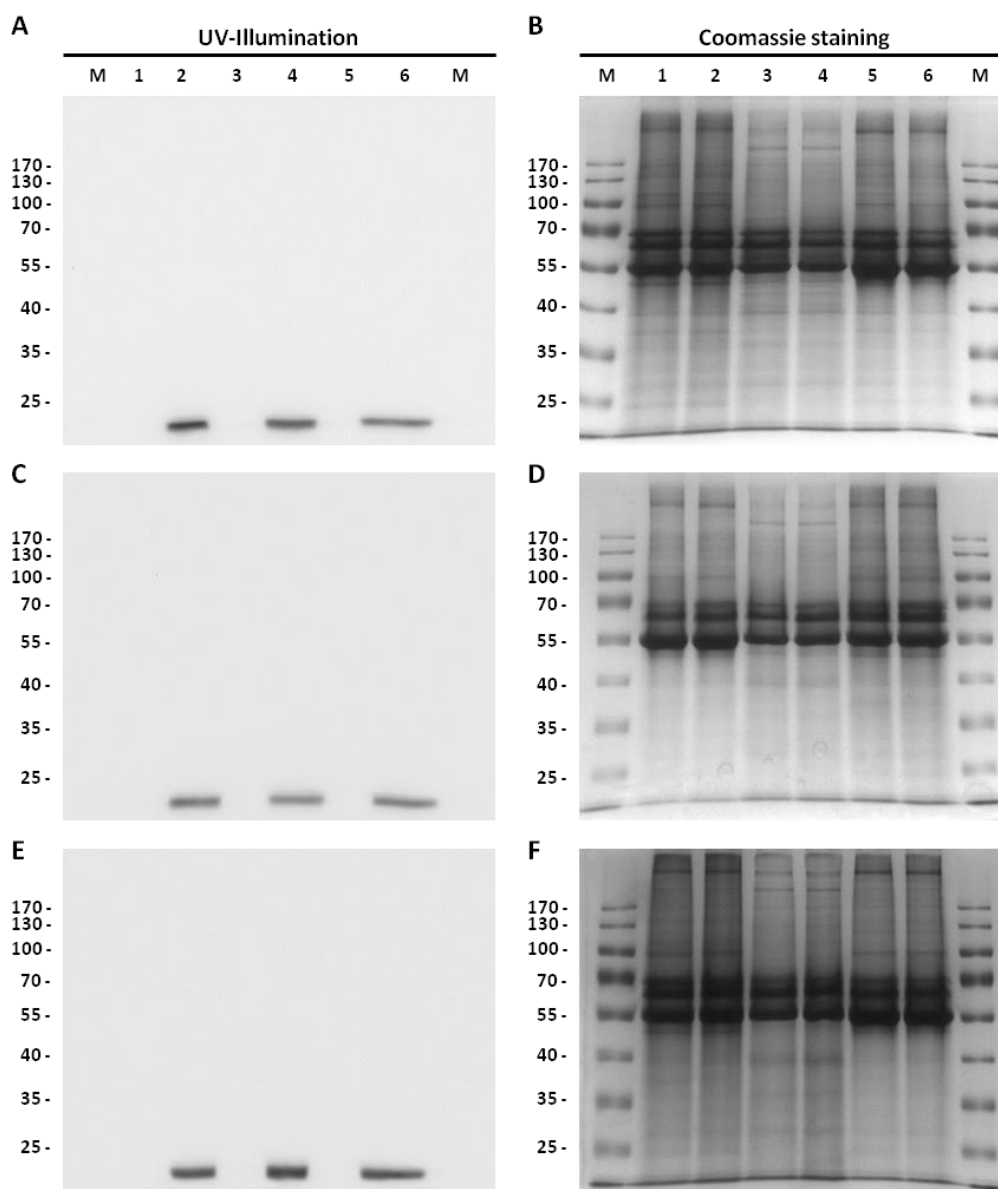


Figure 2.19: Detection of active MT2 by activity-based probes 12 to 14. (A, C, E) UV-illumination after SDS-PAGE. (B, D, F) Coomassie staining of the corresponding gels. 100 μ g of cell supernatant samples were incubated with 100 μ M **12** (A-B), **13** (C-D) or **14** (E-F) for 1 hour at 37 $^{\circ}$ C and were loaded onto a 10% SDS gel. DMSO content was standardized to a concentration of 10% in all samples. After SDS-PAGE UV light was applied to the gel to detect the activity-based probes. 1: HEK-mock; 2: HEK-mock + probe; 3: HEK-MT2-MycHis; HEK-MT2-MycHis + probe; HEK-MT2-S753A-MycHis; HEK-MT2-S753A-MycHis + probe.

However, even under such conditions a protein band representing MT2 could not be detected in HEK cell supernatants by either of the applied SFTI probes (Figure 2.19). Yet, **12** to **14** could still be identified as fluorescent bands at the running front of treated test samples, confirming their detectability and stability.

All three compounds exhibited good inhibitory activity towards MT2 in the low micromolar range in kinetic measurements where a concentration of 100 μM SFTI resulted in complete inhibition of enzymatic activity. These findings indicate that the enzyme-probe complexes established in the incubation step are disrupted prior or during SDS-PAGE experiments. Since **12** to **14** do not possess a covalent warhead structure it is conceivable that the activity-based probes detach from the enzyme under the application of an electric current due to their reversible binding mode. The formation of a covalent bond with the target enzyme seems to be necessary for the successful employment of activity-based probes in this experimental approach. Literature data emphasize this point, as even probes that interact with the non-catalytic portion of a protein, so called affinity-based probes, are generally designed to establish a covalent interaction, either by themselves or through subsequent *in situ* reaction steps.^[219-220] To this end, the introduction of a warhead moiety into the BBI domain of SFTI probes **12** to **14** should be investigated in further studies. However, such alterations in the highly conserved binding domain of these inhibitors might result in undesired changes in binding behavior and could prove difficult to achieve.

In contrast to SFTIs **12** to **14**, active MT2 could be visualized by the CMK activity-based probe **15**. Over the course of this thesis **15** could be successfully employed to label MT2 in a complex protein mixture for the first time.^[205] A distinguishing feature of this probe in comparison to conventional activity-based probes, which often possess a fluorescent reporter group, is its biotin moiety which is accessed in additional labeling steps by streptavidin conjugation. While **15** was identified as an activity-based probe by the use of purified MT2 in the past,^[207] it was believed to be unfit for the labeling of MT2 out of cell supernatants due to a high number of unspecific signals after western blot and streptavidin detection (Figure 2.20C). Further optimization of the labeling protocol could finally mitigate this problem. By stepwise reduction of both, the incubation time and concentration of **15** in supernatant samples to 30 minutes and 5 μM , respectively, unspecific binding signals were minimized and 30 kDa protein bands representing the catalytic domain of MT2 could be identified in HEK-MT2-MycHis samples (Figure 2.20D). These protein bands were apparent in all applied supernatant amounts ranging from 20 to 100 μg in coherence with α -Myc antibody staining (Figure 2.20B). The HEK-mock supernatant sample lacked the 30 kDa MT2 protein band but some unspecific staining signals did appear (Figure 2.20D, lane 1*).

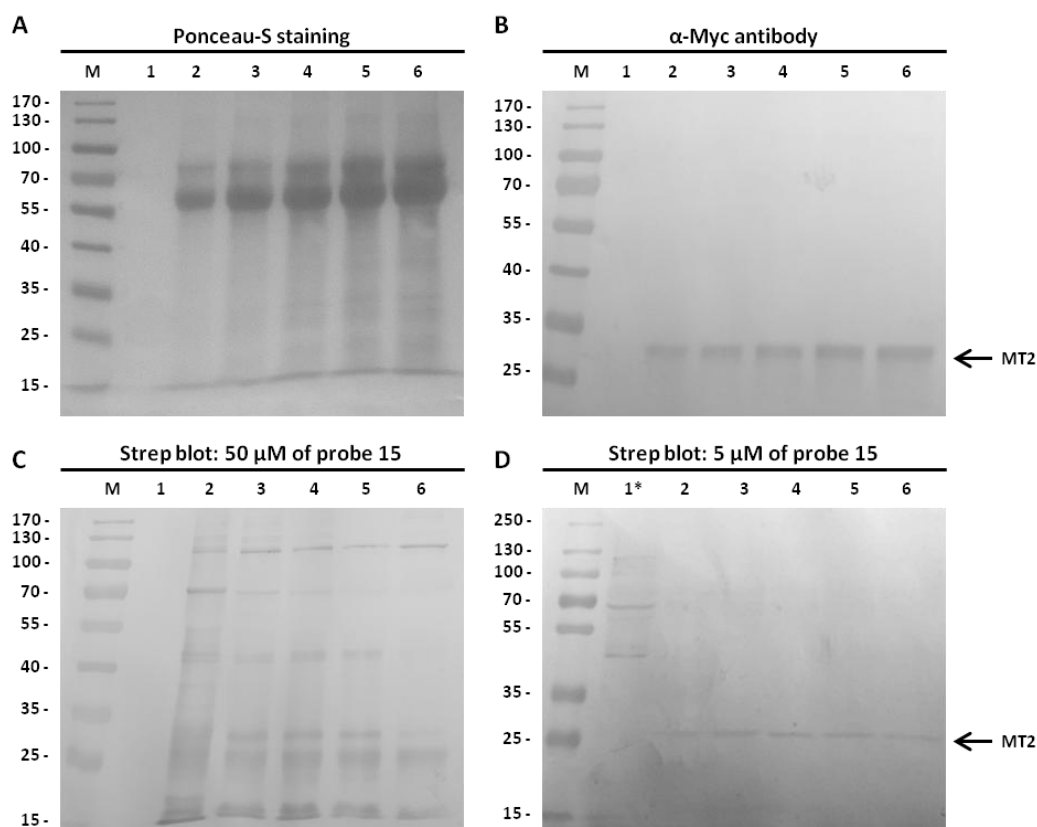


Figure 2.20: Detection of active MT2 in supernatant samples by activity-based probe 15. (A) Ponceau-S staining of the α -Myc blot. (B) Detection of Myc-tagged MT2 in supernatant samples derived from transfected HEK-MT2-MycHis cell cultures. (C-D) Detection of biotin-labeled activity-based probe **15** by the application of strep-avidin alkaline phosphatase conjugate. Increasing amounts of HEK-MT2-MycHis supernatant were loaded onto a 10% SDS gel. Samples were incubated with 50 μ M (C) or 5 μ M (D) of activity-based probe **15** for 30 minutes at 37 $^{\circ}$ C prior to SDS-PAGE. DMSO content was standardized to a concentration of 10% in all samples. Detected MT2 is indicated by arrows at approximately 30 kDa. 1: 0 μ g HEK-MT2-MycHis; 2: 20 μ g HEK-MT2-MycHis; 3: 40 μ g HEK-MT2-MycHis; 4: 60 μ g HEK-MT2-MycHis; 5: 80 μ g HEK-MT2-MycHis; 6: 100 μ g HEK-MT2-MycHis; 1*: 100 μ g HEK-mock.

While the catalytic domain MT2 could be detected in an equivalent of 30 μ g of HEK-MT2 supernatant by **15** comparable to antibody staining, samples derived from either HEK-mock or HEK-MT2-S753A cell cultures lacked the distinct 30 kDa protein band (Figure 2.21B), further emphasizing that the probe successfully labeled the enzyme. But as observed before unspecific staining did occur in the absence of MT2 as apparent in the HEK-MT2-S753A sample treated with **15**. That the observed protein bands can be contributed to background signals and not to MT2 fragments was highlighted by the application of a α -Myc antibody addressing the Myc-tag of the recombinant enzyme (Figure 2.21C).

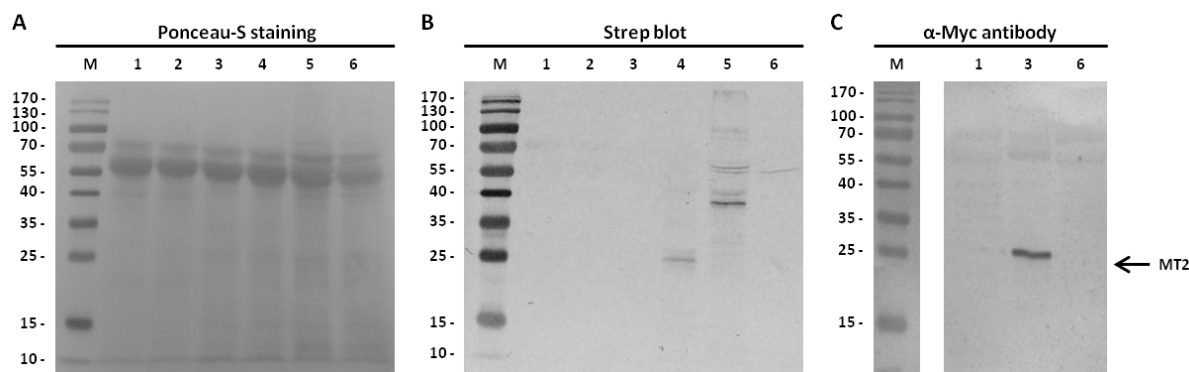


Figure 2.21: Detection of active MT2 in supernatant samples of transfected HEK cell cultures by activity-based probe 15. (A) Ponceau-S staining of the strep blot. (B) Detection of labeled MT2 in supernatant samples derived from transfected HEK cell cultures by the application of strep-avidin alkaline phosphatase conjugate. (C) Detection of Myc-tagged MT2 in supernatant samples. 30 μ g of cell supernatant samples were incubated with 5 μ M of activity-based probe **15** for 30 minutes at 37 °C and loaded onto a 10% SDS gel. DMSO content was standardized to a concentration of 10% in all samples. Detected MT2 is indicated by the arrow at approximately 30 kDa. 1: HEK-mock; 2: HEK-mock + probe; 3: HEK-MT2-MycHis; 4: HEK-MT2-MycHis + probe; 5: HEK-MT2-S753A-MycHis + probe; 6: HEK-MT2-S753A-MycHis.

Subsequently, phosphono bisbenzguanidine probe **16** was employed to label active MT2 in SDS-PAGE experiments. This activity-based probe possesses a fluorescent reporter group in the form of 7-diethylamino-coumarin and forms a covalent with MT2.^[100] Thus, in contrast to **15** no additional labeling steps or western blotting were needed to visualize **16** after SDS-PAGE. MT2 could be visualized in these experiments as an approximately 30 kDa protein band in the supernatant of HEK-MT2 cells (Figure 2.22). Supernatants derived from HEK-mock or HEK-MT2-S753A cell cultures lacked this distinct protein band similar to the experiments with probe **15**. These findings mark both activity-based probes **15** and **16** as applicable tools for the labeling of MT2.

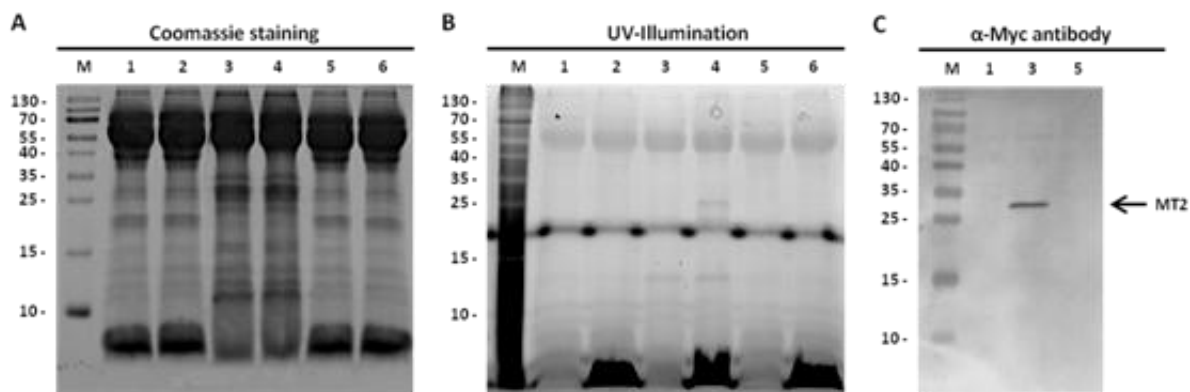


Figure 2.22: Detection of active MT2 in supernatant samples of transfected HEK cell cultures by activity-based probe 16. (A) Coomassie staining of the SDS gel. (B) Detection of labeled MT2 in supernatant samples derived from transfected HEK cell cultures by UV-illumination. 100 μg of cell supernatant samples were incubated with 100 μM of activity-based probe **16** for 1 hour at 37 $^{\circ}\text{C}$ and loaded onto a 12% SDS gel. DMSO content was standardized to a concentration of 10% in all samples. Detected MT2 is indicated by the arrow at approximately 30 kDa. 1: HEK-mock; 2: HEK-mock + probe; 3: HEK-MT2-MycHis; 4: HEK-MT2-MycHis + probe; 5: HEK-MT2-S753A-MycHis; 6: HEK-MT2-S753A-MycHis + probe.

2.2.4 Matriptase-2 competition experiments

Additional competition experiments were designed to investigate the binding mode and interaction of established activity-based probes **15** and **16** with MT2. For this purpose, aprotinin, a broad spectrum serine protease inhibitor was selected.^[221] Kinetic experiments highlighted aprotinin as a potent irreversible inhibitor of MT2 activity (Figure 2.23) which, with a k_{inac}/K_i value of $124200 \text{ M}^{-1} \text{ s}^{-1}$, exceeded both, **15** and **16**. Thus, the peptide inhibitor was chosen as means to irreversibly accommodate the MT2 active site to protect it from further attack by the activity-based probes. To this end, aprotinin was added to supernatant samples in a concentration of 50 μM for 2 hours at room temperature (rt) prior to probe treatment to ensure complete inhibition of the enzyme.

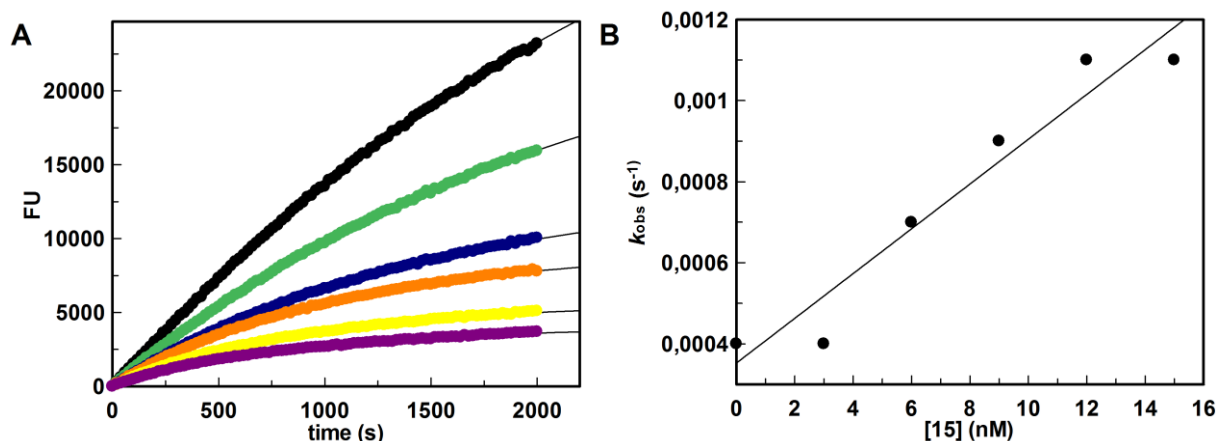


Figure 2.23: MT2 activity in the supernatant of transfected HEK cells in the presence of increasing concentrations of aprotinin. (A) Fluorescence units (FU) plotted versus time. (B) The observed rate constant for inhibition k_{obs} plotted versus probe concentrations. Colored progress curves represent reactions in the presence of different inhibitor concentrations (● uninhibited reaction, ● 3 nM, ● 6 nM, ● 9 nM, ● 12 nM, ● 15 nM of aprotinin). Depicted binding curves are generated from duplicate measurements.

In turn, the ability of both activity-based probes to label MT2 pre-treated with aprotinin was investigated as stated previously, after western blotting in case of **15** or SDS-PAGE in case of **16**. Again, **15** could be employed to label the 30 kDa fragment of MT2 similar to previous experiments (Figure 2.24D lane 2). However, this protein signal was not apparent in samples pre-treated with aprotinin and **15** or aprotinin alone (Figure 2.24D lanes 3 and 4). Since antibody staining confirmed the presence of MT2 in all three samples (Figure 2.24B) the lack of an activity-based probe based signal clearly indicated that the inhibited enzyme is not able to accommodate the probe. This confirmed that the MT2 active site serine is in fact the point of attack for the activity-based probe **15** like it is for aprotinin. Similar observations were made for activity-based probe **16** (Figure 2.25B). Aprotinin pre-treatment resulted in a nearly complete loss of the 30 kDa probe MT2 signal compared to untreated samples further emphasizing a shared binding mode with aprotinin and **15**.

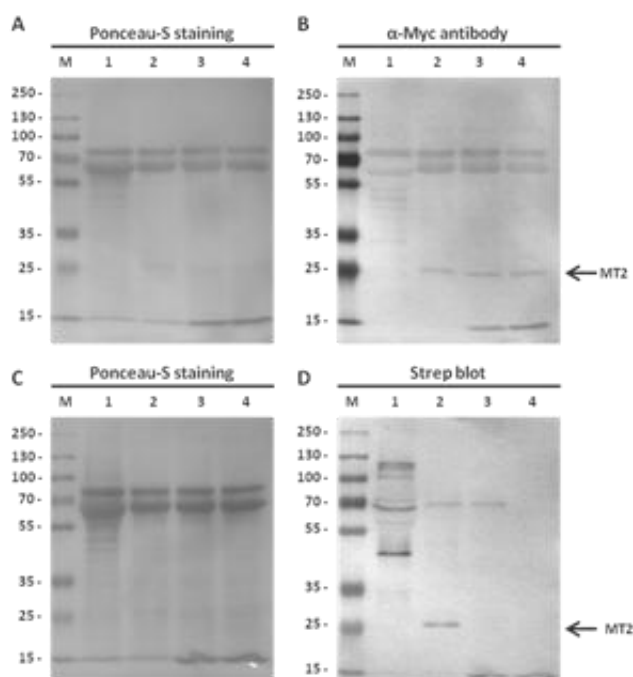


Figure 2.24: Labeling of active MT2 by activity-based probe 15 after application of aprotinin. (A, C) Ponceau-S staining of corresponding western blots B and D. (B, D) Detection of MT2 in supernatant samples derived from transfected HEK cell cultures by the application of an α -Myc antibody (B) or strep-avidin alkaline phosphatase conjugate (D), respectively. 30 μ g of cell supernatant samples were incubated with 50 μ M aprotinin for 2 hours at room temperature (RT) and 5 μ M **15** for 30 minutes at 37 $^{\circ}$ C and loaded onto 10% SDS gels. DMSO content was standardized to a concentration of 10% in all samples. Detected MT2 is indicated by arrows at approximately 30 kDa. 1: HEK-mock; 2: HEK-MT2-MycHis + **15**; 3: HEK-MT2-MycHis + **15** + aprotinin; 4: HEK-MT2-MycHis + aprotinin.

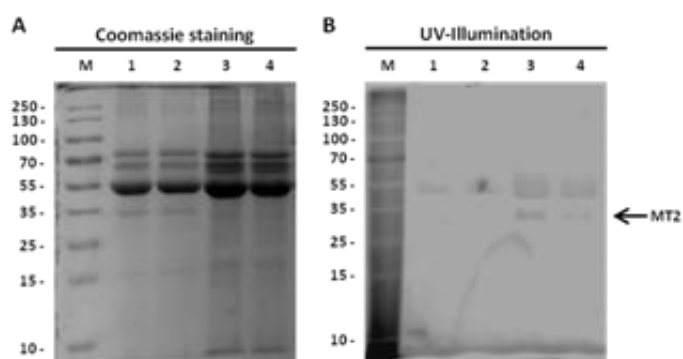


Figure 2.25: Labeling of active MT2 by activity-based probe 16 after application of aprotinin. (A) Coomassie staining of SDS gel. (B) Detection of labeled MT2 in supernatant samples derived from transfected HEK cell cultures by UV-illumination. 30 μ g of cell supernatant samples were incubated with 50 μ M aprotinin for 2 hours at room temperature (RT) and 100 μ M **16** for 1 hour at 37 $^{\circ}$ C and loaded onto a 10% SDS gel. DMSO content was standardized to a concentration of 10% in all samples. Detected MT2 is indicated by the arrow at approximately 30 kDa. 1: HEK-mock + **16**; 2: HEK-mock + **16** + aprotinin; 3: HEK-MT2-MycHis + **16**; 4: HEK-MT2-MycHis + **16** + aprotinin.

2.2.5 Fluorescence probing of matriptase-2 in confocal microscopy experiments

MT2 can be found in solution as well as at the cell surface as a membrane-bound enzyme in cell cultures.^[37-38] Both of these forms can express enzymatic activity, since the activated catalytic domain of MT2 remains attached to its membrane-anchored stem region between the first and second autocatalytic cleavage steps.^[45] Activity-based probes **13**, **14**, **15** and **16** were employed in microscopy experiments in an attempt to visualize this portion of active membrane-bound MT2. For this purpose, HEK cell cultures expressing the empty vector, MT2 or the inactive mutated form MT2-S753A were subjected to probe treatment over different time periods in accordance with previously conducted cell viability tests (Chapter 2.2.2, figure 2.17). Antibody-staining, addressing the Myc-tag of the recombinant MT2 forms was performed to label the total amount of active and inactive enzyme.

While MT2 could be identified both, in its active and inactive form by the employment of the α -Myc antibody and matching Alexa Fluor 488 secondary antibody, indicated by the green fluorescence signal outlining the cell membrane (Figure 2.26 panels B and C), probe-treatment did not result in the detection of active MT2 signals. Subsequently, probe concentrations ranging from 100 nM to 10 μ M were applied for time periods of 1 hour to 24 hours, ultimately with the same outcome. Only in the case of CMK probe **15** weak staining was observed at the cell surface of HEK-MT2-MycHis cells (Figure 2.26 panel K). However, while this staining was exclusive for cells expressing active MT2, it has to be noted that only a small amount of cells could be labeled this way.

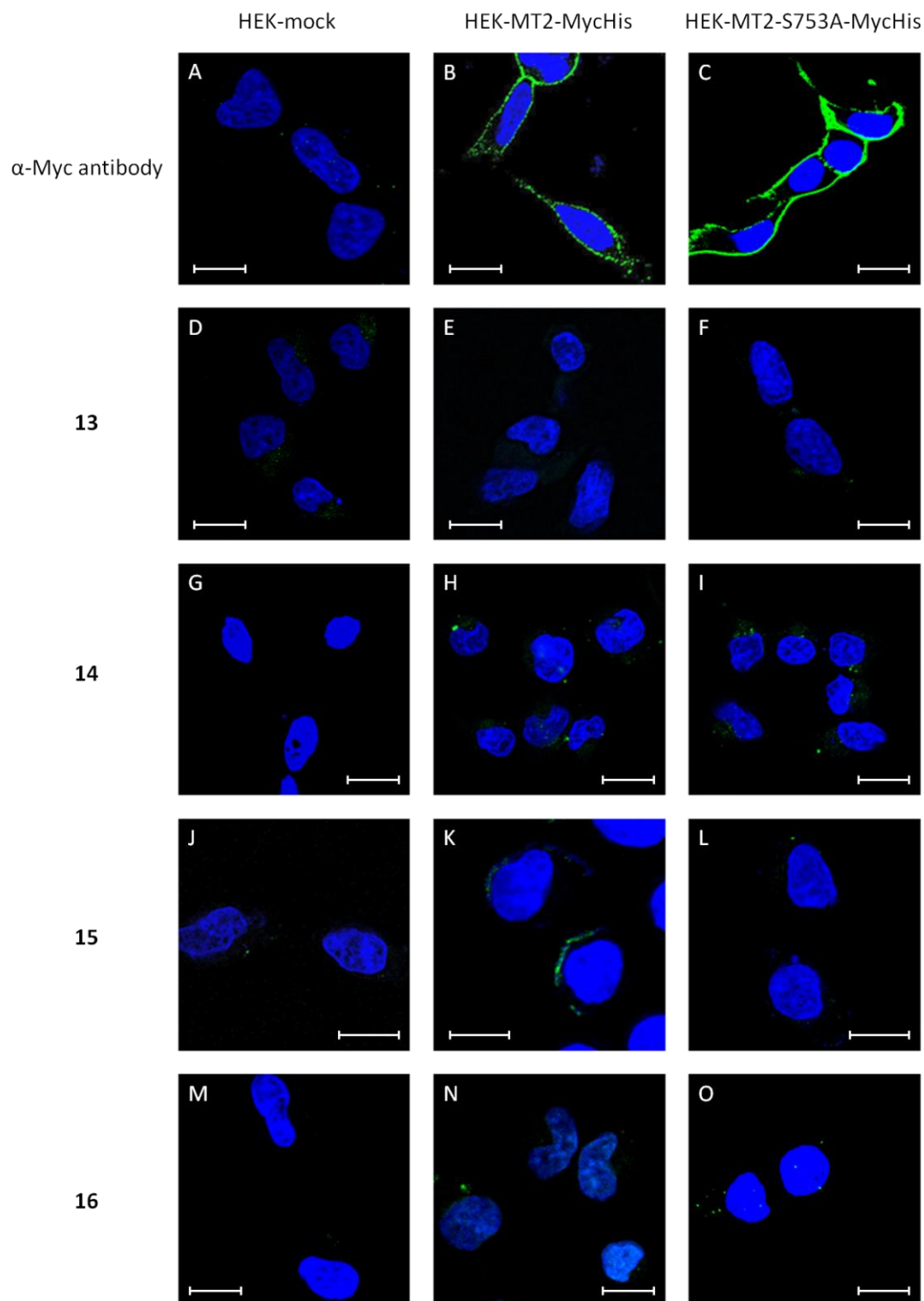


Figure 2.26: Confocal microscopy images of HEK cell cultures treated with activity-based probes 13 to 16. HEK-mock, HEK-MT2-MycHis and HEK-MT2-S753A-MycHis cell cultures were treated with activity-based probes **13**, **14**, **15** or **16** in a concentration of 50 μ M for 30 minutes. After fixation with paraformaldehyde, antibody staining with α -Myc antibody and Alexa Fluor 488 secondary antibodies and DAPI staining was performed. Nuclei are depicted in blue, MT2 in green. Scale bars indicate 10 μ m.

These findings seem to indicate that only a marginal amount of MT2 expressed by cells is activated and accessible for binding of activity-based probes, while most of the enzymes fraction remains as inactive zymogens at the cell surface. Even though it is known that membrane-bound MT2 can express enzymatic activity, the rate of the second autocatalytic cleavage and subsequent shedding event remains to be uncovered. Possibly, the time period between the first and second cleavage steps is too short for the probes to attach to and inhibit MT2. The absent MT2 signals in comparison to previous SDS-PAGE and western blot experiments (Chapter 2.2.3) could result from this and various other reasons. Apart from insufficient labeling due to too small amounts of active MT2 at the cell surface or a higher affinity to the soluble MT2 fragment, the spatial distribution of active enzyme could also impair the detection of probe signals. While soluble MT2 fragments were accumulated over the course of two days, concentrated and focused to a dense protein band in SDS-PAGE experiments, this was of course not the case in the whole cell imaging approach where the enzyme is spread equally over the cell surface. On this note, it should also be taken into account that an antibody's interaction with its antigen is defined by a very high affinity, which exceeds that of enzyme-probe interactions and would thus further enhance the observed difference in antibody and probe signals. In addition, the properties of the lasers and filters used for detection in this confocal microscopy approach deviated from the emission and excitation maxima of **13**, **14** and **16**. Even though these deviations were only minor, they could still influence the signal acquisition from the activity-based probes. Yet, the weak fluorescent signals observed after treatment with CMK probe **15**, which was visualized by a strep-avidin conjugated Alexa Fluor 488 dye, further emphasize the lack of sufficient levels of active MT2 at the cell surface, since this dye was easily detected before as indicated by antibody staining. To investigate this hypothesis additional confocal microscopy experiments using MT2 with a mutation at the second autocatalytic cleavage site should be conducted to induce higher amounts of membrane-bound active MT2 and achieve enzyme labeling.

2.2.6 Conclusion

Since both, its physiological, as well as pathological functions are linked to its enzymatic activity, MT2 presents itself as a promising marker for secondary iron overload diseases.^[74-75] Thus, new biochemical tool compounds for detecting and distinguishing the level of activated enzyme from inactive zymogens could prove helpful for further research and treatment of these diseases.

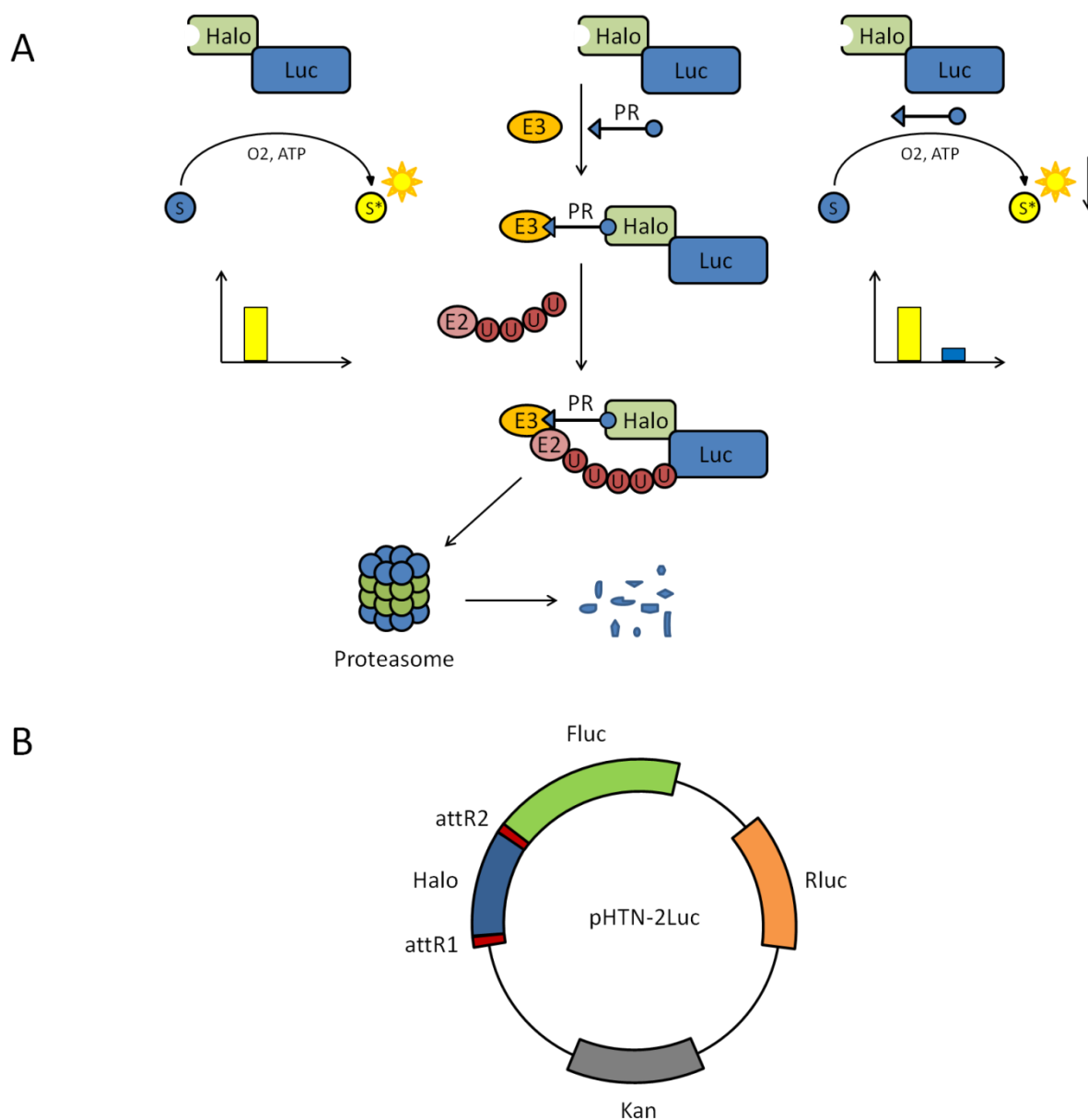
To this end, five activity-based probes, **12** to **16**, were investigated for their abilities to label active MT2. Such compounds are defined by an inhibitor portion which addresses and binds to an enzyme's active site and a detection group which allows for the visualization of the bound probe. The activity-based probes were employed in SDS-PAGE and confocal microscopy applications to assess their capabilities in complex protein mixtures as well as at the cellular level. Reversible probes **12** to **14** could not be applied in either of these experimental approaches, even though they expressed good inhibitory properties in kinetic evaluations. These findings emphasize the importance of an irreversible binding mode for the design and functionality of activity-based probes. In turn, irreversible probes **15** and **16** could be successfully applied in SDS-PAGE experiments. Competition experiments with both compounds, as well as the use of mutated inactive MT2, underlined the proposed binding mode at the active site serine of MT2. However, as with reversible probes, **15** and **16** were not applicable in the visualization of active membrane-bound MT2 in confocal microscopy experiments. Whether this is due to low concentrations of active MT2 at the cell surface or due to insufficient detection of probe signals in this experimental setup remains to be verified.

2.3 Evaluation of proteolysis targeting chimeras

Recent years saw the development and synthesis of proteolysis targeting chimeras (PROTACs). These molecules induce the ubiquitination and subsequent degradation of a target protein by the proteasomal system. While the synthesis of new PROTACs is reported frequently, there is a lack and strong need for additional experimental techniques and evaluation systems for these types of compounds. Over the course of the presented doctoral thesis a small library of PROTACs was investigated by different means. For this purpose a novel assay system which could allow the assessment of cellular uptake, as well as the degradation capabilities of PROTACs was to be conceptualized and established.

2.3.1 Design of a test system for proteolysis targeting chimeras

A suitable assay system for the evaluation of PROTACs needed to fulfill several requirements. Apart from the easy assessment and reproducibility of test results, a fast and straight forward operability were taken into account. The designed test system was supposed to be compatible with cell cultures and include an intracellular target for PROTAC-induced degradation by the UPS. For this purpose, a luciferase-based approach was chosen. Firefly luciferase degradation should be induced by PROTACs via an attached protein tag and monitored by subsequent loss of luciferase activity (Scheme 2.7A). Renilla luciferase was co-expressed as a transfection control which should not be influenced by PROTAC treatment. The HaloTag technology^[222] was selected as means to induce PROTAC selectivity and reduce unspecific degradation events. The HaloTag is a protein tag derived from a haloalkane dehalogenase enzyme of *Rhodococcus rhodochrous*. The dehalogenase activity of this enzyme was modified to form a permanent covalent bond with a halogenated molecule which is utilized concurrently with its deep binding pocket to allow for selective labeling.^[222] Subsequently, the HaloTag gene was cloned as an N-terminal tag into an expression vector containing the firefly luciferase gene, as well as the control renilla luciferase gene (Scheme 2.7B). A gateway cloning system was employed to ensure correct insertion and expression of the fusion protein.

Scheme 2.7: Luciferase-based test system for the evaluation of PROTACs.

(A) Schematic depiction of PROTAC test system. PROTACs targeted towards the HaloTag attached to luciferase induce complex formation with an E3 ligase. Subsequently, luciferase gets ubiquitinated and designated for degradation by the proteasome. Luciferase levels are monitored by luminescence measurement assessing luciferase substrate conversion. (B) Produced expression vector pHTN-2Luc for the PROTAC test system. Halo: HaloTag, Fluc: firefly luciferase, Rluc: renilla luciferase, S: substrate, S*: luminescent substrate, E3: E3 ubiquitin ligase, E2: E2 ubiquitin carrier, U: ubiquitin, PR: PROTAC molecule, Kan: kanamycin resistance, attR1/attR2: attR insert sequences.

2.3.2 Establishment of a luciferase-based test system for proteolysis targeting chimeras

After verification of the correct insertion of the HaloTag gene by replication in *E. coli* and Sanger sequencing, human hepatoma (Huh7) cells were transiently transfected with increasing amounts of the expression plasmid to establish the test system. Huh-7 cell cultures were grown in 96-well plates coated with poly-D-lysine to improve attachment to the plate surface. Luciferase activity was measured 48 hours after transfection by lysis of transfected cell cultures and the addition of luciferase substrates. Expression of increasing amounts of the expression plasmid resulted in a significant increase in luciferase activity compared to untransfected control samples (Figure 2.27). Subsequently, a concentration of 500 ng was determined as a sufficient amount for further experiments.

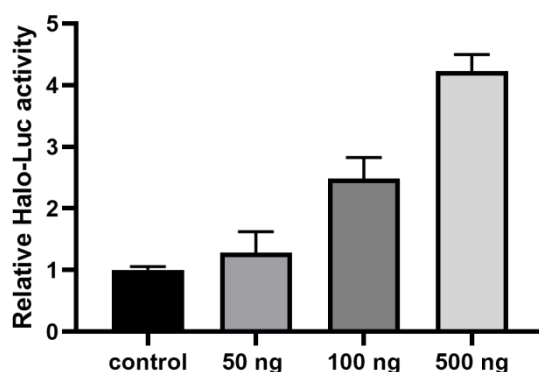


Figure 2.27: Luciferase activity of transfected Huh-7 cell cultures. Luciferase activities of Huh-7 cells transiently transfected with increasing amounts (50 ng, 100 ng, 500 ng) of pHTN-2Luc expression vector were measured. The histogram shows the mean luciferase activity derived from firefly luciferase activity relative to the control renilla luciferase signal. Activity ratios are normalized to a control mean value of 1 derived from untransfected cell cultures. All data points are averages of at least three independent biological replicates and are expressed as means \pm standard deviation.

2.3.3 Influence of proteolysis targeting chimeras on cell viability

In the following experiments a series of six PROTACs **54** to **59** was to be evaluated for their ability to induce degradation of HaloTag-luciferase fusion proteins (Table 2.7). These compounds were synthesized and provided by Christian Steinebach.

Table 2.7: Chemical structures of PROTAC molecules.

Compound	Structure
54	
55	
56	
57	
58	
59	

PROTACs **54** to **59** were synthesized and provided by Christian Steinebach. Stock solutions were prepared in DMSO at a concentration of 10 mM.

They share a chlorohexyl group, which acts as an irreversible ligand for the HaloTag of the fusion protein, as a common feature. Alkane or polyethylene glycol linkers of variable length were chosen to connect this group to an E3 ligase ligand of choice. In case of **54** to **57** this was thalidomide, a ligand of the E3 ligase cereblon (CRBN),^[189] and in case of **58** and **59** the VHL ligand 1, a known interaction partner of the E3 ligase von Hippel-Lindau (VHL).^[222] PROTAC **57** was included as a negative control for **54** due to the addition of a methyl group at the piperidinedione nitrogen which prevents interaction with CRBN. On a similar note, PROTAC **59**, a stereoisomer of **58**, was chosen as a negative control for the VHL E3 ligase. **58** was described previously as a functional PROTAC for the degradation of VHL and was thus included as a positive control.^[223]

To assess suitable concentrations for the application of PROTACs in cell-based experiments MTT viability assays were performed (Figure 2.28). For this purpose, **54** to **59** were applied to Huh-7 cell cultures in concentrations of 100 nM to 100 μ M for 1 hour up to 24 hours. Test results indicated a correlation of increasing application time and PROTAC concentration with decreasing cell viability. In general, concentrations up to 10 μ M were well tolerated by cell cultures for an incubation time of up to 4 hours (decrease of cell viability < 20%). However, concentrations of 100 μ M had a higher impact on cell viability for the majority of test compounds, similar to incubation times of 24 hours. In this regard, **54** and **57** protruded since both PROTACs remained applicable in concentrations of up to 10 μ M for incubation times up to 24 hours with a reduction of cell viability under 20% (Figure 2.28A and D).

These results were taken into account for the design of further experiments. 10 μ M and 4 hours were specified as the highest PROTAC concentrations and incubation times which would be applied to living cell cultures, respectively. Subsequently, PROTACs **54** to **59** were applied in concentrations of 10 pM to 10 μ M for 2 hours to assess their abilities to degrade the Halo-Luc fusion protein.

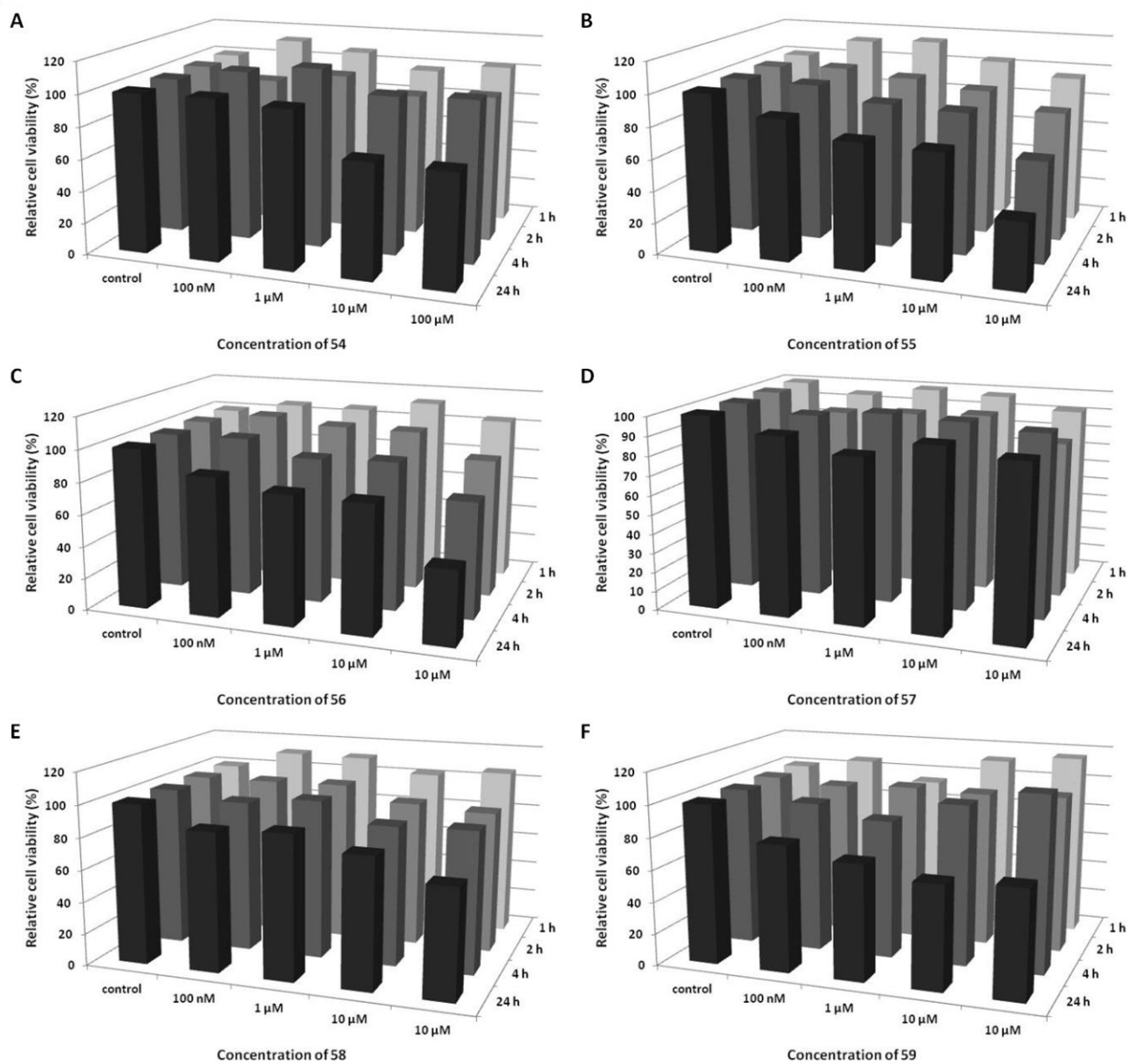


Figure 2.28: Normalized cell viability of PROTACs 54 to 59. Huh-7 cells were treated with 100 nM to 100 μM of PROTACs 54 to 59 (A to F) for 1 hour up to 24 hours at 37 °C. After MTT treatment and lysis the formation of formazan was monitored at 595 nm. Test values were normalized relative to positive controls of untreated cells and negative controls of cells treated with 100% DMSO. Bars were generated from test values of three independent experiments.

2.3.4 Application of PROTACs in a luciferase-based test system

Subsequently, PROTACs **54** to **59** were applied in the fusion protein test system to assess their ability to induce HaloTag-luciferase fusion protein degradation. For this purpose, test compounds were applied to Huh-7 cell cultures 48 hours after transfection with the pHTN-2Luc expression plasmid in concentrations ranging from 10 pM to 10 μ M for a time period of 2 hours. Luciferase activity was measured after lysis of cell cultures and the level of firefly luciferase fusion protein activity was determined relative to renilla luciferase activity.

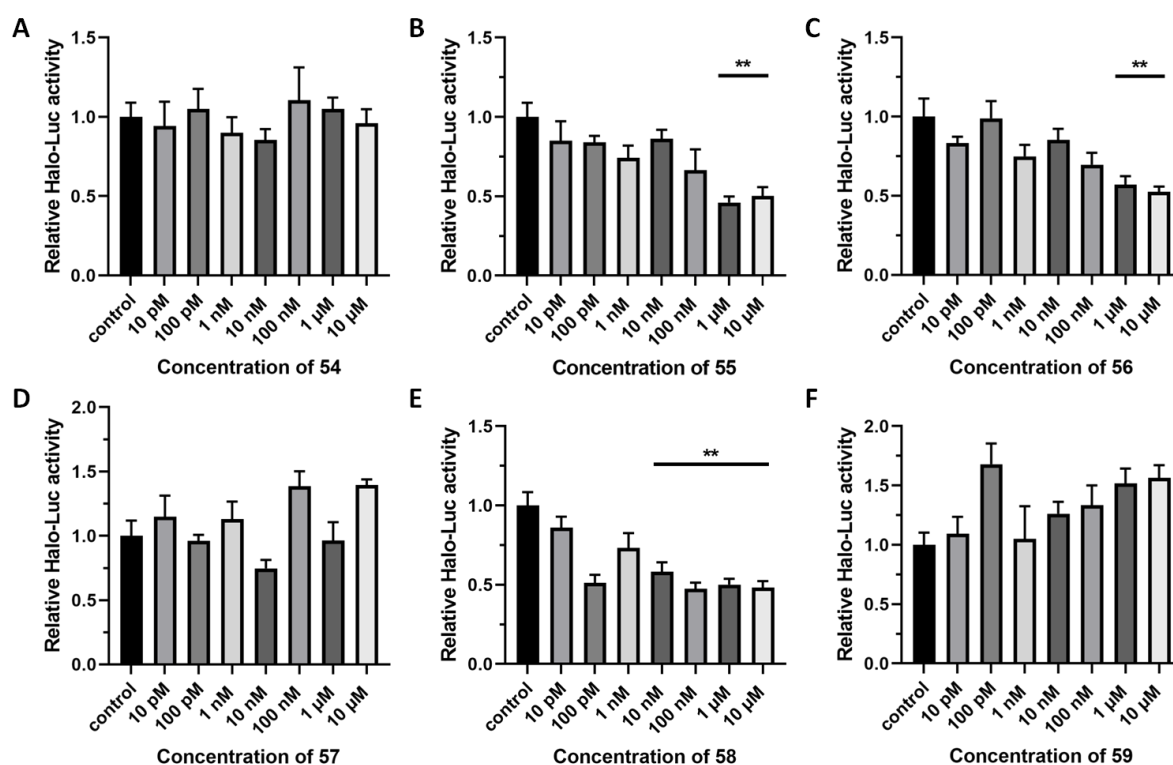


Figure 2.29: Halo-Luc activity in the presence of increasing amounts of PROTACs 54 to 59 (A to F). Luciferase activities of Huh-7 cells transiently transfected with the expression vector pHTN-2Luc and treated with increasing amounts of **54** to **59** for 2 hours at 37 °C were measured. The histograms show the mean luciferase activity derived from the ratio of firefly luciferase activity relative to control renilla luciferase activity. Activity ratios are normalized to a control mean value of 1 derived from cells transfected with pHTN-2Luc which did not undergo PROTAC treatment. All data points are averages of at least three independent biological replicates and are expressed as means \pm standard error of the means. ** indicate $P < 0.001$.

Test results indicated a reduction of firefly luciferase activity dependent on PROTAC levels for three of the tested compounds after the application time of 2 hours (Figure 2.29). While no significant decrease in Halo-Luc activity was observed in the presence of CRBN-directed **54** (Figure 2.29A) treatment with both PROTACs **55** and **56**, which also feature the CRBN ligand thalidomide, resulted in reduced Halo-Luc activity (Figure 2.29B and C). This reduction was dependent on the applied PROTAC concentration. A significant reduction of the relative Halo-Luc activity to a level of approximately 50% compared to control samples was observed in the presence 1 to 10 μM in both cases. Treatment with **57** did not result in significant reduction of Halo-Luc activity (Figure 2.29D). This compound was included as a negative sample for CRBN-directed PROTACs due to an additional methylation in its thalidomide moiety, which should prevent interaction with CRBN and subsequent degradation by the UPS. A significant reduction of the luciferase activity was observed in cells treated with 10 nM to 10 μM **58** (Figure 2.29E). This VHL-directed PROTAC induced a decrease of relative Halo-Luc activity to a level of under 50% in test samples. A similar decrease was not observed in the presence of its inactive analog **59** (Figure 2.29F).

These findings demonstrate the applicability of the presented test system for the evaluation of PROTACs. A reduction of Halo-Luc fusion protein activity to different extents by PROTACs **55**, **56** and **58** could be observed in the luciferase test system. Surprisingly, the same decreasing effect was not apparent in the presence of **54**. Since this compound shares the majority of its molecular structure with **55** a similar induction of degradation was expected. Possibly, the additional oxygen in the linker structure of **54** promotes linker flexibility and its ability to induce ternary complex formation between the target protein and the proteins involved in the ubiquitination process. Several studies point out the importance of both linker length and flexibility for the successful formation of ternary complexes.^[224-225] Since the inactive CRBN-directed PROTAC **57** shares its linker structure and E3 ligand with **54**, additional inactive PROTACs featuring the linker structures of **55** and **56** should be employed to further investigate this possibility and to serve as suitable negative controls. The additional elongation of the linker structure in **56** did not result in an improvement of PROTAC activity. In the case of **58** and **59** this principle of active positive and inactive negative control was successfully employed. The previously established PROTAC **58** could induce a significant decrease in Halo-Luc activity by over 50% in comparison to control samples in contrast to the inactive **59**.

2.3.5 Detection of Halo-Luc fusion protein by immunoblotting

To verify the test results obtained in the Halo-Luc PROTAC assay, the influence of compounds **54** to **59** on the Halo-Luc fusion protein levels in transfected cell cultures was investigated by immunoblotting. For this purpose, HEK cell cultures were seeded into 6 well culture plates and transfected with pHTN-2Luc expression plasmid.

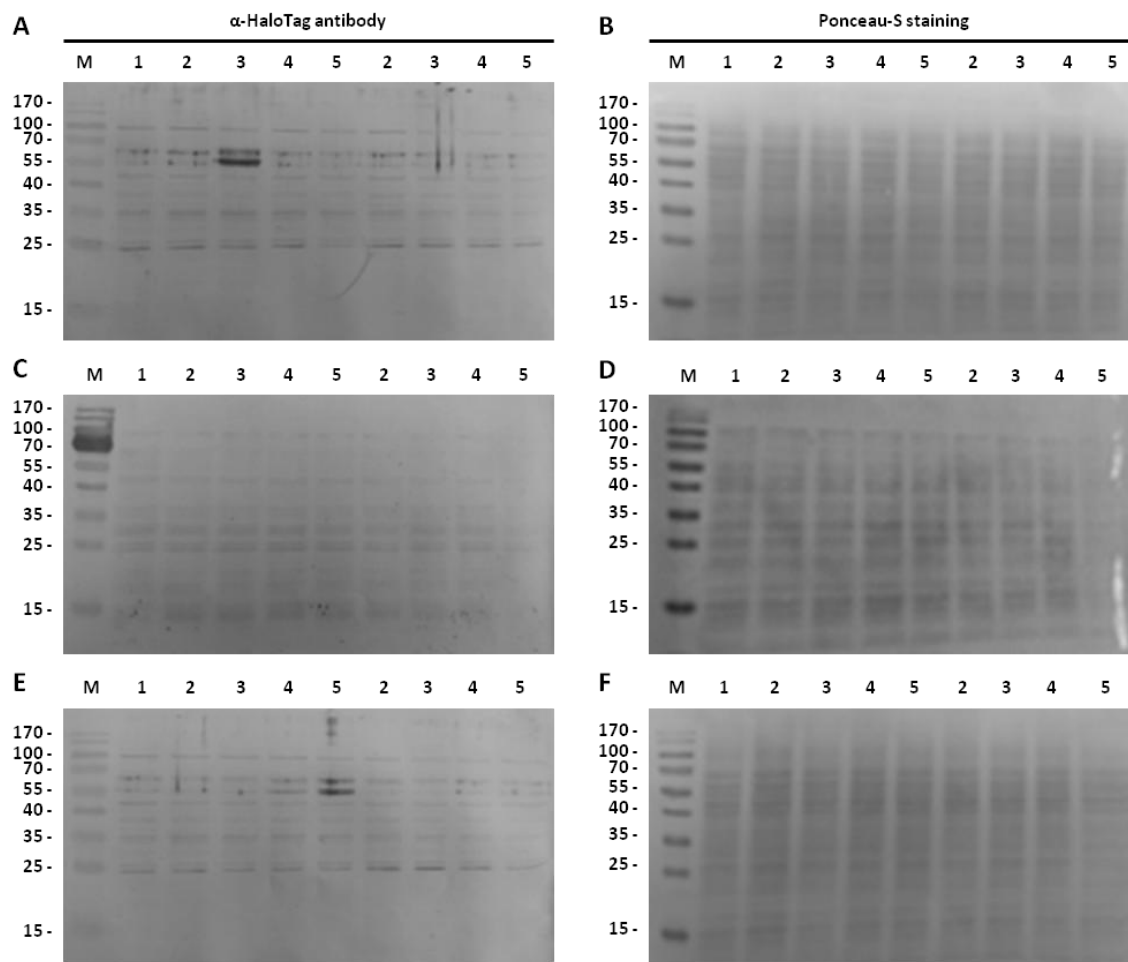


Figure 230: Detection of Halo-Luc fusion protein by western blotting. (A, C, E) α -HaloTag western blot. (B, D, F) Ponceau-S staining of the corresponding blots. 50 μ g of cell lysates derived from cell cultures treated with 10 nM to 10 μ M **54** or **55** (A-B), **56** or **57** (C-D) and **58** or **59** (E-F) for 2 hours at 37 $^{\circ}$ C were loaded onto 12% SDS gels. After western blotting and antibody staining with α -HaloTag and secondary AP-conjugated antibody, Halo-Luc fusion protein was detected by the addition of BCIP and NBT solutions. 1: HEK-Halo-Luc; 2: HEK-Halo-Luc + 10 nM PROTAC; 3: HEK-Halo-Luc + 100 nM PROTAC; 4: HEK-Halo-Luc + 1 μ M PROTAC; 5: HEK-Halo-Luc + 10 μ M PROTAC.

After 24 hours PROTACS **54** to **59** were added to cell cultures in concentrations of 10 nM to 10 μ M for 2 hours at 37 °C. Cells were lysed and 30 to 50 μ g of lysate samples were applied to SDS gels. Subsequently, Halo-Luc fusion proteins should be visualized by the use of a α -HaloTag antibody. However, no fusion protein protein band could be detected even in 50 μ g of lysate samples (Figure 2.30A, C, E). The Halo-Luc fusion protein designed in the presented experimental approach should be expressed as an approximately 100 kDa protein band (61 kDa firefly luciferase, HaloTag 33 kDa). Yet, neither in control samples which did not receive PROTAC treatment (Figure 2.30 lane 1), nor in lysate samples derived from transfected cell cultures treated with 10 nM to 10 μ M PROTAC (Figure 2.30 lanes 2-5) such a protein band was apparent. To ensure that these results did not occur due to insufficient binding of the employed α -HaloTag antibody, a second antibody directed towards the firefly portion of the fusion protein, was employed. Through the use of this α -firefly luciferase antibody a distinct double protein band could be visualized in the HEK cell lysate samples (Figure 2.31A).

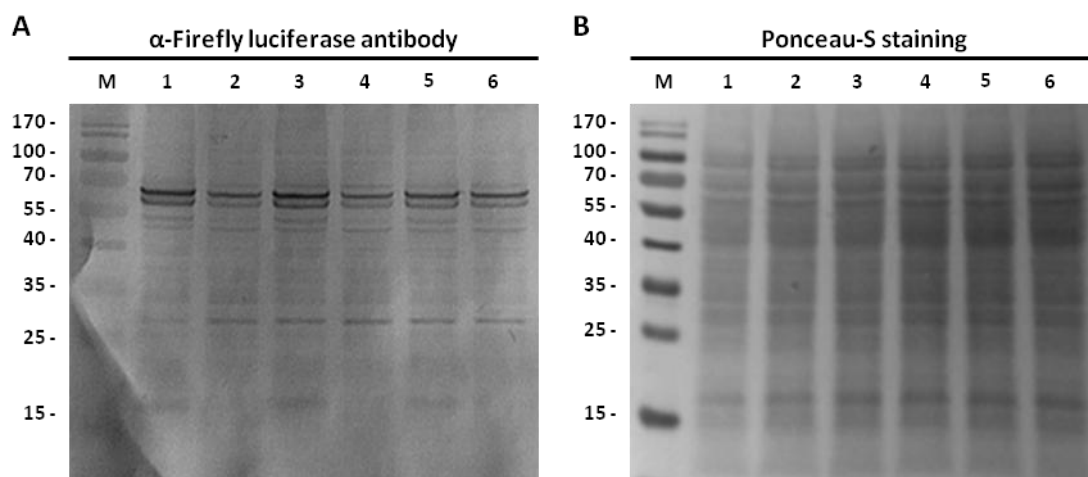


Figure 2.31: α -Firefly luciferase immunoblot of HEK lysates transfected with pHTN-2Luc expression vector. (A) α -Firefly luciferase western blot. (B) Ponceau-S staining of the corresponding blot. 50 μ g of cell lysates derived from cell cultures treated with 10 μ M PROTACs for 2 hours at 37 °C were loaded onto 12% SDS gels. After western blotting and antibody staining with α -firefly luciferase and secondary AP-conjugated antibody, Halo-Luc fusion protein was detected by the addition of BCIP and NBT solutions. 1: HEK-Halo-Luc; 2: HEK-Halo-Luc + 10 μ M **54**; 3: HEK-Halo-Luc + 10 μ M **55**; 4: HEK-Halo-Luc + 10 μ M **56**; 5: HEK-Halo-Luc + 10 μ M **58**; 6: HEK-Halo-Luc + 10 μ M **59**.

However, this protein band possessed a size of approximately 60 kDa, which is in coherence with native firefly luciferase but not with the designed fusion protein, indicating that the detected band represented in fact the untagged firefly luciferase protein.

Since the correct gene sequence was verified by Sanger sequencing, an incorrect insertion of the HaloTag gene into the expression vector is unlikely and could be excluded. Likewise, the Gly-rich linker structure present between tag and luciferase protein should be expressed correctly and did not contain additional start- or stop-codons. Even though protein stability was supported by the preparation of cell lysates in the presence of protease inhibitor cocktail and the application of non-reducing SDS-PAGE conditions, the possibility that the HaloTag detached from the Halo-Luc fusion protein during the lysis process or SDS-PAGE and western blotting still persists. To investigate this possibility additional experiments, such as native electrophoresis should be performed.

2.3.6 Conclusion

In recent years PROTACs emerged as a promising new drug class which possesses the potential to revolutionize the treatment of diseases and the process of drug discovery.^[184] New test systems that allow for the easy and fast assessment of PROTAC activity are necessary tools to promote this emerging research field.

Over the course of this thesis, a luciferase-based test system for the evaluation of PROTACs was designed and established. A series of PROTAC molecules was tested for their ability to induce fusion protein degradation. In case of three compounds **55**, **56** and **58** a concentration-dependent reduction of HaloLuc activity was observed. However, whether this reduced luciferase activity was actually caused by the degradation of fusion proteins remains to be proven since those results could not be verified by immunoblotting. In the case that only untagged firefly luciferase was expressed, cytotoxicity of the tested PROTACs as a cause of reduced fusion protein levels can be largely ruled out due to the results of extensive cell viability experiments. To this end, additional cloning approaches which yield a fusion construct detectable in western blot should be employed to investigate its behavior in the proposed test system and to verify the results presented in this thesis. As the applicability of both, HaloTag and firefly luciferase as targets for targeted protein degradation by PROTACs was demonstrated recently,^[223,226] such a test system might help to further the ongoing research in the PROTAC field.

3 Experimental section

3.1 Methods

3.1.1 Cultivation of cells

Experimental procedures were performed with either human embryonic kidney (HEK 293) cells, or human hepatoma (Huh-7) cells. Cells were cultivated under a humidified atmosphere at 37 °C and 5% CO₂. HEK cells were cultivated in Dulbecco's Modified Eagle Medium (DMEM) supplemented with 10% fetal calf serum (FCS), 100 U/mL penicillin and 100 µg/mL streptomycin. Huh-7 cells were cultivated in Roswell Park Memorial Institute (RPMI) medium supplemented with 10% FCS, 2 mM L-glutamine and non-essential amino acids at a final concentration of 0.1 mM. For the transfer of a cell culture to a new culture flask or culture plates cells were washed twice with phosphate buffered saline (PBS) buffer and detached from the culture surface by incubation in trypsin/EDTA solution for 5 minutes at room temperature (all substances and media were purchased from Thermo FisherScientific, Karlsruhe, Germany). Detached cell cultures were counted and a defined amount of cells was transferred into new culture vessels containing an appropriate amount of new medium. Final volumes of 5 mL for 25 cm², 10 mL for 75 cm² and 20 mL for 175 cm² flasks were used.

3.1.2 Counting of cells

Cell numbers of a cell culture were determined by using a Neubauer counting chamber (Merck Millipore, Darmstadt, Germany). After cultivation, the culture medium was removed and cells were washed with sterile PBS buffer. Cells were detached from culture flasks with trypsin/EDTA solution and diluted in culture medium. 10 µL of cell suspension were diluted with 90 µL PBS and 10 µL of this dilution were put in one part of a Neubauer counting chamber. Eight large squares were counted each run. The cell number in 1 µL cell suspension was calculated using the following formula:

$$\text{cell number per } \mu\text{L} = \frac{\text{number of cells counted}}{\text{surface area counted (mm}^2\text{) x depth of chamber (mm) x dilution factor}}$$

Example: number of cells counted = 104
 counted surface area = 8 large squares (8 mm²)
 chamber depth = 0.1 mm
 dilution factor = 1:10

$$\frac{104 \times 10}{8 \times 0.1 \times 1} = 1300 \text{ cells}/\mu\text{L}$$

3.1.3 MTT viability assay

3-(4,5-dimethylthiazol-2-yl)-2,5-diphenyltetrazolium bromide (MTT) was used to stain catalytically active cells of a cell culture to determine possible cytotoxic effects of used test substances. 12000 HEK or 10000 Huh-7 cells in a volume of 100 μL RPMI medium were seeded into consecutive wells of a 96-well cell culture plate. Unoccupied wells were filled with 100 μL RPMI medium to avoid an uneven evaporation between different wells of the plate. Cells were cultivated in the culture plates at 37 °C and 5% CO₂ for two further days. Afterwards, the culture supernatant was discarded, cells were washed with PBS once and 100 μL Modified Eagle's Minimum Essential Medium (OptiMEM), containing 1% DMSO and test compound in the desired concentration, were added to each culture well. Following an incubation step of 1, 2, 4 or 24 hours the OptiMEM supplemented with the test compound was replaced by 110 μL of a freshly prepared 1 mM MTT solution in OptiMEM. Cells were incubated for 4 hours at 37 °C and 5% CO₂ to allow the viable cell portion to take up MTT and reduce it to water-insoluble formazan. Afterwards 85 μL of the MTT-OptiMEM solution was discarded and cells were lysed by the addition of 50 μL DMSO for 15 minutes at 450 rpm and rt. Formazan was detected by absorbance measurement at 595 nm at a FLUOstar Optima fluorimeter (BMG Labtech, Offenburg, Germany).

3.1.4 Transfection of cells

Cells were transfected by cationic lipid mediated transfection using LipofectamineTM 2000 reagent (GIBCO[®] Life Technologies, ThermoFisher Scientific). Cell cultures were cultivated to a confluence of approximately 70%, at which point the culture medium was removed and the cells were washed twice with PBS buffer to remove remnants of serum. Serum free medium (4 mL in case of 25 cm² flasks or 50 μ L per well in a 96-well plate) was added to the cell culture. For optimal transfection efficacy serum-free reduced OptiMEM was used in further incubation and selection steps. Appropriate volumes of Lipofectamine (24 μ L per 25 cm² culture flask or 1 μ L per well in a 96-well plate) and expression plasmids were prepared in separated reaction tubes and supplemented with OptiMEM (500 μ L in case of 25 cm² flasks or 25 μ L per well in a 96-well plate). After 5 minutes of incubation at rt the Lipofectamine-OptiMEM solution was added carefully, drop by drop, to the plasmid-OptiMEM solution followed by a second incubation step of 20 minutes at room temperature. The Lipofectamine-plasmid mixture (1 mL in case of 25 cm² flasks or 50 μ L per well in a 96-well plate) was added to the cell culture. After two days of incubation at 37 °C and 5% CO₂ transfected cell cultures were harvested to produce cell lysates and culture supernatants.

The generation of stably transfected cell lines HEK-mock, HEK-MT2-Myc-His and HEK-MT2-S753A was described previously by Stirnberg *et al.*^[45]

3.1.5 Preparation of cell lysates and culture supernatants

For the generation of cell lysates the conditioned supernatant of cell cultures was removed 48 hours after addition and cultivation in serum-free medium. The cells were washed twice with PBS buffer containing Halt protease inhibitor cocktail (ThermoFisher Scientific) and detached from the culture flask surface by a cell scraper followed by 15 aspirations through a 25-gauge needle. Cell debris and intact cells were separated by centrifugation at 2000g and 4 °C for 10 minutes. The resulting supernatant represented the cell lysate.

The conditioned medium of a cell culture was collected to obtain culture supernatants. After centrifugation at 4 °C and 2000g for 10 minutes to separate detached cells, the resulting supernatant was concentrated by the use of Amicon size exclusion filter tubes (Merck Millipore) at 4 °C and 7500g to obtain concentrated culture supernatants.

3.1.6 Protein determination

To quantify the total protein amount of a test sample a method based on the Bradford assay was used.^[227] For this purpose, ROTI-Nanoquant solution (Carl Roth, Karlsruhe, Germany) was diluted 1:5 with distilled water. 800 μL of this dilution, 198 μL distilled water and 2 μL test sample were mixed in a cuvette and the absorption was measured at 465 nm and 595 nm in a Cary 50 UV-VIS spectrophotometer (Agilent Technologies, Böblingen, Germany). By comparison of the absorbance ratio of the test samples with data of a calibration curve, which was obtained by measurement of defined amounts of a bovine serum albumin (BSA) solution, protein amounts in the test sample could be calculated.

3.1.7 Enzyme inhibition assays with purified enzymes and cell culture supernatants

Enzymatic activity assays of human chymotrypsin, human matriptase, human matriptase-2 and human thrombin were performed in 96 well flat bottom plates (Sarstedt, Nümbrecht, Germany) at a FLUOstar Optima fluorimeter (BMG Labtech). The enzymatic reactions were monitored at an excitation wavelength of 340 nm and an emission wavelength of 460 nm. Inhibitors and substrates were prepared as stock solutions with a concentration of 10 mM in DMSO. The substrates Boc-Gln-Ala-Arg-AMC (human matriptase, human matriptase-2) and Cbz-Gly-Gly-Arg-AMC (human thrombin) were purchased from Bachem (Bachem, Bubendorf, Switzerland).

Human matriptase inhibition assay

The assay was performed in a 50 mM TRIS, 150 mM NaCl, pH 8.0 buffer. A solution of 2 g BSA in 10 mL of a 154 mM NaCl solution was diluted 1:200 with a 154 mM NaCl solution. This BSA solution was used for a 1:10 dilution of the enzyme stock solution (0.1 $\mu\text{g}/\text{mL}$) (R&D systems, Wiesbaden-Nordenstadt, Germany). This diluted enzyme solution was kept at 0 °C. A 10 mM stock solution of the fluorogenic substrate Boc-Gln-Ala-Arg-AMC in DMSO was diluted with water to a concentration of 800 μM before the measurement. 162 μL assay

buffer, 8 μL of an inhibitor solution in DMSO and 20 μL of the substrate dilution were mixed in the well of a 96-well plate. The final assay concentration of the substrate was 80 μM , of DMSO was 6% and of human matriptase was 0.0005 $\mu\text{g}/\text{mL}$. The reaction was started by the addition of 10 μL enzyme dilution and followed at 37 $^{\circ}\text{C}$.

Human matriptase-2 inhibition assay

The assay was performed in a 50 mM TRIS, 150 mM NaCl, pH 8.0 buffer. The conditioned medium of transfected HEK cells was used as a source of matriptase-2 activity. The conditioned medium was collected and concentrated with amicon filter tubes. The resulting concentrate was stored at -20 $^{\circ}\text{C}$. After thawing, it was diluted with assay buffer and kept at 0 $^{\circ}\text{C}$. A 10 mM stock solution of the fluorogenic substrate Boc-Gln-Ala-Arg-AMC in DMSO was diluted with assay buffer to a concentration of 800 μM before the measurement. 158.8 μL assay buffer, 11.2 μL of an inhibitor solution in DMSO and 10 μL of the substrate dilution were mixed in the well of a 96-well plate. The final assay concentration of the substrate was 40 μM and of DMSO was 6%. The reaction was started by the addition of 20 μL conditioned medium dilution and followed at 37 $^{\circ}\text{C}$.

Human thrombin inhibition assay

The assay was performed in a 50 mM TRIS, 150 mM NaCl, pH 8.0 buffer. The enzyme stock solution (1 U/ μL) (Enzo Life Sciences) was prepared in water, kept at 0 $^{\circ}\text{C}$ and diluted 1:50 with assay buffer before the measurement. A 10 mM stock solution of the fluorogenic substrate Cbz-Gly-Gly-Arg-AMC in DMSO was diluted with assay buffer to a concentration of 800 μM before the assay. 158.8 μL assay buffer, 11.2 μL of an inhibitor solution in DMSO and 10 μL of the substrate dilution were mixed in the well of a 96-well plate. The final assay concentration of the substrate was 40 μM , of DMSO was 6% and of human thrombin was 2 U/mL. The reaction was started by the addition of 20 μL enzyme dilution and followed at 25 $^{\circ}\text{C}$.

3.1.8 MT2 inhibition assay with intact cells

Stably transfected HEK cells expressing matriptase-2 were seeded into 96-well plates coated with poly-D-lysine solution (Thermofisher Scientific) for 5 minutes at rt. Cell cultures were cultivated for two days at 37 °C and 5% CO₂, at which point the culture medium was discarded and, following three wash steps with PBS buffer, replaced with 178.8 µL 50 mM pre-warmed TRIS-HCl, 150 mM NaCl, pH 8.0 buffer and 11.2 µL of an inhibitor solution in DMSO. A 10 mM stock solution of the fluorogenic substrate Boc-Gln-Ala-Arg-AMC in DMSO was diluted with assay buffer to a concentration of 800 µM before the measurement. The reaction was started by the addition of 10 µL substrate dilution and followed at 37 °C. The final assay concentration of the substrate was 40 µM and of DMSO was 6%.

3.1.9 Solution-based synthesis of prolineamide inhibitors

Prolineamide inhibitors **17A** to **20F** were prepared prior to measurements by combining one type of lactone (**17** to **20**) with one type of amine/amide (**A** to **F**). For this purpose, equal amounts of lactone and amine/solutions were combined in one reaction tube. Incubation of these reaction mixtures for 24 hours at 45 °C in a heating block (Eppendorf) yielded inhibitor solutions of **17A** to **20F**. For the purpose of applicability, inhibitor solutions were considered to contain 100% of formed inhibitor and no adducts.

3.1.10 SDS-PAGE

Sodium dodecyl sulphate polyacrylamide gel electrophoresis (SDS-PAGE) was used to separate protein samples prior to the in-gel detection of activity-based probes or immunoblotting. The samples for one SDS-PAGE experiment were adjusted to the same final volume with distilled water and appropriate volumes of 5x SDS loading buffer were added before applying the samples to the gel. SDS-PAGE were performed either under non-reducing or reducing conditions. In the case of reducing SDS-PAGE experiments the 5× SDS loading buffer was supplemented with 10% 2-Mercaptoethanol and samples were incubated at 95 °C for 5 minutes before application to the gel.

3.1.11 In-gel detection

Activity-based probes that allowed for visualization under UV-light were examined by in-gel detection after SDS-PAGE. For this purpose protein samples were incubated with the activity-based probe at 37 °C for 30 minutes to 1 hour before application to the SDS gel. If the activity-based probe was still bound to its target after SDS-PAGE the corresponding protein band was visualized under UV-light in a gel doc photo documentator (BioRad Laboratories, Basel, Switzerland).

3.1.12 Immunoblotting

Protein samples were transferred from SDS gels to nitrocellulose membrane and subjected to western blot analysis to specifically detect and to evaluate the level of expression of selected target proteins. For this purpose several antibodies and one activity-based probe were used. Murine 9E10 anti-Myc antibody for the detection of Myc-tagged MT2 was applied in a dilution of 1:100. An antibody against Halotag from mouse (Promega, Walldorf, Germany) and an antibody against firefly luciferase from rabbit (ThermoFisher) were applied in a dilution of 1:1000. The bound biotinylated CMK probe **15** or primary antibodies were detected by using strep-tactin alkaline phosphatase (AP) conjugate (IBA Lifesciences, Göttingen, Germany) or AP-conjugated anti-mouse/anti-rabbit secondary antibodies (Merck Millipore) in a dilution of 1:10000. Visualization of protein bands was performed in reaction buffer supplemented with 40 µL nitro tetrazolium blue chloride (NBT) solution and 120 µL 5-bromo-4-chloro-3-indolyl phosphate (BCIP) solution. Successful protein transfer was confirmed by Ponceau S staining.

3.1.13 Confocal microscopy

Stably transfected HEK-mock, HEK-MT2-MycHis and HEK-MT2-S753A-MycHis cells were grown in 25 cm² culture flasks until a confluence of approximately 70% was reached. As the desired confluence of cell cultures was reached, glass slides with a diameter of 10 mm were put in subsequent wells of 12 well culture plates. Each slide was coated with poly-D-lysine

solution (Sigma-Aldrich) for 5 minutes at rt. The poly-D-lysine solution was discarded and slides were washed twice with PBS buffer. Cells were detached and counted and an amount of 10000 cells was transferred into each used well in a volume of 1 mL DMEM. Transferred cells were cultivated for 24 hours at 37 °C and 5% CO₂. Afterwards, the culture medium was removed and cells were washed twice with PBS buffer. Activity-based probes were added in 1 mL OptiMEM and cell cultures were incubated for 30 minutes at 37 °C and 5% CO₂. Samples incubated with CMK probe **15** were treated with 1 µg/mL FITC-Avidin (Thermo Fisher Scientific) in PBS for 10 minutes in the dark at rt. Cells were washed three times with PBS buffer and fixed with a 4% paraformaldehyde solution for 30 minutes at rt. Antibody samples were washed again with PBS buffer and blocked with 5% BSA/PBS for 1 hour at rt. Samples were incubated with α-Myc antibody (1:100) in the dark for 1 hour and then 30 minutes with the secondary Alexa Fluor 488 antibody (Thermofisher Scientific), both diluted 1:10000 in a 2.5% BSA/PBS solution. In between and after antibody incubations, cells were washed three times with PBS buffer. Visualization of cell nuclei was achieved by DAPI staining. At last coverslips were mounted using Immumount reagent (Thermo Fisher Scientific) and stored in the dark at 4 °C. A Nikon A1 spectral confocal microscope (Nikon, Minato, Japan) was used for imaging. Each staining was repeated three times and at least ten squares (60x objective) containing 3 to 15 cells each were imaged for each sample. The cells that were most representative of the majority of each condition were shown.

3.1.14 Cloning

The construction of expression plasmids pcDNA4-MT2-Myc-His, pcDNA4-MT2-S753A and pGL3-Hampro and the generation of the stably transfected cell lines HEK-mock, HEK-MT2-Myc-His and HEK-MT2-S753A was described previously by Stirnberg *et al.*^[45] For the construction of expression plasmid pHTN-2Luc for the expression of HaloTag-firefly luciferase under the CMV promoter the HaloTag sequence was amplified by polymerase chain reaction (PCR) using the attB1 forward primer 5'-ggggacagttgtacaaaaagcaggcttaacctggcgatcgctccgaattcagagctcaaccg-3' and the attB2 reverse primer 5'-ggggaccactttgtacaagaaagctgggtc gaaagaacatgtttcacca-3' to generate HaloTag gene with suitable attB recombination sites for the integration into the donor vector. Subsequently, 150 ng of PCR products were cloned into a pDONR223 donor vector (Invitrogen) using a BP clonase enzyme mix (Thermofisher Scientific). *E. coli* cultures were

transformed with the resulting vector and selected by streptomycin resistance to generate an entry clone. After verification of the desired sequence by Sanger sequencing, 150 ng of the entry clone were incubated with 150 ng of the destination vector pIRIGF (Addgene, Cambridge, USA) using a LR clonase enzyme mix (ThermoFisher Scientific) to yield the fusion protein expression vector pHTN-2Luc.

3.1.15 Proteolysis targeting chimera evaluation assay

The PROTAC evaluation assay established in this thesis is a modification of the Dual-Glo® reporter gene assay from Promega.^[228] A number of 4000 Huh-7 cells was seeded into the wells of a 96-well white bottom cell culture plate (Sarstedt) and cultivated for two days at 37 °C and 5% CO₂. Cells were transfected as described in 3.1.4 with 50-500 ng of pHTN-2Luc expression plasmid. After 24 hours of incubation at 37 °C and 5% CO₂ culture supernatants were removed and cells were washed two times with PBS buffer. 100 µL OptiMEM containing PROTACs in DMSO were added followed by further incubation at 37 °C and 5% CO₂ for 2 hours. Supernatants were removed and cells were lysed in 1x passive lysis buffer (Promega) for 15 minutes at 450 rpm and rt. Successively, the auto-luminescence, firefly luminescence activity and renilla luminescence activity were measured at a FLUOstar Optima fluorimeter (BMG Labtech) after the addition of 50 µL LarII substrate solution and 50 µL S&G substrate solution, respectively. The level of halotag-firefly expression was determined by the division of firefly luciferase activity by the renilla luciferase activity thereby calculating in the transfection efficiency.

3.1.16 Transformation of *Escherichia coli* cells

Competent *Escherichia coli* (*E. coli*) DH5α cells (Thermo Fisher Scientific) were stored at -80 °C and thawed on ice upon usage. 2 µg of plasmid DNA were added to the thawed cells followed by incubation on ice for 30 minutes. After a heat shock of 42 °C for 1 minute, the *E. coli* suspension was incubated on ice for two further minutes. 300 µL super optimal broth with catabolite repression (SOC) were added and the mixture was incubated at 37 °C and 550

rpm for 1 hour. Successfully transformed bacteria were selected by cultivation on lysogeny broth (LB) agar plates containing antibiotics (ampicillin or kanamycin) over night at 37 °C.

3.1.17 Cultivation of *Escherichia coli* cells

For the multiplication of expression plasmids successfully transformed *E. coli* were transferred from a LB agar plate to liquid medium. Depending on the method 4 mL (Mini-Prep) or 75 mL (Midi-Prep) of LB medium supplemented with 4 µL or 75 µL of ampicillin solution (100 mg/mL) were inoculated with one colony of transformed *E. coli* and incubated at 37 °C and 200 rpm for 16 hours.

3.1.18 Plasmid isolation from transformed *Escherichia coli* cells

Plasmid-DNA was isolated from transformed *E. coli* cultures using a QIAGEN Plasmid Midi Kit (Qiagen, Hilden, Germany) or a PureLink Quick Plasmid Miniprep Kit (ThermoFisher Scientific) depending on the culture volume. In both cases a cell pellet was formed by centrifugation at 2000g for 15 minutes at 4 °C and the supernatant was discarded. Pellets were resuspended in resuspension buffer containing RNase and lysis buffer was added. The suspension was thoroughly mixed and incubated for 5 minutes at rt after which precipitation buffer was added immediately. The mixture was inverted until a homogenous solution was obtained followed by a second incubation step on ice for 15 minutes.

For Midi-Preps the mixture was centrifuged at 20000g and 4 °C for 45 minutes. A Quiagen Tip column was equilibrated with equilibration buffer and the supernatant from the centrifugation step was added. The column was washed twice with washing buffer and plasmid-DNA was eluted by using elution buffer. The DNA was precipitated by isopropanol and centrifugation at 20000g for 30 minutes at 4 °C. After a washing step in ethanol solution the DNA-pellet was dried and re-dissolved in 100 µL water.

For Mini-Preps the mixture was centrifuged at 12000g and 4 °C for 10 minutes. The supernatant was added onto a spincolumn placed in a wash tube and centrifuged at 12000g and 4 °C for 1 minute. The flow-through was discarded followed by two wash steps with wash buffer. The flow-through wash buffer was removed and the column was centrifuged

again to remove any residual fluids. The DNA-plasmid was eluted by the addition of 50 μL on the spincolumn and subsequent centrifugation at 12000g and 4 °C for 1 minute.

Total DNA-plasmid concentrations were determined at a Colibri microvolume spectrometer (Titertek Berthold, Pforzheim, Germany).

3.1.19 Statistical analysis

Statistical analysis was performed with standard statistical functions of GraphPad Prism using a two-tailed t test. If not stated otherwise, all values represent means \pm SEM. The error probability was set at $p < 0.05$ (indicated in figures by *), $p < 0.01$ (**) or $p < 0.001$ (***)).

3.2 Devices and Materials

3.2.1 Devices

The following table 3.1 contains a list of the devices that were used in this thesis.

Devices	Suppliers
Analytical balance	770, Kern
Autoclave	Varioclav steam sterilizer 75T, H+P, 3850 ELV, Systec
Balance	PLS 4000-2, Kern
Cell counting chamber	Merck
Centrifuges	Biofuge primo R, Heraeus Z 216 MK, Hermle
Colibri microvolume spectrometer	Titertek Berthold
Confocal microscope	Nikon A1 Spectral confocal microscope, Nikon
Electrophoresis chamber for agarose gels	Amersham Bioscience
Electrophoresis chamber for electro-blotting	TE-22, Amersham Bioscience
Electrophoresis chamber for SDS-PAGE	Mini-Protean Tetra Cell, BioRad
Electrophoresis power supply unit	EV 243, Consort EPS 301, Amersham Bioscience
Fluorimeter	FLUOstar Optima, BMG Labtech
Gel dock photo documentator	Universal hood II geldoc, BioRad
Heating block	Thermomixer comfort, Eppendorf
Hot plate with magnetic stirrer	MR 2002, Heidolph
Incubator for bacterial cell culture	TH 15, KS 15, Edmund Bühler GmbH
Incubator for human cell culture	Jouan IG 650, HERAcell, Heraeus
Laboratory shaker	Mini Rocker MR-1, Kisker
Light microscope	Axiovert 25, Zeiss
Microwave	Severin
pH Meter	691 pH meter, Metrohm
Pipettes	0,5-10 µl, 2-20 µl, 10-100 µl, 20-200 µl, 100-1000 µl, Eppendorf

Pipetting aids	Pipettus Akku, Eppendorf; Accu jet, Brand
Spectrophotometers	Cary 50 Bio, Varian Cary 100 Bio, Varian
Sterile Bench	NUNC Safe flow 1.2
Test Tube Rotor	Kisker-Biotech
Thermo Cycler	T Professional standard Gradient 96, Biometra
Transferpette-12	20-200 µl, Roth
Water bath	Memmert

Table 3.1 List of used devices.

3.2.2 Consumables

The following table 3.2 contains a list of the consumables that were used in this thesis.

Consumables	Suppliers
25-Gauge needle	Omnifix-R, B Braun
White flat bottom plates	96 well, sterile, Sarstedt
Bacteria culture tubes	13 ml, Sarstedt
Cell culture flasks	25 cm ² , 75 cm ² , 175 cm ² , sterile, Sarstedt
Cell culture plates	12 well, 96 well, sterile, clear, flat bottom, Sarstedt
Cell scrapers	25 cm, Sarstedt
Columns for the concentration of media	Amicon Ultra-4, Ultracel-3k, Millipore
Cover slips	10 mm, round, Sigma-Aldrich
Culture dishes	10 cm, Sarstedt
Cuvettes	1.5 ml, Brand, Roth
Disposable serological pipettes	5 ml, 10 ml, 25 ml, sterile, Sarstedt
Falcon Tubes	15 ml, 50 ml, Sarstedt
Glass slides	75 mm x 25 mm, Sigma-Aldrich
His-column	HisPur ^{1M} Cobalt Spin Column, Pierce
Nitrocellulose membrane	Whatman, Protan BA 85, Roth
Parafilm	Bemis
PCR-Cups	Multiply-Pro® 0.2 mL, Sarstedt
Petri dishes	10 cm diameter, Sarstedt
Pipette tips	Sarstedt
Pipetting reservoirs	Bio-Pure, Sigma-Aldrich
Reaction tubes	Safe Seal Tubes, 1,5 ml, 2,0 ml, Sarstedt

Table 3.2 List of used consumables.

3.2.3 Materials

The following table 3.3 contains a list of the materials that were used in this thesis.

Materials	Suppliers
30% Acrylamide, 0,8% N,N'-Methylenebisacrylamide	Rotiphorese [®] Gel 20 (37,5:1), Roth
Agarose ultra pure	Ultrapure ^{1M} Agarose, Invitrogen
Ampicillin	AppliChem
Ammonium persulphate	Acros Organics
Bacto tryptone	Thermo Fisher Scientific
Bacto yeast extract	Thermo Fisher Scientific
BCIP	Roth
Bromophenol blue	AppliChem
BSA/ albumine fraction V	Roth
Cell lysis buffer	Promega
Disodium phosphate	Roth
DMEM	GIBCO [®] Invitrogen
DMF	ZVE, University of Bonn
DMSO	Fluka
Dry milk powder	Roth
EDTA	Fluka
Ethanol	ZVE, University of Bonn
FCS	Life Technologies
Gateway BP clonase enzyme mix	ThermoFisher Scientific
Gateway LR clonase enzyme mix	ThermoFisher Scientific
Gel Extraction Kit	MiniElute gel extraction kit, Qiagen
GelRed ^{1M} Nucleic Acid Gel Stain	Biotium
Glacial acetic acid	Merck
Glucose	Roth
Glycerol	AppliChem
Glycine	Roth
Halt Protease Inhibitor Cocktail (100x)	ThermoFisher Scientific

Hydrochloric acid 37%	ZVE, University of Bonn
Imidazole	AppliChem
Isopropyl alcohol	ZVE, University of Bonn
Kanamycin	Sigma-Aldrich
Lambda DNA/EcoRI + HindIII marker for agarose gels	Fermentas
LB-Agar-mixture	Invitrogen
LB-Broth powder	AppliChem
L-Glutamine	Life Technologies
Lipofectamine ^{1M} 2000	GIBCO [®] Life Technologies
Magnesium chloride	ZVE, University of Bonn
Magnesium sulfate	ZVE, University of Bonn
MES-monohydrate	AppliChem
Methanol	Sigma-Aldrich
Midi Präp Kit	Plasmid Midi Kit, Qiagen
Mini Präp Kit	PureLink Quick Plasmid Miniprep Kit, Thermo Fisher Scientific
MEM Non Essential Amino Acids	Invitrogen
MTT	Merck
NBT	Roth
Opti-MEM [®] Reduced Serum Medium	GIBCO [®] Life Technologies
Paraformaldehyde	Sigma-Aldrich
Penicillin-Streptomycin solution	Invitrogen
Phenol red	Sigma-Aldrich
Poly-D-lysine	Sigma-Aldrich
Ponceau S	AppliChem
Potassium chloride	ZVE, University of Bonn
Potassium dihydrogen phosphate	ZVE, University of Bonn
Protein staining solution	PageBlue Protein Staining Solution, Thermo Scientific
Protein-Marker	PageRuler Prestained Protein Ladder, Fermentas
RPMI	GIBCO [®] Life Technologies
Roti [®] -Nanoquant	Roth

SDS	Roth
SOC-Medium	Invitrogen
Sodium chloride	Grüssing
Sodium hydroxide	ZVE, University of Bonn
Sodium phosphate	ZVE, University of Bonn
Streptomycin	Sigma-Aldrich
TEMED	Roth
Trichloroacetic acid	Fluka
Trisodium phosphate	ZVE, University of Bonn
TRIS	Roth
Trypsin	Invitrogen
Tween-20	AppliChem
Zeocin	Thermo Fisher Scientific
β -Mercaptoethanol	AppliChem

Table 3.3 List of used materials.

3.2.4 Cell lines

In the following table 3.4 cell lines which were used in this thesis are listed.

Cell line	Characterization	Supplier
HEK	Human embryonic kidney cells	Stirnberg <i>et al.</i> ^[45]
HEK-mock	Human embryonic kidney cells stably transfected with mock	Stirnberg <i>et al.</i> ^[45]
HEK-MT2-Myc-His	HEK-cells stably transfected with MT2-Myc-His	Stirnberg <i>et al.</i> ^[45]
HEK-MT2-S753A	HEK-cells stably transfected with MT2-S753A	Stirnberg <i>et al.</i> ^[45]
Huh-7	Human hepatoma cells	Nakabayashi <i>et al.</i> ^[229]

Table 3.4 List of used cell lines.

3.2.5 Vectors

In the following table 3.5 the genetic vectors which were used and generated in this thesis are listed.

Vector name	Characterization	Supplier
pcDNA4-HJV	pcDNA4 vector encoding HJV	Stirnberg <i>et al.</i> ^[113]
pcDNA4-MT2-Myc-His	pcDNA4 vector encoding MT2-Myc-His	Stirnberg <i>et al.</i> ^[45]
pDONR223	Donor vector for the generation of gateway entry clones	Invitrogen
pGL3-HAMP	Reporter vector encoding the <i>Firefly</i> luciferase gene under control of the <i>HAMP</i> promoter	Maurer <i>et al.</i> ^[230]
pHTN-Halotag	Expression vector encoding the Halotag gene under control of the CMV promoter, ampicillin and neomycin resistance	Promega
pHTN-2Luc	Expression vector encoding Halotag-firefly luciferase and renilla luciferase under control of the CMV promoter, kanamycin resistance	This dissertation
pIRIGF	Destination vector encoding a gateway cassette, firefly luciferase and renilla luciferase under control of the CMV promoter, kanamycin resistance	Addgene
pRluc-N1	Expression vector encoding the <i>Renilla</i> luciferase gene under control of the CMV promoter, ampicillin and neomycin resistance	BioSignal Packard

Table 3.5 List of used vectors.

3.2.6 Enzymes

The following table 3.6 contains a list of the enzymes that were used in kinetic evaluation studies.

Enzyme	Source	Supplier
Matriptase	Human	R&D Systems
Matriptase-2	Human	HEK-MT2-MycHis cell cultures
Thrombin	Human	Enzo Life Sciences

Table 3.6 List of used enzymes.

3.2.7 Substrates

The following table 3.7 contains a list of the enzyme substrates that were used in this thesis.

Substrate	Substrate specificity	Supplier
Boc-Gln-Ala-Arg-AMC	MT1, MT2	Bachem
Cbz-Gly-Gly-Arg-AMC	Thrombin	Bachem
LarII	Firefly luciferase	Promega
Stop & Glo	Renilla luciferase	Promega

Table 3.7 List of enzyme substrates.

3.2.8 Antibodies, commercially available probes and dyes

The following table 3.8 contains a list of the antibodies, commercially available probes and dyes that were used in this thesis.

Antibody/ probe/ dye	Supplier
Alexa Fluor 488 secondary antibody (anti-mouse)	Thermo Fisher Scientific
Anti-firefly luciferase antibody	Thermo Fisher Scientific
Anti-HaloTag® monoclonal antibody	Promega
AP-conjugated secondary antibody (anti-mouse)	Merck Millipore
AP-conjugated secondary antibody (anti-rabbit)	Merck Millipore
Anti-Myc antibody 9E10	Evan <i>et al.</i> ^[251]
Chloromethyl ketone probe	American Peptide Company
DAPI	Thermo Fisher Scientific
FITC-Avidin	Thermo Fisher Scientific
Strep-Tactin-AP-conjugate	IBA Lifesciences

Table 3.8 List of antibodies, commercially available probes and dyes .

3.2.9 Buffers and solutions

In the following table 3.9 the buffers and solutions which were used in this thesis are listed.

Name of buffer or solution	Ingredients	Concentration of ingredients
1x PBS	KH ₂ PO ₄	4 mM
	NaCl	115 mM
	Na ₂ HPO ₄	16 mM
	in aqua dest.	
	Adjusted to pH 7.4	
1x PBS-T	KH ₂ PO ₄	4 mM
	NaCl	115 mM
	Na ₂ HPO ₄	16 mM
	Tween-20	0.1%
	in aqua dest. Adjusted to pH 7.4	
1x TBS	TRIS	20 mM
	NaCl	150 mM
	in aqua dest. Adjusted to pH 7.6	
1x TBS-T	TRIS	20 mM
	NaCl	150 mM
	Tween-20	0.1%
	in aqua dest. Adjusted to pH 7.6	
5x SDS loading buffer for SDS-PAGE	Bromphenol blue	0.05%
	Glycerol	30%
	SDS	20%
	TRIS	250 mM
	in aqua dest. Adjusted to pH 6.8	

Experimental section

6x loading buffer for agarose gels	Bromphenol blue	0.25%
	Glycerol in aqua dest.	50%
50x TAE buffer for agarose gel elektrophoresis	TRIS	2 M
	EDTA	50 mM
	Glacial acetic acid	5.71%
	in aqua dest	
BCIP solution	BCIP	5%
	in DMF	
Blocking buffer with BSA	BSA	3%
	KH ₂ PO ₄	4 mM
	NaCl	115 mM
	Na ₂ HPO ₄	16 mM
	Tween-20	0.1%
	in aqua dest.	
Blocking buffer with milk	Milk powder	5%
	NaCl	150 mM
	TRIS	20 mM
	Tween-20	0.1%
	in aqua dest.	
Factor Xa assay buffer	CaCl ₂	10 mM
	NaCl	100 mM
	TRIS	50 mM
	in aqua dest.	
	Adjusted to pH 8.0	
Matriptase-2 assay buffer	NaCl	150 mM
	TRIS	50 mM
	in aqua dest.	
	Adjusted to pH 8.0	
NBT solution	DMF	20%
	NBT	7.5%
	in aqua dest.	

Experimental section

Ponceau S solution	Ponceau S	0.2%
	Trichloro acetic acid in aqua dest.	3%
Reaction buffer for immunoblotting	MgCl ₂	
	NaCl	
	TRIS	
	in aqua dest. Adjusted to pH 8.8	
SDS running buffer for SDS- PAGE	Glycine	200 mM
	SDS	0.1%
	TRIS	25 mM
	in aqua dest.	
Transfer buffer for western blotting	Glycine	200 mM
	Methanol	20%
	TRIS	25 mM
	in aqua dest.	

Table 3.9 List of buffers and solutions.

4 References

1. Hartley, B. S. Proteolytic Enzymes. *Annu. Rev. Biochem.* **1960**, *29*, 45-72. doi:10.1146/annurev.bi.29.070160.000401
2. Paschkowsky, S.; Hsiao, J. M.; Young, J.; Munter, L. M. The Discovery of Proteases and Intramembrane Proteolysis. *Biochem. Cell Biol.* **2018**, [Epub ahead of print]. doi:10.1139/bcb-2018-0186
3. Schechter, I.; Berger, A. On the Size of the Active Site in Proteases. I. Papain. *Biochem. Biophys. Res. Commun.* **1967**, *27*, 157-162.
4. Fujinaga, M.; Cherney, M. M.; Oyama, H.; Oda, K.; James, M. N. The Molecular Structure and Catalytic Mechanism of a Novel Carboxyl Peptidase from *Scytalidium lignicolum*. *Proc. Natl. Acad. Sci. USA.* **2004**, *101*, 3364-3369. doi:10.1073/pnas.0400246101
5. Jensen, K.; Ostergaard, P. R.; Wilting, R.; Lassen, S. F. Identification and Characterization of a Bacterial Glutamic Peptidase. *BMC Biochem.* **2010**, *11*, 47. doi:10.1186/1471-2091-11-47
6. Sims, A. H.; Dunn-Coleman, N. S.; Robson, G. D.; Oliver, S. G. Glutamic Protease Distribution is Limited to Filamentous Fungi. *FEMS Microbiol. Lett.* **2004**, *239*, 95-101. doi:10.1016/j.femsle.2004.08.023
7. Quesada, V.; Ordóñez, G. R.; Sánchez, L. M.; Puente, X. S.; López-Otín, C. The Degradome Database: Mammalian Proteases and Diseases of Proteolysis. *Nucleic Acids Res.* **2009**, *37* (Database issue), D239-243. doi: 10.1093/nar/gkn570
8. Rawlings, N. D.; Barrett, A. J.; Thomas, P. D.; Huang, X.; Bateman, A.; Finn, R. D. The MEROPS Database of Proteolytic Enzymes, their Substrates and Inhibitors in 2017 and a Comparison with Peptidases in the PANTHER Database. *Nucleic Acids Res.* **2018**, *46* (Database issue), D624-632. doi: 10.1093/nar/gkx1134
9. Kappelhoff, R.; Puente, X. S.; Wilson, C. H.; Seth, A.; López-Otín, C.; Overall, C. M. Overview of Transcriptomic Analysis of All Human Proteases, Non-Proteolytic Homologs and Inhibitors: Organ, Tissue and Ovarian Cancer Cell Line Expression Profiling of the Human Protease Degradome by the CLIP-CHIP™ DNA Microarray. *Biochim. Biophys. Acta Mol. Cell Res.* **2017**, *1864*, 2210-2219. doi: 10.1016/j.bbamcr.2017.08.004
10. Chakraborti, S.; Chakraborti, T.; Dhalla, N.S. Proteases in Human Diseases. Springer, Singapore **2017**, doi: 10.1007/978-981-10-3162-5
11. Page, M. J.; Di Cera, E. Serine Peptidases: Classification, Structure and Function. *Cell. Mol. Life Sci.* **2008**, *65*, 1220-1236. doi: 10.1007/s00018-008-7565-9
12. Polgár, L. The Catalytic Triad of Serine Peptidases. *Cell. Mol. Life Sci.* **2005**, *62*, 2161-2172. doi: 10.1007/s00018-005-5160-x
13. Hedstrom, L. Serine Protease Mechanism and Specificity. *Chem. Rev.* **2002**, *102*, 4501-4524. doi: 10.1021/cr000033x

14. Di Cera, E. Serine Proteases. *IUBMB Life* **2009**, *61*, 510-515. doi: 10.1002/iub.186
15. Tanaka, K. A.; Key, N. S.; Levy, J. H. Blood Coagulation: Hemostasis and Thrombin Regulation. *Anesth. Analg.* **2009**, *108*, 1433-1446. doi: 10.1213/ane.0b013e31819bcc9c
16. Rothman, S. S. The Digestive Enzymes of the Pancreas: a Mixture of Inconstant Proportions. *Annu. Rev. Physiol.* **1977**, *39*, 373-389. doi: 10.1146/annurev.ph.39.030177.002105
17. Heutinck, K. M.; ten Berge, I. J.; Hack, C. E.; Hamann, J.; Rowshani, A. T. Serine Proteases of the Human Immune System in Health and Disease. *Mol. Immunol.* **2010**, *47*, 1943-1955. doi: 10.1016/j.molimm.2010.04.020
18. Pavlov, I. P. The Work of the Digestive Glands. *Bristol Med. Chir. J.* **1883**, *21*, 158-159 (1903).
19. Hooper, J. D.; Clements, J. A.; Quigley, J. P.; Antalis, T. M. Type II Transmembrane Serine Proteases. Insights into an Emerging Class of Cell Surface Proteolytic Enzymes. *J. Biol. Chem.* **2001**, *276*, 857-860. doi: 10.1074/jbc.R109.021006
20. Yan, W.; Wu, F.; Morser, J.; Wu, Q. Corin, a Transmembrane Cardiac Serine Protease, Acts as a Pro-Atrial Natriuretic Peptide-Converting Enzyme. *Proc. Natl. Acad. Sci. USA.* **2000**, *97*, 8525-8529. doi: 10.1073/pnas.150149097
21. Huber, R.; Bode, W. Structural Basis of the Activation and Action of Trypsin. *Acc. Chem. Res.* **1978**, *11*, 114-122.
22. List, K.; Haudenschild, C. C.; Szabo, R, *et al.* Matriptase/MT-SP1 is Required for Postnatal Survival, Epidermal Barrier Function, Hair Follicle Development, and Thymic Homeostasis. *Oncogene* **2002**, *21*, 3765-3779. doi: 10.1038/sj.onc.1205502
23. Donaldson, S. H.; Hirsh, A.; Li, D. C.; *et al.* Regulation of the Epithelial Sodium Channel by Serine Proteases in Human Airways. *J. Biol. Chem.* **2002**, *277*, 8338-8345. doi: 10.1074/jbc.M105044200
24. Murray, A. S.; Varela, F. A.; List, K. Type II Transmembrane Serine Proteases as Potential Targets for Cancer Therapy. *Biol. Chem.* **2016**, *397*, 815-826. doi: 10.1515/hsz-2016-0131
25. Webb, S. L.; Sanders, A. J.; Mason, M. D.; Jiang, W. G. Type II Transmembrane Serine Protease (TTSP) Deregulation in Cancer. *Front. Biosci. (Landmark Ed.)* **2011**, *16*, 539-555.
26. Tanabe, L. M.; List, K. The Role of Type II Transmembrane Serine Protease-Mediated Signaling in Cancer. *FEBS J.* **2017**, *284*, 1421-1436. doi: 10.1111/febs.13971
27. Shin, W. J.; Seong, B. L. Type II Transmembrane Serine Proteases as Potential Target for Anti-Influenza Drug Discovery. *Expert Opin. Drug Discov.* **2017**, *12*, 1139-1152. doi: 10.1080/17460441.2017.1372417
28. Choi, S. Y.; Bertram, S.; Glowacka, I.; Park, Y. W.; Pöhlmann, S. Type II Transmembrane Serine Proteases in Cancer and Viral Infections. *Trends Mol. Med.* **2009**, *15*, 303-312. doi: 10.1016/j.molmed.2009.05.003

29. Lee, S. L.; Dickson, R. B.; Lin, C. Y. Activation of Hepatocyte Growth Factor and Urokinase/Plasminogen Activator by Matriptase, an Epithelial Membrane Serine Protease. *J. Biol. Chem.* **2000**, *275*, 36720–36725. doi: 10.1074/jbc.M007802200
30. Lin, B.; Ferguson, C.; White, J. T.; Wang, S.; Vessella, R.; True, L. D.; Hood, L.; Nelson, P. S. Prostate-Localized and Androgen-Regulated Expression of the Membrane-Bound Serine Protease TMPRSS2. *Cancer Res.* **1999**, *59*, 4180–4184.
31. Szabo, R.; Bugge, T. H. Type II Transmembrane Serine Proteases in Development and Disease. *Int. J. Biochem. Cell Biol.* **2008**; *40*, 1297–1316. doi: 10.1016/j.biocel.2007.11.013
32. Bugge, T. H.; Antalis, T. M.; Wu, Q. Type II Transmembrane Serine Proteases. *J. Biol. Chem.* **2009**; *284*, 23177–23181. doi: 10.1074/jbc.R109.021006
33. Cal, S.; Quesada, V.; Llamazares, M.; Díaz-Perales, A.; Garabaya, C.; López-Otín, C. Human Polyserase-2, a Novel Enzyme with Three Tandem Serine Protease Domains in a Single Polypeptide Chain. *J. Biol. Chem.* **2005**, *280*, 1953–1961. doi: 10.1074/jbc.M409139200
34. Cal, S.; Peinado, J. R.; Llamazares, M.; Quesada, V.; Moncada-Pazos, A.; Garabaya, C.; López-Otín, C. Identification and Characterization of Human Polyserase-3, a Novel Protein with Tandem Serine-Protease Domains in the Same Polypeptide Chain. *BMC Biochem.* **2006**, *7*, 9. doi: 10.1186/1471-2091-7-9
35. Netzel-Arnett, S.; Hooper, J. D.; Szabo, R.; Madison, E. L.; Quigley, J. P.; Bugge, H.; Antalis, T. M. Membrane Anchored Serine Proteases : A Rapidly Expanding Group of Cell Surface Proteolytic Enzymes with Potential Roles in Cancer. *Cancer Metastasis Rev.* **2003**, *22*, 237–258.
36. Stirnberg, M.; Gütschow, M. Matriptase-2, a Regulatory Protease of Iron Homeostasis: Possible Substrates, Cleavage Sites and Inhibitors. *Curr. Pharm. Des.* **2013**, *19*, 1052–1061. doi: 10.3324/haematol.2008.001867
37. Velasco, G.; Cal, S.; Quesada, V.; Sánchez, L. M.; López-Otín, C. Matriptase-2, a Membrane-Bound Mosaic Serine Proteinase Predominantly Expressed in Human Liver and Showing Degrading Activity against Extracellular Matrix Proteins. *J. Biol. Chem.* **2002**, *277*, 37637–37646. doi: 10.1074/jbc.M203007200
38. Velasco, G.; Cal, S.; Quesada, V.; Sánchez, L. M.; López-Otín, C. Withdrawal: Matriptase-2, a Membrane-Bound Mosaic Serine Proteinase Predominantly Expressed in Human Liver and Showing Degrading Activity against Extracellular Matrix Proteins. *J. Biol. Chem.* **2019**, *294*, 1430. doi: 10.1074/jbc.W118.007324
39. Hooper, J. D.; Campagnolo, L.; Goodarzi, G.; Truong, T. N.; Stuhlmann, H.; Quigley, J. P. Mouse Matriptase-2: Identification, Characterization and Comparative mRNA Expression Analysis with Mouse Hepsin in Adult and Embryonic Tissues. *Biochem. J.* **2003**, *373*, 689–702. doi: 10.1042/bj20030390
40. Dion, S. P.; Béliveau, F.; Désilets, A.; Ghinet, M. G.; Leduc, R. Transcriptome Analysis Reveals TMPRSS6 Isoforms with Distinct Functionalities. *J. Cell. Mol. Med.* **2018**, *22*, 2498–2509. doi: 10.1111/jcmm.13562

41. Ramsay, A. J.; Reid, J. C.; Velasco, G.; Quigley, J. P.; Hooper, J. D. The Type II Transmembrane Serine Protease Matriptase-2. Identification, Structural Features, Enzymology, Expression Pattern and Potential Roles. *Front. Biosci.* **2008**, *13*, 569-579.
42. Béliveau, F.; Brule, C.; Desilets, A.; Zimmerman, B.; Laporte, S. A.; Lavoie, C. L.; and Leduc, R. Essential Role of Endocytosis of the Type II Transmembrane Serine Protease TMPRSS6 in Regulating its Functionality. *J. Biol. Chem.* **2011**, *286*, 29035-29043. doi: 10.1074/jbc.M111.223461
43. Mao, P.; Wortham, A. M.; Enns, C. A.; Zhang, A. S. The Catalytic, Stem, and Transmembrane Portions of Matriptase-2 are Required for Suppressing the Expression of the Iron-Regulatory Hormone Hepcidin. *J. Biol. Chem.* **2019**, *294*, 2060-2073. doi: 10.1074/jbc.RA118.006468
44. McDonald, C. J.; Ostini, L.; Bennett, N.; Subramaniam, N.; Hooper, J.; Velasco, G.; Wallace, D. F.; Subramaniam, V. N. Functional Analysis of Matriptase-2 Mutations and Domains: Insights into the Molecular Basis of Iron-Refractory Iron Deficiency Anemia. *Am. J. Physiol. Cell. Physiol.* **2015**, *308*, C539-C547. doi: 10.1152/ajpcell.00264.2014
45. Stirnberg, M.; Maurer, E.; Horstmeyer, A.; Kolp, S.; Frank, S.; Bald, T.; Arenz, K.; Janzer, A.; Prager, K.; Wunderlich, P.; Walter, J.; Gütschow, M. Proteolytic Processing of the Serine Protease Matriptase-2: Identification of the Cleavage Sites Required for its Autocatalytic Release from the Cell Surface. *Biochem. J.* **2010**, *430*, 87-95. doi: 10.1042/BJ20091565
46. Jiang, J.; Yang, J.; Feng, P.; Dong, N.; Wu, Q.; He, Y. N-Glycosylation is Required for Matriptase-2 Autoactivation and Ectodomain Shedding. *J. Biol. Chem.* **2014**, *289*, 19500-19507. doi: 10.1074/jbc.M114.555110
47. Andrews, N. C. Forging a Field: The Golden Age of Iron Biology. *Blood* **2008**, *112*, 219-230. doi: 10.1182/blood-2007-12-077388
48. Du, X.; She, E.; Gelbart, T.; Truksa, J.; Lee, P.; Xia, Y.; Khovananth, K.; Mudd, S.; Mann, N.; Moresco, E. M.; Beutler, E.; Beutler, B. The Serine Protease TMPRSS6 is Required to Sense Iron Deficiency. *Science* **2008**, *320*, 2539-2545. doi: 10.1126/science.1157121
49. Finberg, K. E.; Heeney, M. M.; Campagna, D. R.; Aydmok, Y.; Pearson, H. A.; Hartman, K. R.; Mayo, M. M.; Samuel, S. M.; Strouse, J. J.; Markianos, K.; Andrews, N. C.; Fleming, M. D. Mutations in TMPRSS6 Cause Iron-Refractory Iron Deficiency Anemia (IRIDA). *Nat. Genet.* **2008**, *40*, 569-571. doi: 10.1038/ng.130
50. Folgueras, A. R.; de Lara, F. M.; Pendás, A. M.; Garabaya, C.; Rodriguez, F.; Astudillo, A.; Bernal, T.; Cabanillas, R.; López-Otín, C. Membrane-Bound Serine Protease Matriptase-2 (Tmprss6) Is an Essential Regulator of Iron Homeostasis. *Blood* **2008**, *112*, 2539-2546. doi: 10.1182/blood-2008-04-149773
51. Shayeghi, M.; Latunde-Dada, G. O.; Oakhill, J. S.; Laftah, A. H.; Takeuchi, K.; Halliday, N.; Khan, Y.; Warley, A.; McCann, F. E.; Hider, R. C.; Frazer, D. M.; Anderson, G. J.; Vulpe, C. D.; Simpson, R. J.; McKie, A. T. Identification of an Intestinal Heme Transporter. *Cell* **2005**, *122*, 789-801. doi:10.1016/j.cell.2005.06.025

-
52. Yuan, X.; Fleming, M. D.; Hamza, I. Heme Transport and Erythropoiesis. *Curr. Opin. Chem. Biol.* **2013**, *17*, 204–211. doi: 10.1016/j.cbpa.2013.01.010
53. Donovan, A.; Lima, C. A.; Pinkus, J. L.; Pinkus, G. S.; Zon, L. I.; Robine, S.; Andrews, N. C. The Iron Exporter Ferroportin/Slc40a1 Is Essential for Iron Homeostasis. *Cell Metab.* **2005**, *1*, 191–200. doi:10.1016/j.cmet.2005.01.003
54. Nemeth, E.; Tuttle, M. S.; Powelson, J.; Vaughn, M. B.; Donovan, A.; Ward, D. M.; Ganz, T.; Kaplan, J. Hepcidin Regulates Cellular Iron Efflux by Binding to Ferroportin and Inducing its Internalization. *Science* **2004**, *306*, 2090–2093. doi: 10.1126/science.1104742
55. Nemeth, E. Targeting the Hepcidin-Ferroportin Axis in the Diagnosis and Treatment of Anemias. *Adv. Hematol.* **2010**, *750643*, doi:10.1155/2010/750643
56. Ganz, T.; Nemeth, E. Hepcidin and Iron Homeostasis. *Biochim. Biophys. Acta* **2012**, *1823*, 1434–1443. doi: 10.1016/j.bbamcr.2012.01.014
57. Folgueras, A. R.; Freitas-Rodríguez, S.; Ramsay, A. J.; Garabaya, C.; Rodríguez, F.; Velasco, G.; López-Otín, C. Matriptase-2 Deficiency Protects from Obesity by Modulating Iron Homeostasis. *Nat. Commun.* **2018**, *9*, 1350. doi: 10.1038/s41467-018-03853-1
58. Finberg, K. E.; Whittlesey, R. L.; Fleming, M. D.; Andrews, N. C. Down-Regulation of Bmp/Smad Signaling by Tmprss6 Is Required for Maintenance of Systemic Iron Homeostasis. *Blood* **2010**, *115*, 3817–3826. doi:10.1182/blood-2009-05-224808
59. Zhang, A. S.; Xiong, S.; Tsukamoto, H.; Enns, C. A. Localization of Iron Metabolism-Related MRNAs in Rat Liver Indicate That HFE Is Expressed Predominantly in Hepatocytes. *Blood* **2003**, *103*, 1509–1514. doi:10.1182/blood-2003-07-2378
60. Zhang, A. S.; Yang, F.; Wang, J.; Tsukamoto, H.; Enns, C. A. Hemojuvelin-Neogenin Interaction Is Required for Bone Morphogenic Protein-4-Induced Hepcidin Expression. *J. Biol. Chem.* **2009**, *284*, 22580–22589. doi:10.1074/jbc.M109.027318
61. Muckenthaler MU, Rivella S, Hentze MW, Galy B. A Red Carpet for Iron Metabolism. *Cell* **2017**, *168*, 344–361.
62. D'Alessio, F.; Hentze, M. W.; Muckenthaler, M. U. The Hemochromatosis Proteins HFE, TfR2, and HJV Form a Membrane-Associated Protein Complex for Hepcidin Regulation. *J. Hepatol.* **2012**, *57*, 1052–1060.
63. Papanikolaou, G.; Samuels, M. E.; Ludwig, E. H.; MacDonald, M. L.; Franchini, P. L.; Dube, M. P.; Andres, L.; MacFarlane, J.; Sakellaropoulos, N.; Politou, M.; Nemeth, E.; Thompson, J.; Risler, J. K.; Zaborowska, C.; Babakoff, R.; Radomski, C. C.; Pape, T. D.; Davidas, O.; Christakis, J.; Brissot, P.; Lockitch, G.; Ganz, T.; Hayden, M. R.; Goldberg, Y. P. Mutations in HFE2 Cause Iron Overload in Chromosome 1q-Linked Juvenile Hemochromatosis. *Nat. Genet.* **2004**, *36*, 77–82. doi: 10.1038/ng1274
64. Lee, P. Role of Matriptase-2 (TMPRSS6) in Iron Metabolism. *Acta Haematol.* **2009**, *122*, 87–96. doi: 10.1159/000243792
65. Silvestri, L.; Pagani, A.; Nai, A.; De Domenico, I.; Kaplan, J.; Camaschella, C. The Serine Protease Matriptase-2 (TMPRSS6) Inhibits Hepcidin Activation by Cleaving

- Membrane Hemojuvelin. *Cell Metab.* **2008**, *8*, 502-511. doi: 10.1016/j.cmet.2008.09.012
66. Wahedi, M.; Wortham, A. M.; Kleven, M. D.; Zhao, N.; Jue, S.; Enns, C. A.; Zhang, A. S. Matriptase-2 Suppresses Heparin Expression by Cleaving Multiple Components of the Heparin Induction Pathway. *J. Biol. Chem.* **2017**, *292*, 18354–18371. doi: 10.1074/jbc.M117.801795
67. Gibert, Y.; Lattanzi, V. J.; Zhen, A. W.; Vedder, L.; Brunet, F.; Faasse, S. A.; Babitt, J. L.; Lin, H. Y.; Hammerschmidt, M.; Fraenkel, P. G. BMP Signaling Modulates Heparin Expression in Zebrafish Embryos Independent of Hemojuvelin. *PLoS One* **2011**, *6*, e14553. doi: 10.1371/journal.pone.0014553
68. Lenoir, A.; Deschemin, J. C.; Kautz, L.; Ramsay, A. J.; Roth, M. P.; López-Otín, C.; Vaulont, S.; Nicolas, G. Iron-Deficiency Anemia from Matriptase-2 Inactivation Is Dependent on the Presence of Functional Bmp6. *Blood* **2011**, *117*, 647–650. doi: 10.1182/blood-2010-07-295147
69. Altamura, S.; Alessio, F. D.; Selle, B.; Muckenthaler, M. U. A Novel TMPRSS6 Mutation That Prevents Protease Auto-Activation Causes IRIDA. *Biochem. J.* **2010**, *431*, 363–371. doi: 10.1042/BJ20100668
70. De Falco, L.; Sanchez, M.; Silvestri, L.; Kannengiesser, C.; Muckenthaler, M. U.; Iolascon, A.; Gouya, L.; Camaschella, C.; Beaumont, C. Iron Refractory Iron Deficiency Anemia. *Haematologica* **2013**, *98*, 845–853. doi: 10.3324/haematol.2012.075515
71. Yaish, H. M.; Farrell, C. P.; Christensen, R. D.; MacQueen, B. C.; Jackson, L. K.; Trochez-Enciso, J.; Kaplan, J.; Ward, D. M.; Salah, W. K.; Phillips, J. D. Two Novel Mutations in TMPRSS6 Associated with Iron-Refractory Iron Deficiency Anemia in a Mother and Child. *Blood Cells Mol. Dis.* **2017**, *65*, 38–40. doi: 10.1016/j.bcmed.2017.04.002
72. Pietrangelo, A. Hereditary Hemochromatosis: Pathogenesis, Diagnosis, and Treatment. *Gastroenterology* **2010**, *139*, 393–408. doi: 10.1053/j.gastro.2010.06.013
73. Babitt, J.; Lin, H. The Molecular Pathogenesis of Hereditary Hemochromatosis. *Semin. Liver Dis.* **2011**, *31*, 280–292. doi: 10.1055/s-0031-1286059
74. Guo, S.; Casu, C.; Gardenghi, S.; Booten, S.; Aghajan, M.; Peralta, R.; Watt, A.; Freier, S.; Monia, B. P.; Rivella, S. Reducing TMPRSS6 Ameliorates Hemochromatosis and β -Thalassemia in Mice. *J. Clin. Invest.* **2013**, *123*, 1531–1541. doi: 10.1172/JCI66969
75. Schmidt, P. J.; Toudjarska, I.; Sendamarai, A. K.; Racie, T.; Milstein, S.; Bettencourt, B. R.; Hettinger, J.; Bumcrot, D.; Fleming, M. D. An RNAi Therapeutic Targeting Tmprss6 Decreases Iron Overload in Hfe^{-/-} Mice and Ameliorates Anemia and Iron Overload in Murine β -Thalassemia Intermedia. *Blood* **2013**, *121*, 1200–1208. doi: 10.1182/blood-2012-09-453977
76. Koblinski, J. E.; Ahram, M.; Sloane, B. F. Unraveling the Role of Proteases in Cancer. *Clin. Chim. Acta.* **2000**, *291*, 113–135.

77. Mason, S. D.; Joyce, J. A. Proteolytic Networks in Cancer. *Trends Cell Biol.* **2011**, *21*, 228–237. doi: 10.1016/j.tcb.2010.12.002
78. Eatemadi, A.; Aiyelabegan, H. T.; Negahdari, B.; Mazlomi, M. A.; Daraee, H.; Daraee, N.; Eatemadi, R.; Sadroddiny, E. Role of Protease and Protease Inhibitors in Cancer Pathogenesis and Treatment. *Biomed. Pharmacother.* **2017**, *86*, 221–231. doi: 10.1016/j.biopha.2016.12.021
79. Shi, Y. E.; Torri, J.; Yieh, L.; Wellstein, A.; Lippman, M. E.; Dickson, R. B. Identification and Characterisation of a Novel Matrix-Degrading Protease from Hormone-Dependent Human Breast Cancer Cells. *Cancer Res.* **1993**, *53*, 1409–1415.
80. Bergum, C.; List, K. Loss of the Matriptase Inhibitor HAI-2 during Prostate Cancer Progression. *Prostate* **2010**, *70*, 1422–1428. doi: 10.1002/pros.21177
81. Murray, A. S.; Varela, F. A.; List, K. Type II Transmembrane Serine Proteases as Potential Targets for Cancer Therapy. *Biol. Chem.* **2016**, *397*, 815–826. doi: 10.1515/hsz-2016-0131
82. Jin, X.; Yagi, M.; Akiyama, N.; Hirosaki, T.; Higashi, S.; Lin, C. Y.; Dickson, R. B.; Kitamura, H.; Miyazaki, K. Matriptase Activates Stromelysin (MMP-3) and Promotes Tumor Growth and Angiogenesis. *Cancer Sci.* **2006**, *97*, 1327–1334. doi: 10.1111/j.1349-7006.2006.00328.x
83. Overall, C. M.; Tam, E. M.; Kappelhoff, R.; Connor, A.; Ewart, T.; Morrison, C. J.; Puente, X.; López-Otín, C.; Seth, A. Protease Degradomics: Mass Spectrometry Discovery of Protease Substrates and the CLIP-CHIP, a Dedicated DNA Microarray of All Human Proteases and Inhibitors. *Biol. Chem.* **2004**, *385*, 493–504. doi: 10.1515/BC.2004.058
84. Parr, C.; Sanders, A. J.; Davies, G.; Martin, T.; Lane, J.; Mason, M. D.; Mansel, R. E.; Jiang, W. G. Matriptase-2 Inhibits Breast Tumor Growth and Invasion and Correlates with Favorable Prognosis for Breast Cancer Patients. *Clin. Cancer Res.* **2007**, *13*, 3568–3576. doi: 10.1158/1078-0432.CCR-06-2357
85. Sanders, A. J.; Parr, C.; Martin, T. A.; Lane, J.; Mason, M. D.; Jiang, W. G. Genetic Upregulation of Matriptase-2 Reduces the Aggressiveness of Prostate Cancer Cells *in Vitro* and *in Vivo* and affects FAK and paxillin localisation. *J. Cell. Physiol.* **2008**, *216*, 780–789. doi: 10.1002/jcp.21460
86. Cheng, M. F.; Lin, L. H.; Huang, M. S.; Lee, H. S.; Ji, D. D.; Lin, C. S.; Hsia, K. T. Downexpression of Matriptase-2 Correlates With Tumor Progression and Clinical Prognosis in Oral Squamous-Cell Carcinoma. *Appl. Immunohistochem. Mol. Morphol.* **2017**, *25*, 481–488. doi: 10.1097/PAI.0000000000000324
87. Tuhkanen, H.; Hartikainen, J. M.; Soini, Y.; Velasco, G.; Sironen, R.; Nykopp, T. K.; Kataja, V.; Eskelinen, M.; Kosma, V. M.; Mannermaa, A. Matriptase-2 Gene (*TMPRSS6*) Variants Associate with Breast Cancer Survival, and Reduced Expression Is Related to Triple-Negative Breast Cancer. *Int. J. Cancer* **2013**, *133*, 2334–2340. doi: 10.1002/ijc.28254
88. Webb, S. L.; Sanders, A. J.; Mason, M. D.; Jiang, W. G. The Influence of Matriptase-2 on Prostate Cancer *in Vitro*: A Possible Role for β -Catenin. *Oncol. Rep.* **2012**, *28*, 1491–1497, doi: 10.3892/or.2012.1945

89. Webb, S. L.; Sanders, A. J.; Mason, M. D.; Jiang, W. G. Matriptase-2 Inhibits HECV Motility and Tubule Formation *in Vitro* and Tumour Angiogenesis *in Vivo*. *Mol. Cell Biochem.* **2013**, *375*, 207-217. doi: 10.1007/s11010-012-1544-z
90. Reichert, C. O.; da Cunha, J.; Levy, D.; Maselli, L. M. F.; Bydlowski, S. P.; Spada, C. Homeostasis and Diseases Related to Iron Metabolism. *Acta Haematol.* **2017**, *137*, 220-236. doi: 10.1159/000471838
91. Ginzburg, Y.; Rivella, S. Beta-Thalassemia: a Model for Elucidating the Dynamic Regulation of Ineffective Erythropoiesis and Iron Metabolism. *Blood* **2011**, *118*, 4321-4330. doi: 10.1182/blood-2011-03-283614
92. Taher, A. T.; Musallam, K. M.; Cappellini, M. D.; Weatherall, D. J. Optimal Management of Beta Thalassaemia Intermedia. *Br. J. Haematol.* **2011**, *152*, 512-523. doi: 10.1097/MPH.0000000000000914
93. Arezes, J.; Nemeth, E. Hepcidin and Iron Disorders: New Biology and Clinical Approaches. *Int. J. Lab. Hematol.* **2015**, *37*, 92-98. doi: 10.1111/ijlh.12358
94. Papanikolaou, G.; Tzilianos, M.; Christakis, J. I.; Bogdanos, D.; Tsimirika, K.; MacFarlane, J.; Goldberg, P. Y.; Sakellaropoulos, N.; Ganz, T.; Nemeth, E. Hepcidin in Iron Overload Disorders. *Blood* **2005**, *105*, 4103-4105. doi: 10.1182/blood-2004-12-4844
95. Origa, R.; Galanello, R.; Ganz, T.; Giagu, N.; Maccioni, L.; Faa, G.; Nemeth, E. Liver Iron Concentrations and Urinary Hepcidin in beta-Thalassemia. *Haematologica* **2007**, *92*, 583-588. doi: 10.3324/haematol.10842
96. Mobarra, N.; Shanaki, M.; Ehteram, H.; Nasiri, H.; Sahmani, M.; Saeidi, M.; Goudarzi, M.; Pourkarim, H.; Azad, M. A Review on Iron Chelators in Treatment of Iron Overload Syndromes. *Int. J. Hematol. Oncol. Stem Cell Res.* **2016**, *10*, 239-247.
97. Finberg, K. E.; Whittlesey, R. L.; Andrews, N. C. Tmprss6 is a Genetic Modifier of the Hfe-Hemochromatosis Phenotype in Mice. *Blood* **2011**, *117*, 4590-4599. doi: 10.1182/blood-2010-10-315507
98. Nai, A.; Pagani, A.; Mandelli, G.; Lidonnici, M. R.; Silvestri, L.; Ferrari, G.; Camaschella, C. Deletion of TMPRSS6 Attenuates the Phenotype in a Mouse Model of beta-Thalassemia. *Blood* **2012**, *119*, 5021-5029. doi: 10.1182/blood-2012-01-401885
99. Lee, P.; Hsu, M. H.; Welser-Alves, J.; Peng, H. Severe Microcytic Anemia but Increased Erythropoiesis in Mice Lacking Hfe or Tfr2 and Tmprss6. *Blood Cells Mol. Dis.* **2012**, *48*, 173-178. doi: 10.1016/j.bcmd.2011.12.005
100. Häußler, D.; Mangold, M.; Furtmann, N.; Braune, A.; Blaut, M.; Bajorath, J.; Stirnberg, M.; Gütschow, M. Phosphono Bisbenzguanidines as Irreversible Dipeptidomimetic Inhibitors and Activity-Based Probes of Matriptase-2. *Chemistry* **2016**, *22*, 8525-8535. doi: 10.1002/chem.201600206
101. Mertens, M. D.; Schmitz, J.; Horn, M.; Furtmann, N.; Bajorath, J.; Mareš, M.; Gütschow, M. A Coumarin-Labeled Vinyl Sulfone as Tripeptidomimetic Activity-Based Probe for Cystein Cathepsins. *Chem. Bio. Chem.* **2014**, *15*, 955-959. doi: 10.1002/cbic.201300806

102. Frizler, M.; Mertens, M. D.; Gütschow, M. Fluorescent Nitrile-Based Inhibitors of Cysteine Cathepsins. *Bioorg. Med. Chem. Lett.* **2012**, *22*, 7715-7718. doi: 10.1016/j.bmcl.2012.09.086
103. Sisay, M. T.; Steinmetzer, T.; Stirnberg, M.; Maurer, E.; Hammami, M.; Bajorath, J.; Gütschow, M. Identification of the First Low-Molecular-Weight Inhibitors of Matriptase-2. *J. Med. Chem.* **2010**, *53*, 5523-5535. doi: 10.1021/jm100183e
104. Duchêne, D.; Colombo, E.; Désilets, A.; Boudreault, P. L.; Leduc, R.; Marsault, E.; Najmanovich, R. Analysis of Subpocket Selectivity and Identification of Potent Selective Inhibitors for Matriptase and Matriptase-2. *J. Med. Chem.* **2014**, *57*, 10198-10204. doi: 10.1021/jm5015633
105. Beckmann, A. M.; Maurer, E.; Lülldorff, V.; Wilms, A.; Furtmann, N.; Bajorath, J.; Gütschow, M.; Stirnberg, M. En Route to New Therapeutic Options for Iron Overload Diseases: Matriptase-2 as a Target for Kunitz-Type Inhibitors. *Chem. Bio. Chem.* **2016**, *17*, 595-604. doi: 10.1002/cbic.201500651
106. St-Georges, C.; Désilets, A.; Béliveau, F.; Ghinet, M.; Dion, S. P.; Colombo, É.; Boudreault, P. L.; Najmanovich, R. J.; Leduc, R.; Marsault, É. Modulating the Selectivity of Matriptase-2 Inhibitors with Unnatural Amino Acids. *Eur. J. Med. Chem.* **2017**, *129*, 110-123. doi: 10.1016/j.ejmech.2017.02.006
107. Rausa, M.; Ghitti, M.; Pagani, A.; Nai, A.; Campanella, A.; Musco, G.; Camaschella, C.; Silvestri, L. Identification of TMPRSS6 Cleavage Sites of Hemojuvelin. *J. Cell Mol. Med.* **2015**, *19*, 879-888. doi: 10.1111/jcmm.12462
108. Wysocka, M.; Gruba, N.; Miecznikowska, A.; Popow-Stellmaszyk, J.; Gütschow, M.; Stirnberg, M.; Furtmann, N.; Bajorath, J.; Lesner, A.; Rolka, K. Substrate Specificity of Human Matriptase-2. *Biochimie* **2014**, *97*, 121-127. doi: 10.1016/j.biochi.2013.10.001
109. Barré, O.; Dufour, A.; Eckhard, U.; Kappelhoff, R.; Béliveau, F.; Leduc, R.; Overall, C. M. Cleavage Specificity Analysis of Six Type II Transmembrane Serine Proteases (TTSPs) Using PICS with Proteome-Derived Peptide Libraries. *PLoS One* **2014**, *9*, e105984. doi: 10.1371/journal.pone.0105984
110. Béliveau, F.; Désilets, A.; Leduc, R. Probing the Substrate Specificities of Matriptase, Matriptase-2, Hepsin and DESC1 with Internally Quenched Fluorescent Peptides. *FEBS J.* **2009**, *276*, 2213-2226. doi: 10.1111/j.1742-4658.2009.06950.x
111. Dosa, S.; Stirnberg, M.; Lülldorff, V.; Häußler, D.; Maurer, E.; Gütschow, M. Active Site Mapping of Trypsin, Thrombin and Matriptase-2 by Sulfamoyl Benzamidines. *Bioorg. Med. Chem.* **2012**, *20*, 6489-6505. doi: 10.1016/j.bmcl.2012.08.042
112. Maxson, J. E.; Chen, J.; Enns, C. A.; Zhang, A. S. Matriptase-2- and Proprotein Convertase-Cleaved Forms of Hemojuvelin Have Different Roles in the Down-Regulation of Heparin Expression. *J. Biol. Chem.* **2010**, *285*, 39021-39028. doi: 10.1074/jbc.M110.183160
113. Stirnberg, M.; Maurer, E.; Arenz, K.; Babler, A.; Jähnen-Dechent, W.; Gütschow, M. Cell Surface Serine Protease Matriptase-2 Suppresses Fetuin-A/AHSG-Mediated Induction of Heparin. *Biol. Chem.* **2015**, *396*, 81-93. doi: 10.1515/hsz-2014-0120

114. Jäckle, F.; Schmidt, F.; Wichert, R.; Arnold, P.; Prox, J.; Mangold, M.; Ohler, A.; Pietrzik, C. U.; Koudelka, T.; Tholey, A.; Gütschow, M.; Stirnberg, M.; Becker-Pauly, C. Metalloprotease Meprin Beta is Activated by Transmembrane Serine Protease Matriptase-2 at the Cell Surface thereby Enhancing APP Shedding. *Biochem. J.* **2015**, *470*, 91-103. doi: 10.1042/BJ20141417
115. Roydeva, P. G.; Beckmann, A. M.; Stirnberg, M.; Cesar, J.; Kikelj, D.; Ilas, J.; Gütschow, M. 3,1-Benzothiazines, 1,4-Benzodioxines and 1,4-Benzoxazines as Inhibitors of Matriptase-2: Outcome of a Focused Screening Approach. *Pharmaceuticals* **2016**, *9*, doi: 10.3390/ph9010002
116. Furtmann, N.; Häußler, D.; Scheidt, T.; Stirnberg, M.; Steinmetzer, T.; Bajorath, J.; Gütschow, M. Limiting the Number of Potential Binding Modes by Introducing Symmetry into Ligands: Structure-Based Design of Inhibitors for Trypsin-Like Serine Proteases. *Chemistry* **2016**, *22*, 610-625. doi: 10.1002/chem.201503534
117. Beckmann, A. M.; Gilberg, E.; Gattner, S.; Huang, T. L.; Vanden Eynde, J. J.; Mayence, A.; Bajorath, J.; Stirnberg, M.; Gütschow, M. Evaluation of Bisbenzamidines as Inhibitors for Matriptase-2. *Bioorg. Med. Chem. Lett.* **2016**, *26*, 3741-3745. doi: 10.1016/j.bmcl.2016.05.071
118. Hammami, M.; Rühmann, E.; Maurer, E.; Heine, A. M.; Gütschow, M.; Klebe, G.; Steinmetzer, T. New 3-Amidinophenylalanine Derived Inhibitors of Matriptase. *MedChemComm* **2012**, *3*, 807-813. doi: 10.1039/c2md20074k
119. Maurer, E.; Sisay, M. T.; Stirnberg, M.; Steinmetzer, T.; Bajorath, J.; Gütschow, M. Insights into Matriptase-2 Substrate Binding and Inhibition Mechanisms by Analyzing Active-Site-Mutated Variants. *ChemMedChem.* **2012**, *7*, 68-72. doi: 10.1002/cmdc.201100350
120. Yuan, C.; Chen, L.; Meehan, E. J.; Daly, N.; Craik, D. J.; Huang, M.; Ngo, J. C. Structure of Catalytic Domain of Matriptase in Complex with Sunflower Trypsin Inhibitor-1. *BMC Struct. Biol.* **2011**, *11*, 30. doi: 10.1186/1472-6807-11-30
121. Fittler, H.; Avrutina, O.; Empting, M.; Kolmar, H. Potent Inhibitors of Human Matriptase-1 Based on the Scaffold of Sunflower Trypsin Inhibitor. *J. Pept. Sci.* **2014**, *20*, 415-420. doi: 10.1002/psc.2629
122. Gitlin, A.; Debowski, D.; Karna, N.; Legowska, A.; Stirnberg, M.; Gütschow, M.; Rolka, K. Inhibitors of Matriptase-2 Based on the Trypsin Inhibitor SFTI-1. *ChemBioChem* **2015**, *16*, 1601-1607.
123. Lockett, S.; Garcia, R. S.; Barker, J. J.; Konarev, A. V.; Shewry, P. R.; Clarke, A. R.; Brady, R. L. High-Resolution Structure of a Potent, Cyclic Proteinase Inhibitor from Sunflower Seeds. *J. Mol. Biol.* **1999**, *290*, 525-533. doi: 10.1006/jmbi.1999.2891
124. Gitlin-Domagalska, A.; Debowski, D.; Legowska, A.; Stirnberg, M.; Okońska, J.; Gütschow, M.; Rolka, K. Design and Chemical Syntheses of Potent Matriptase-2 Inhibitors Based on Trypsin Inhibitor SFTI-1 Isolated from Sunflower Seeds. *Biopolymers* **2017**, *108*, doi: 10.1002/bip.23031
125. Seemüller, E.; Lupas, A.; Stock, D.; Löwe, J.; Huber, R.; Baumeister, W. Proteasome from *Thermoplasma Acidophilum*: a Threonine Protease. *Science* **1995**, *268*, 579-582. doi: 10.1126/science.7725107

126. Guan, C.; Cui, T.; Rao, V.; Liao, W.; Benner, J.; Lin, C. L.; Comb, D. Activation of Glycosylasparaginase. Formation of Active N-Terminal Threonine by Intramolecular Autoproteolysis. *J. Biol. Chem.* **1996**, *271*, 1732-1737. doi: 10.1074/jbc.271.3.1732
127. Guo, H. C.; Xu, Q.; Buckley, D.; Guan, C. Crystal Structures of Flavobacterium Glycosylasparaginase. An N-Terminal Nucleophile Hydrolase Activated by Intramolecular Proteolysis. *J. Biol. Chem.* **1998**, *273*, 20205-20212. doi: 10.1074/jbc.273.32.20205
128. Brannigan, J. A.; Dodson, G.; Duggleby, H. J.; Moody, P. C.; Smith, J. L.; Tomchick, D. R.; Murzin, A. G. A Protein Catalytic Framework with an N-Terminal Nucleophile is Capable of Self-Activation. *Nature* **1995**, *378*, 416-419. doi: 10.1038/378416a0
129. Dodson, G.; Wlodawer, A. Catalytic Triads and their Relatives. *Trends Biochem Sci.* **1998**, *23*, 347-352. doi: 10.1016/S0968-0004(98)01254-7
130. Corey, D. R.; Craik, C. S. An Investigation into the Minimum Requirements for Peptide Hydrolysis by Mutation of the Catalytic Triad of Trypsin. *J. Am. Chem. Soc.* **1992**, *114*, 1784-1790.
131. Baird, T. T. Jr.; Wright, W. D.; Craik, C. S. Conversion of Trypsin to a Functional Threonine Protease. *Protein Sci.* **2006**, *15*, 1229-1238. doi: 10.1110/ps.062179006
132. Buller, A. R.; Townsend, C. A. Intrinsic Evolutionary Constraints on Protease Structure, Enzyme Acylation, and the Identity of the Catalytic Triad. *Proc. Natl. Acad. Sci. USA.* **2013**, *110*, E653-E661. doi: 10.1073/pnas.1221050110
133. Storer AC1, Ménard R. Catalytic Mechanism in Papain Family of Cysteine Peptidases. *Methods Enzymol.* **1994**, *244*, 486-500. doi: 10.1016/0076-6879(94)44035-2
134. Schoenheimer, R.; Rittenberg, D.; Foster, G. L.; Keston, A. S.; Ratner, S. The Application of the Nitrogen Isotope N15 for the Study of Protein Metabolism. *Science* **1938**, *88*, 599-600. doi: 10.1126/science.88.2295.599
135. Olson, R. E. The Dynamic State of Body Constituents (Schoenheimer, 1939). *J. Nutr.* **1997**, *127*, 1041S-1043S.
136. Simpson, M. V. The Release of Labeled Amino Acids from the Proteins of Rat Liver Slices. *J. Biol. Chem.* **1953**, *201*, 143-154.
137. De Duve, C.; Gianetto, R.; Appelmans, F.; Wattiaux, R. Enzymic Content of the Mitochondria Fraction. *Nature* **1953**, *172*, 1143-1144. doi: 10.1038/1721143a0
138. Gianetto, R.; De Duve, C. Tissue Fractionation Studies. 4. Comparative Study of the Binding of Acid Phosphatase, Beta-Glucuronidase and Cathepsin by Rat-Liver Particles. *Biochem. J.* **1955**, *59*, 433-438. doi: 10.1042/bj0590433
139. Schneider, D. L. ATP-Dependent Acidification of Intact and Disrupted Lysosomes. Evidence for an ATP-Driven Proton Pump. *J. Biol. Chem.* **1981**, *256*, 3858-3864.
140. Hayashi, M.; Hiroi, Y.; Natori, Y. Effect of ATP on Protein Degradation in Rat Liver Lysosomes. *Nat. New Biol.* **1973**, *242*, 163-166.

141. Poole, B.; Ohkuma, S.; Warburton, M. J. The Accumulation of Weakly Basic Substances in Lysosomes and the Inhibition of Intracellular Protein Degradation. *Acta Biol. Med. Ger.* **1977**, *36*, 1777-1788.
142. Ciechanover, A.; Hod, Y.; Hershko, A. A Heat-Stable Polypeptide Component of an ATP-Dependent Proteolytic System from Reticulocytes. *Biochem. Biophys. Res. Commun.* **1978**, *81*, 1100–1105.
143. Ciechanover, A.; Heller, H.; Elias, S.; Haas, A. L.; Hershko, A. ATP-Dependent Conjugation of Reticulocyte proteins with the Polypeptide Required for Protein Degradation. *Proc. Natl Acad. Sci. USA* **1980**, *77*, 1365–1368.
144. Wilkinson, K. D., Urban, M. K. & Haas, A. L. Ubiquitin is the ATP-dependent proteolysis factor I of rabbit reticulocytes. *J. Biol. Chem.* **1980**, *255*, 7529–7532.
145. Hershko, A., Heller, H., Elias, S. & Ciechanover, A. Components of ubiquitin-protein ligase system: resolution, affinity purification and role in protein breakdown. *J. Biol. Chem.* **1983**, *258*, 8206–8214.
146. Hough, R.; Pratt, G.; Rechsteiner, M. Ubiquitin–Lysozyme Conjugates. Identification and Characterization of an ATP-Dependent Protease from Rabbit Reticulocyte Lysates. *J. Biol. Chem.* **1986**, *261*, 2400–2408.
147. Waxman, L.; Fagan, J. M.; Goldberg, A. L. Demonstration of Two Distinct High Molecular Weight Proteases in Rabbit Reticulocytes, One of which Degrades Ubiquitin Conjugates. *J. Biol. Chem.* **1987**, *262*, 2451-2457.
148. Tomko, R. J. Jr.; Hochstrasser, M. Molecular Architecture and Assembly of the Eukaryotic Proteasome. *Annu. Rev. Biochem.* **2013**, *82*, 415-445. doi: 10.1146/annurev-biochem-060410-150257
149. Kunjappu, M. J.; Hochstrasser, M. Assembly of the 20S Proteasome. *Biochim. Biophys. Acta.* **2014**, *1843*, 2-12. doi: 10.1016/j.bbamcr.2013.03.008
150. Budenholzer, L.; Cheng, C. L.; Li, Y.; Hochstrasser, M. Proteasome Structure and Assembly. *J. Mol. Biol.* **2017**, *429*, 3500-3524. doi: 10.1016/j.jmb.2017.05.027
151. Groll, M.; Bajorek, M.; Köhler, A.; Moroder, L.; Rubin, D. M.; Huber, R.; Glickman, M. H.; Finley, D. A Gated Channel into the Proteasome Core Particle. *Nat. Struct. Biol.* **2000**, *7*, 1062-1067. doi: 10.1038/80992
152. Deveraux, Q.; Ustrell, V.; Pickart, C.; Rechsteiner, M. A 26 S Protease Subunit that Binds Ubiquitin Conjugates. *J. Biol. Chem.* **1994**, *269*, 7059-7061.
153. Liu, C. W.; Jacobson, A. D. Functions of the 19S Complex in Proteasomal Degradation. *Trends Biochem. Sci.* **2013**, *38*, 103–110. doi: 10.1016/j.tibs.2012.11.009
154. Murata, S.; Takahama, Y.; Kasahara, M.; Tanaka, K. The Immunoproteasome and Thymoproteasome: Functions, Evolution and Human Disease. *Nat. Immunol.* **2018**, *19*, 923-931. doi: 10.1038/s41590-018-0186-z
155. Naujokat, C.; Hoffmann, S. Role and Function of the 26S Proteasome in Proliferation and Apoptosis. *Lab. Invest.* **2002**, *82*, 965–980.

156. Asher, G.; Bercovich, Z.; Tsvetkov, P.; Shaul, Y.; Kahana, C. 20S Proteasomal Degradation of Ornithine Decarboxylase is Regulated by NQO1. *Mol. Cell.* **2005**, *17*, 645–655. doi: 10.1016/j.molcel.2005.01.020
157. Strehl, B.; Seifert, U.; Krüger, E.; Heink, S.; Kuckelkorn, U.; Kloetzel, P. M. Interferon- γ , the Functional Plasticity of the Ubiquitin-Proteasome System, and MHC Class I Antigen Processing. *Immunol. Rev.* **2005**, *207*, 19–30. doi: 10.1111/j.0105-2896.2005.00308.x
158. Cavo M. Proteasome Inhibitor Bortezomib for the Treatment of Multiple Myeloma. *Leukemia* **2006**, *20*, 1341–1352. doi: 10.1038/sj.leu.2404278
159. Hobler, S. C.; Williams, A.; Fischer, D.; Wang, J. J.; Sun, X.; Fischer, J. E.; Monaco, J. J.; Hasselgren, P. O. Activity and Expression of the 20S Proteasome are Increased in Skeletal Muscle During Sepsis. *Am. J. Physiol.* **1999**, *277*, R434-440. doi: 10.1152/ajpregu.1999.277.2.R434
160. Keck, S.; Nitsch, R.; Grune, T.; Ullrich, O. Proteasome Inhibition by Paired Helical Filament-Tau in Brains of Patients with Alzheimer's Disease. *J. Neurochem.* **2003**, *85*, 115–122. doi: 10.1046/j.1471-4159.2003.01642.x
161. McNaught, K. S. P.; Jenner, P. Proteasomal Function is Impaired in Substantia Nigra in Parkinson's Disease. *Neurosci. Lett.* **2001**; *297*, 191–194. doi: 10.1016/S0304-3940(00)01701-8
162. Seeger, M.; Ferrel, K.; Frank, R.; Dubiel, W. HIV-1 Tat Inhibits the 20S Proteasome and its 11S Regulator-Mediated Activation. *J. Biol. Chem.* **1997**, *272*, 8145–8148. doi: 10.1074/jbc.272.13.8145
163. Hu, Z.; Zhang, Z.; Doo, E.; Coux, O.; Goldberg, A. L.; Liang, T. J. Hepatitis B Virus X Protein is both a Substrate and a Potential Inhibitor of the Proteasome Complex. *J. Virol.* **1999**, *73*, 7231–7240.
164. Jagannath, S.; Barlogie, B.; Berenson, J.; Siegel, D.; Irwin, D.; Richardson, P. G.; Niesvizky, R.; Alexanian, R.; Limentani, S. A.; Alsina, M.; Adams, J.; Kauffman, M.; Esseltine, D. L.; Schenkein, D. P.; Anderson, K. C. A Phase 2 Study of Two Doses of Bortezomib in Relapsed or Refractory Myeloma. *Br. J. Haematol.* **2004**, *127*, 165-72. doi: 10.1111/j.1365-2141.2004.05188.x
165. Muchamuel, T.; Basler, M.; Aujay, M. A.; Suzuki, E.; Kalim, K. W.; Lauer, C.; Sylvain, C.; Ring, E. R.; Shields, J.; Jiang, J.; Shwonek, P.; Parlati, F.; Demo, S. D.; Bennett, M. K.; Kirk, C. J.; Groettrup, M. A Selective Inhibitor of the Immunoproteasome Subunit LMP7 Blocks Cytokine Production and Attenuates Progression of Experimental Arthritis. *Nat. Med.* **2009**, *15*, 781–787. doi: 10.1038/nm.1978
166. Sakamoto, K. M.; Kim, K. B.; Kumagai, A.; Mercurio, F.; Crews, C. M.; Deshaies, R. J. Protacs: Chimeric Molecules that Target Proteins to the Skp1-Cullin-F Box Complex for Ubiquitination and Degradation. *Proc. Natl. Acad. Sci. USA* **2001**, *98*, 8554-9. doi: 10.1073/pnas.141230798
167. Hochstrasser, M. Ubiquitin-Dependent Protein Degradation. *Annu. Rev. Genet.* **1996**, *30*, 405-439. doi: 10.1146/annurev.genet.30.1.405

-
168. Haas, A. L.; Rose, I. A. The Mechanism of Ubiquitin Activating Enzyme. A Kinetic and Equilibrium Analysis. *J. Biol. Chem.* **1982**, *257*, 10329-10337.
169. Jentsch, S. The Ubiquitin-Conjugation System. *Annu. Rev. Genet.* **1992**, *26*, 179-207. doi: 10.1146/annurev.ge.26.120192.001143
170. Handley, P. M.; Mueckler, M.; Siegel, N. R.; Ciechanover, A.; Schwartz, A. L. Molecular Cloning, Sequence, and Tissue Distribution of the Human Ubiquitin-Activating Enzyme E1. *Proc. Natl. Acad. Sci. USA* **1991**, *88*, 258-262. doi: 10.1073/pnas.88.1.258
171. Scheffner, M.; Nuber, U.; Huibregtse, J. M. Protein Ubiquitination Involving an E1-E2-E3 Enzyme Ubiquitin Thioester Cascade. *Nature* **1995**, *373*, 81-83. doi: 10.1038/373081a0
172. Lecker, S. H.; Goldberg, A. L.; Mitch, W. E. Protein Degradation by the Ubiquitin-Proteasome Pathway in Normal and Disease States. *J. Am. Soc. Nephrol.* **2006**, *17*, 1807-1819. doi: 10.1681/ASN.2006010083
173. Mosesson, Y.; Yarden, Y. Monoubiquitylation: a Recurrent Theme in Membrane Protein Transport. *Isr. Med. Assoc. J.* **2006**, *8*, 233-237.
174. Lonard, D. M.; O'Malley, B. W. Emerging Roles of the Ubiquitin Proteasome System in Nuclear Hormone Receptor Signaling. *Prog. Mol. Biol. Transl. Sci.* **2009**, *87*, 117-135. doi: 10.1016/S1877-1173(09)87004-X
175. Amerik, A. Y.; Hochstrasser, M. Mechanism and Function of Deubiquitinating Enzymes. *Biochim. Biophys. Acta* **2004**, *1695*, 189-207. doi: 10.1016/j.molcel.2018.03.022
176. Shi, Y.; Chen, X.; Elsasser, S.; Stocks, B. B.; Tian, G.; Lee, B. H.; Shi, Y.; Zhang, N.; de Poot, S. A.; Tuebing, F.; Sun, S.; Vannoy, J.; Tarasov, S. G.; Engen, J. R.; Finley, D.; Walters, K. J. Rpn1 Provides Adjacent Receptor Sites for Substrate Binding and Deubiquitination by the Proteasome. *Science* **2016**, *351*. pii: aad9421. doi: 10.1126/science.aad9421
177. de Poot, S. A. H.; Tian, G.; Finley, D. Meddling with Fate: The Proteasomal Deubiquitinating Enzymes. *J. Mol. Biol.* **2017**, *429*, 3525-3545. doi: 10.1016/j.jmb.2017.09.015
178. Martin, A.; Baker, T. A.; Sauer, R. T. Pore Loops of the AAA+ ClpX Machine Grip Substrates to Drive Translocation and Unfolding. *Nat. Struct. Mol. Biol.* **2008**, *15*, 1147-1151. doi: 10.1038/nsmb.1503
179. Aubin-Tam, M. E.; Olivares, A. O.; Sauer, R. T.; Baker, T. A.; Lang, M. J. Single-Molecule Protein Unfolding and Translocation by an ATP-Fueled Proteolytic Machine. *Cell* **2011**, *145*, 257-267. doi: 10.1016/j.cell.2011.03.036
180. Kisselev, A. F.; Akopian, T. N.; Woo, K. M.; Goldberg, A. L. The Sizes of Peptides Generated from Protein by Mammalian 26 and 20 S Proteasomes. Implications for Understanding the Degradative Mechanism and Antigen Presentation. *J. Biol. Chem.* **1999**, *274*, 3363-3371. doi: 10.1074/jbc.274.6.3363

-
181. Saric, T.; Graef, C. I.; Goldberg, A. L. Pathway for Degradation of Peptides Generated by Proteasomes: a Key Role for Thimet Oligopeptidase and other Metallopeptidases. *J. Biol. Chem.* **2004**, *279*, 46723-46732. doi: 10.1074/jbc.M406537200
182. Palombella, V. J.; Rando, O. J.; Goldberg, A. L.; Maniatis, T. The Ubiquitin-Proteasome Pathway is Required for Processing the NF-kappa B1 Precursor Protein and the Activation of NF-kappa B. *Cell.* **1994**, *78*, 773-785. doi: 10.1016/s0092-8674(94)90482-0
183. Zhang, D.; Baek, S. H.; Ho, A.; Lee, H.; Jeong, Y. S.; Kim, K. Targeted Degradation of Proteins by Small Molecules: A Novel Tool for Functional Proteomics. *Comb. Chem. High Throughput Screen.* **2004**, *7*, 689-697.
184. Pettersson, M.; Crews, C. M. PROteolysis TArgeting Chimeras (PROTACs) - Past, Present and Future. *Drug Discov. Today Technol.* **2019**, *31*, 15-27. doi: 10.1016/j.ddtec.2019.01.002
185. Hopkins, A. L.; Groom, C. R. The Druggable Genome. *Nat. Rev. Drug Discov.* **2002**, *1*, 727-730. doi: 10.1038/nrd892
186. Valeur, E.; Guéret, S. M.; Adihou, H.; Gopalakrishnan, R.; Lemurell, M.; Waldmann, H.; Grossmann, T. N.; Plowright, A. T. New Modalities for Challenging Targets in Drug Discovery. *Angew. Chem. Int. Ed. Engl.* **2017**, *56*, 10294-10323. doi: 10.1002/anie.201611914
187. Lu, J.; Qian, Y.; Altieri, M.; Dong, H.; Wang, J.; Raina, K.; Hines, J.; Winkler, J. D.; Crew, A. P.; Coleman, K.; Crews, C. M. Hijacking the E3 Ubiquitin Ligase Cereblon to Efficiently Target BRD4. *Chem. Biol.* **2015**, *22*, 755-763. doi: 10.1016/j.chembiol.2015.05.009
188. Bondeson, D. P.; Mares, A.; Smith, I. E.; Ko, E.; Campos, S.; Miah, A. H.; Mulholland, K. E.; Routly, N.; Buckley, D. L.; Gustafson, J. L.; Zinn, N.; Grandi, P.; Shimamura, S.; Bergamini, G.; Faeltz-Savitski, M.; Bantscheff, M.; Cox, C.; Gordon, D. A.; Willard, R. R.; Flanagan, J. J.; Casillas, L. N.; Votta, B. J.; den Besten, W.; Famm, K.; Kruidenier, L.; Carter, P. S.; Harling, J. D.; Churcher, I.; Crews, C. M. Catalytic *in Vivo* Protein Knockdown by Small-Molecule PROTACs. *Nat. Chem. Biol.* **2015**, *11*, 611-617. doi: 10.1038/nchembio.1858
189. Ito, T.; Ando, H.; Suzuki, T.; Ogura, T.; Hotta, K.; Imamura, Y.; Yamaguchi, Y.; Handa, H. Identification of a Primary Target of Thalidomide Teratogenicity. *Science* **2010**, *327*, 1345-1350. doi: 10.1126/science.1177319
190. Buckley, D. L.; Van Molle, I.; Gareiss, P. C.; Tae, H. S.; Michel, J.; Noblin, D. J.; Jorgensen, W. L.; Ciulli, A.; Crews, C. M. Targeting the Von Hippel-Lindau E3 Ubiquitin Ligase Using Small Molecules to Disrupt the VHL/HIF-1 α Interaction. *J. Am. Chem. Soc.* **2012**, *134*, 4465-4468. doi: 10.1021/ja209924v
191. Itoh, Y.; Ishikawa, M.; Naito, M.; Hashimoto, Y. Protein Knockdown Using Methyl Bestatin-Ligand Hybrid Molecules: Design and Synthesis of Inducers of Ubiquitination-Mediated Degradation of Cellular Retinoic Acid-Binding Proteins. *J. Am. Chem. Soc.* **2010**, *132*, 5820-5826. doi: 10.1021/ja100691p

192. Han, T.; Goralski, M.; Gaskill, N.; Capota, E.; Kim, J.; Ting, T. C.; Xie, Y.; Williams, N. S.; Nijhawan, D. Anticancer Sulfonamides Target Splicing by Inducing RBM39 Degradation via Recruitment to DCAF15. *Science* **2017**, *356*, pii: eaal3755. doi: 10.1126/science.aal3755
193. Maniaci, C.; Hughes, S. J.; Testa, A.; Chen, W.; Lamont, D. J.; Rocha, S.; Alessi, D. R.; Romeo, R.; Ciulli, A. Homo-PROTACs: Bivalent Small-Molecule Dimerizers of the VHL E3 Ubiquitin Ligase to Induce Self-Degradation. *Nat. Commun.* **2017**, *8*, 830. doi: 10.1038/s41467-017-00954-1
194. Steinebach, C.; Lindner, S.; Udeshi, N. D.; Mani, D. C.; Kehm, H.; Köpff, S.; Carr, S. A.; Gütschow, M.; Krönke, J. Homo-PROTACs for the Chemical Knockdown of Cereblon. *ACS Chem. Biol.* **2018**, *13*, 2771-2782. doi: 10.1021/acscchembio.8b00693
195. Neklesa, T.; Snyder, L. B.; Willard, R. R.; Vitale, N.; Raina, K.; Pizzano, J.; Gordon, D. A.; Bookbinder, M.; Macaluso, J.; Dong, H.; Liu, Z.; Ferraro, C.; Wang, G.; Wang, J.; Crews, C. M.; Houston, J.; Crew, A. P.; Taylor, I. An Oral Androgen Receptor PROTAC Degradator for Prostate Cancer. *J. Clin. Oncol.* **2018**, *36*, 381. doi: 10.1200/JCO.2018.36.6_suppl.381
196. Flanagan, J. J.; Qian, Y.; Gough, S. M.; Andreoli, M.; Bookbinder, M.; Cadelina, G.; Bradley, J.; Rousseau, E.; Willard, R.; Pizzano, J.; Crews, C. M.; Crew, A. P.; Taylor, I.; Houston, J. Abstract P5-04-18: ARV-471, an Oral Estrogen Receptor PROTAC Degradator for Breast Cancer. *Cancer Res.* **2019**, *79*, doi: 10.1158/1538-7445.SABCS18-P5-04-18
197. Newman, D. J., Cragg, G. M., Snader, K. M. The Influence of Natural Products Upon Drug Discovery. *Nat. Prod. Rep.* **2000**, *17*, 215–234. doi: 10.1039/a902202c
198. Clardy, J.; Walsh, C. Lessons from Natural Molecules. *Nature* **2004**, *432*, 829-837. doi: 10.1038/nature03194
199. Kingston, D. G. Modern Natural Products Drug Discovery and its Relevance to Biodiversity Conservation. *J. Nat. Prod.* **2011**, *74*, 496-511. doi: 10.1021/np100550t
200. Lesner, A.; Łęgowska, A.; Wysocka, M.; Rolka, K. Sunflower Trypsin Inhibitor 1 as a Molecular Scaffold for Drug Discovery. *Curr. Pharm. Des.* **2011**, *17*, 4308-4317. doi: 10.2174/138161211798999393
201. Gitlin-Domagalska, A.; Mangold, M.; Dębowski, D.; Ptaszyńska, N.; Łęgowska, A.; Gütschow, M.; Rolka, K. Matriptase-2: Monitoring and Inhibiting its Proteolytic Activity. *Future Med. Chem.* **2018**, *10*, 2745-2761. doi: 10.4155/fmc-2018-0346
202. Qi, R. F.; Song, Z. W.; Chi, C. W. Structural Features and Molecular Evolution of Bowman-Birk Protease Inhibitors and their Potential Application. *Acta Biochim. Biophys. Sin.* **2005**, *37*, 283-92. doi: 10.1111/j.1745-7270.2005.00048.x
203. Hilpert, K.; Hansen, G.; Wessner, H.; Volkmer-Engert, R.; Höhne, W. Complete Substitutional Analysis of a Sunflower Trypsin Inhibitor with Different Serine Proteases. *J. Biochem.* **2005**, *138*, 383-390. doi: 10.1093/jb/mvi140
204. Qvit, N.; Rubin, S. J. S.; Urban, T. J.; Mochly-Rosen, D.; Gross, E. R. Peptidomimetic Therapeutics: Scientific Approaches and Opportunities. *Drug Discov. Today* **2017**, *22*, 454–462. doi: 10.1016/j.drudis.2016.11.003

205. Mangold, M.; Gütschow, M.; Stirnberg, M. A Short Peptide Inhibitor as an Activity-Based Probe for Matriptase-2. *Pharmaceuticals (Basel)*. **2018**, *11*, pii: E49. doi: 10.3390/ph11020049
206. Godiksen, S.; Soendergaard, C.; Friis, S.; Jensen, J. K.; Bornholdt, J.; Sales, K. U.; Huang, M.; Bugge, T. H.; Vogel, L. K. Detection of Active Matriptase Using a Biotinylated Chloromethyl Ketone Peptide. *PLoS One* **2013**, *8*, e77146. doi: 10.1371/journal.pone.0077146
207. Mangold, M. Untersuchungen zur Reinigung und Aktivitätsregulation der Rekombinanten Humanen Serinprotease Matriptase-2. Master thesis, University of Bonn **2015**.
208. Vindigni, A.; Dang, Q. D.; Di Cera, E. Site-Specific Dissection of Substrate Recognition by Thrombin. *Nat. Biotechnol.* **1997**, *15*, 891-895. doi: 10.1038/nbt0997-891
209. Gallwitz, M.; Enoksson, M.; Thorpe, M.; Hellman, L. The Extended Cleavage Specificity of Human Thrombin. *PLoS One* **2012**, *7*, e31756. doi: 10.1371/journal.pone.0031756
210. Stefanachi, A.; Leonetti, F.; Pisani, L.; Catto, M.; Carotti, A. Coumarin: A Natural, Privileged and Versatile Scaffold for Bioactive Compounds. *Molecules* **2018**, *23*, pii: E250. doi: 10.3390/molecules23020250
211. Borghi, S. M.; Carvalho, T. T.; Staurengo-Ferrari, L.; Hohmann, M. S.; Pinge-Filho, P.; Casagrande, R.; Verri, W. A. Jr. Vitexin Inhibits Inflammatory Pain in Mice by Targeting TRPV1, Oxidative Stress, and Cytokines. *J. Nat. Prod.* **2013**, *76*, 1141-1149. doi: 10.1021/np400222v
212. de Souza, L. G.; Rennã, M. N.; Figueroa-Villar, J. D. Coumarins as Cholinesterase Inhibitors: A Review. *Chem. Biol. Interact.* **2016**, *254*, 11-23. doi: 10.1016/j.cbi.2016.05.001
213. Revankar, H. M.; Bukhari, S. N.; Kumar, G. B.; Qin, H. L. Coumarins Scaffolds as COX Inhibitors. *Bioorg. Chem.* **2017**, *71*, 146-159. doi: 10.1016/j.bioorg.2017.02.001
214. Miao, J.; Cui, H.; Jin, J.; Lai, F.; Wen, H.; Zhang, X.; Ruda, G. F.; Chen, X.; Yin, D. Development of 3-Alkyl-6-Methoxy-7-Hydroxy-Chromones (AMHCs) from Natural Isoflavones, a New Class of Fluorescent Scaffolds for Biological Imaging. *Chem. Commun.* **2015**; *51*, 881-884. doi: 10.1039/c4cc06762b
215. Lemke, C.; Christmann, J.; Yin, J.; Alonso, J. M.; Serrano, E.; Chioua, M.; Ismaili, L.; Martínez-Grau, M. A.; Beadle, C. D.; Vetman, T.; Dato, F. M.; Bartz, U.; Elsinghorst, P. W.; Pietsch, M.; Müller, C. E.; Iriepa, I.; Wille, T.; Marco-Contelles, J.; Gütschow, M. Chromenones as Multineurotargeting Inhibitors of Human Enzymes. *ACS Omega*. **2019**, *4*, 22161–22168. doi: 10.1021/acsomega.9b03409
216. Huggins, D. J.; Sherman, W.; Tidor, B. Rational Approaches to Improving Selectivity in Drug Design. *J. Med. Chem.* **2012**, *55*, 1424-1444. doi: 10.1021/jm2010332
217. Zhang, P.; Wang, F.; Hu, J.; Sorrentino, R. Exploring the Relationship Between Drug Side-Effects and Therapeutic Indications. *AMIA Annu. Symp. Proc.* **2013**, *2013*, 1568-1577.

219. Heal, W. P.; Dang, T. H.; Tate, E. W. Activity-Based Probes: Discovering New Biology and New Drug Targets. *Chem. Soc. Rev.* **2011**, *40*, 246-257. doi: 10.1039/c0cs00004c
219. Yang, X.; Michiels, T. J. M.; de Jong, C.; Soethoudt, M.; Dekker, N.; Gordon, E.; van der Stelt, M.; Heitman, L. H.; van der Es, D.; IJzerman, A. P. An Affinity-Based Probe for the Human Adenosine A_{2A} Receptor. *J. Med. Chem.* **2018**, *61*, 7892-7901. doi: 10.1021/acs.jmedchem.8b00860
220. Tam, E. K.; Li, Z.; Goh, Y. L.; Cheng, X.; Wong, S. Y.; Santhanakrishnan, S.; Chai, C. L.; Yao, S. Q. Cell-Based Proteome Profiling Using an Affinity-Based Probe (AfBP) Derived from 3-Deazaneplanocin A (DzNep). *Chem. Asian J.* **2013**, *8*, 1818-1828. doi: 10.1002/asia.201300303
221. Fritz, H.; Wunderer, G. Biochemistry and Applications of Aprotinin, the Kallikrein Inhibitor from Bovine Organs. *Arzneimittelforschung* **1983**, *33*, 479-494.
222. Zengerle, M.; Chan, K. H.; Ciulli, A. Selective Small Molecule Induced Degradation of the BET Bromodomain Protein BRD4. *ACS Chem. Biol.* **2015**, *10*, 1770-1777. doi: 10.1021/acscchembio.5b00216
223. Buckley, D. L.; Raina, K.; Darricarrere, N.; Hines, J.; Gustafson, J. L.; Smith, I. E.; Miah, A. H.; Harling, J. D.; Crews, C. M. HaloPROTACS: Use of Small Molecule PROTACs to Induce Degradation of HaloTag Fusion Proteins. *ACS Chem. Biol.* **2015**, *10*, 1831-1837. doi: 10.1021/acscchembio.5b00442
224. Cyrus, K.; Wehenkel, M.; Choi, E. Y.; Han, H. J.; Lee, H.; Swanson, H.; Kim, K. B. Impact of Linker Length on the Activity of PROTACs. *Mol. Biosyst.* **2011**, *7*, 359-364. doi: 10.1039/c0mb00074d
225. Wang, Y.; Jiang, X.; Feng, F.; Liu, W.; Sun, H. Degradation of Proteins by PROTACs and Other Strategies. *Acta Pharm. Sin. B.* **2020**, *10*, 207-238. doi: 10.1016/j.apsb.2019.08.001
226. Riching, K. M.; Mahan, S.; Corona, C. R.; McDougall, M.; Vasta, J. D.; Robers, M. B.; Uhr, M.; Daniels, D. L. Quantitative Live-Cell Kinetic Degradation and Mechanistic Profiling of PROTAC Mode of Action. *ACS Chem. Biol.* **2018**, *13*, 2758-2770. doi: 10.1021/acscchembio.8b00692
227. Bradford, M. M. A Rapid and Sensitive Method for the Quantitation of Microgram Quantities of Protein Utilizing the Principle of Protein-Dye Binding. *Anal. Biochem.* **1976**, *72*, 248-254. doi: 10.1006/abio.1976.9999
228. Fan, F.; Wood, K. V. Bioluminescent Assays for High-Throughput Screening. *Assay Drug. Dev. Technol.* **2007**, *5*, 127-136. doi: 10.1089/adt.2006.053
229. Nakabayashi, H.; Taketa, K.; Miyano, K.; Yamane, T.; Sato, J. Growth of Human Hepatoma Cells Lines with Differentiated Functions in Chemically Defined Medium. *Cancer Res.* **1982**, *42*, 3858-3863.
230. Maurer, E.; Gütschow, M.; Stirnberg, M. Hepatocyte Growth Factor Activator Inhibitor Type 2 (HAI-2) Modulates Hecpudin Expression by Inhibiting the Cell Surface Protease Matriptase-2. *Biochem. J.* **2013**, *450*, 583-593. doi: 10.1042/BJ20121518.

231. Evan, G. I.; Lewis, G. K.; Ramsay, G.; Bishop, J. M. Isolation of monoclonal antibodies specific for human c-myc proto-oncogene product. *Mol. Cell Biol.* **1985**, *5*, 3610-3616.

5 Registers

5.1 List of abbreviations

AAA+	ATPases associated with various cellular activities
Abz	2-Aminobenzoyl
AMC	7-Amino-4-methylcoumarin
AP	Alkaline phosphatase
Arg	Arginine
Asp	Aspartic acid
ATP	Adenosine triphosphate
BBI	Bowman Birk inhibitor
BCIP	5-Bromo-4-chloro-3-indolyl Phosphate
BMP	Bone morphogenetic protein
BMPR	Bone morphogenetic protein receptor
Boc	<i>tert</i> -Butyloxycarbonyl
BSA	Bovine serum albumin
Cbz	Carboxybenzyl
CMK	Chloromethyl ketone
CP	Core particle
CRBN	Cereblon
CUB	Cls/Clr, urchin embryonic growth factor and bone morphogenic protein-1
Cys	Cysteine
DAPI	4',6-Diamidino-2-phenylindole
DMEM	Dulbecco's Modified Eagles Medium
DMSO	Dimethylsulfoxide
DNA	Deoxyribonucleic Acid
<i>E. coli</i>	<i>Escherichia coli</i>
EDTA	Ethylenediaminetetraacetic Acid
FCS	Fetal calf serum
FU	Fluorescence units
Gln	Glutamine
Gly	Glycine
HAT/DESC	Human airway trypsin-like protease/differentially expressed in squamous cell carcinoma gene
HCP	Heme carrier protein
HEK cells	Human embryonic kidney cells

Hepsin/TMPRSS	Hepsin/transmembrane serine protease
HFE	Hemochromatosis protein
HIF	Hypoxia inducible factor
His	Histidine
HJV	Hemojuvelin
Huh7 cells	Human hepatoma cells
Ile	Isoleucine
IMiD	Immunomodulatory imide drug
IRIDA	Iron refractory iron deficiency anemia
LB	lysogeny broth
LDLRA	Low-density lipoprotein receptor class A
Lys	Lysine
MAM	Meprin, A-5 protein and receptor protein-tyrosine phosphatase mu
MAO	Monoamine oxidases
MT1	Matriptase
MT2	Matriptase-2
MT3	Matriptase-3
MTT	3-(4,5-Dimethylthiazol-2-yl)-2,5-Diphenyltetrazolium Bromide
n.i.	No inhibition
NBT	Nitro blue tetrazolium chloride
PA	Proteases of mixed nucleophile, superfamily A
PBS	Phosphate buffered saline
PEG	8-Amino-3,6-Dioxaoctanoic Acid
Phe	Phenylalanine
PICS	Proteomic Identification of Protease Cleavage Sites
pNA	<i>para</i> -Nitroaniline
POI	Protein of interest
Pro	Proline
PROTAC	Proteolysis targeting chimera
OptiMEM	Modified Eagle's Minimum Essential Medium
RP	Regulatory particle
RPMI	Roswell Park Memorial Institute
rt	Room temperature
SCAV	Group A scavenger receptor
SDS	Sodium dodecyl sulfate
SDS-PAGE	SDS-Polyacrylamide Gel Electrophoresis
SEA	Sea urchin sperm protein, enteropeptidase, agrin

Ser	Serine
SFTI	Sunflower trypsin inhibitor
SFTI-1	Sunflower trypsin inhibitor 1
SMAD	Son of the Mothers Against Decapentaplegic
SOC	Super optimal broth with catabolite repression
Suc	Succinyl
TfR2	Transferrin receptor-2
Thr	Threonine
TMPRSS	Transmembrane protease serine
TRIS	Tris(hydroxymethyl)aminomethane
TTSP	Type II transmembrane serine protease
UPS	Ubiquitin proteasome system
UV	Ultraviolet
Val	Valine
VIS	Visible
VHL	von Hippel-Lindau

5.2 List of figures

1.1	Chemical structures of synthetic MT2 inhibitors.	15
1.2	Chemical structures of sunflower trypsin inhibitors.	17
2.1	Matriptase-2 activity in the supernatant of transfected HEK cells.	25
2.2	Chemical structures of SFTI-1 analogs.	29
2.3	MT2 activity in the supernatant of transfected HEK cells in the presence of increasing concentrations of SFTI inhibitors 11 and 12 .	30
2.4	MT2 activity in the supernatant of transfected HEK cells in the presence of increasing concentrations of SFTI inhibitors 13 and 14 .	31
2.5	Chemical structure of biotinylated CMK peptide probe 15 .	34
2.6	MT2 activity in the supernatant of transfected HEK cells in the presence of increasing concentrations of CMK probe 15 .	34
2.7	Chemical structure of activity-based probe 16 .	35
2.8	MT2 activity in the supernatant of transfected HEK cells in the presence of increasing concentrations of phosphono bisbenzguanidine 16 .	36
2.9	Inhibition of human thrombin by prolineamide 19B .	41
2.10	MT2 activity at the surface of transfected HEK cells in the presence of increasing concentrations of SFTI inhibitors 11 to 13 .	48
2.11	MT2 activity at the surface of transfected HEK cells in the presence of increasing concentrations of SFTI inhibitors 14 to 16 .	49
2.12	Modulation of hepcidin expression by inhibitors 11 and 13 to 16 .	52
2.13	Chemical structure of detection groups of activity-based probe 12 to 16 .	54
2.14	Enzymatic activity of native MT2 and mutated MT2-S753A.	55
2.15	Detection of MT2 in the supernatant and membrane fractions of transfected HEK cells.	56
2.16	Normalized absorption and emission spectra of fluorescent activity-based probes.	57
2.17	Normalized cell viability of activity-based probes 13 to 16 .	58
2.18	Screening for detection of active MT2 in HEK cell supernatants by activity-based probes 13 and 14 .	59
2.19	Detection of active MT2 by activity-based probes 12 to 14 .	60
2.20	Detection of active MT2 in supernatant samples by activity-based probe 15 .	62
2.21	Detection of active MT2 in supernatant samples of transfected HEK cell	

	cultures by activity-based probe 15 .	63
2.22	Detection of active MT2 in supernatant samples of transfected HEK cell cultures by activity-based probe 16 .	64
2.23	MT2 activity in the supernatant of transfected HEK cells in the presence of increasing concentrations of aprotinin.	65
2.24	Labeling of active MT2 by activity-based probe 15 after application of aprotinin.	66
2.25	Labeling of active MT2 by activity-based probe 16 after application of aprotinin	66
2.26	Confocal microscopy images of HEK cell cultures treated with activity-based probes 13 to 16 .	68
2.27	Luciferase activity of transfected Huh-7 cell cultures.	73
2.28	Normalized cell viability of PROTACs 54 to 59 .	76
2.29	Halo-Luc activity in the presence of increasing amounts of PROTACs 54 to 59	77
2.30	Detection of Halo-Luc fusion protein by western blotting.	79
2.31	α -Firefly luciferase immunoblot of HEK lysates transfected with pHTN-2Luc expression vector	80

5.3 List of tables

2.1	Chemical structures of lactone and amine/amide molecules.	37
2.2	Inhibition of MT2 and thrombin by prolineamides 17A to 20F , as well as lactones 17 to 20 and amines/amides A to F .	38
2.3	Chemical structures of chromenone derivatives and inhibition of MT2.	43
2.4	Inhibition of MT2 by phosphonates 49 to 53 .	44
2.5	Selectivity profiles of inhibitors 11 to 16 .	45
2.6	Inhibition of soluble MT2 and MT2 at the cell surface by compounds 11 to 16 .	50
2.7	Chemical structures of PROTAC molecules.	74
3.1	List of used devices.	93
3.2	List of used consumables.	95
3.3	List of used materials.	96
3.4	List of used cell lines.	99
3.5	List of used vectors.	100
3.6	List of used enzymes.	101
3.7	List of enzyme substrates.	102
3.8	List of antibodies, commercially available probes and dyes.	103
3.9	List of buffers and solutions.	104

5.4 List of schemes

1.1	Schematic depiction of the active site of a protease and its substrate.	1
1.2	Schematic representation of the TTSP family and its four subfamilies. HAT/DESC, hepsin/TMPRSS, matriptase and corin	4
1.3	Schematic structure of matriptase proteins.	5
1.4	MT2 activation mechanism and release.	7
1.5	Influence of MT2 on hepcidin expression.	9
1.6	Functionality of activity-based probes.	12
1.7	Schematic depiction of endogenous versus targeted protein degradation induced by PROTACs.	23
2.1	Schematic depiction of the general mechanism of competitive reversible inhibition.	26
2.2	Equations used for the determination of IC_{50} and K_i values.	26
2.3	Schematic depiction of the general mechanism of competitive irreversible inhibition.	27
2.4	Equations used for the determination of k_{obs} and k_{inac}/K_i values.	27
2.5	Synthesis of prolineamide inhibitors based on the example of 17A .	38
2.6	Proposed binding mode of 19B in the thrombin active site.	40
2.7	Luciferase-based test system for the evaluation of PROTACs.	72

6 Summary

This thesis was focused on the identification and characterization of irreversible inhibitors and activity-based probes of the cell surface serine protease matriptase-2, as well as inducers of targeted protein degradation. Matriptase-2, also known as Tmprss6, was identified as a key regulator of the systemic iron homeostasis due to its role in the regulation of the peptide hormone hepcidin. Its involvement in iron overload disorders, especially β -thalassemia, promotes matriptase-2 as a promising target for the treatment of these diseases. Activity-based probes could be used in this context to further the research and understanding of this enzyme as a pathological marker. Proteolysis targeting chimeras (PROTACs) on the other hand, represent an emerging drug class which can be employed to induce the proteasomal degradation of target proteins. While the synthesis and evaluation of small series of PROTACs in cell cultures is described by various studies, there is still a strong need for experimental approaches that allow for the easy and fast evaluation of such compounds.

In the first project, peptide and peptidomimetic inhibitors were evaluated for their inhibitory activity towards matriptase-2. Small series of sunflower trypsin inhibitors, phosphonates, prolineamides, chromenones and a peptide inhibitor were employed for this purpose. This way, six compounds out of the sun flower trypsin inhibitors, phosphonates and the peptide inhibitor could be identified as inhibitors of matriptase-2 activity. Subsequently, inhibitory properties of these inhibitors were characterized further in additional cell-based assays and towards related serine proteases. While the identified compounds also inhibited the serine proteases matriptase-1 and thrombin to different extents, sunflower trypsin inhibitors exhibited the highest selectivity for matriptase-2. Furthermore, these inhibitors could be successfully employed in a cell-based assay and a reporter gene assay to investigate their potency towards membrane-bound matriptase-2 and their influence on the expression of down-stream targets of the enzyme. Even though the series of prolineamides, which was synthesized in a novel solution-based approach, did not exhibit inhibitory activity towards matriptase-2, these compounds could be identified as inhibitors of thrombin activity. Subsequently, this experimental approach was established as a screening system for the fast synthesis and evaluation of such inhibitors.

In the following project, five activity-based probes which were characterized as inhibitors of matriptase-2 in the first project were evaluated for their ability to label active matriptase-2. First, fluorescence properties and toxicity of these compounds were determined to establish experimental parameters suitable for the following investigations. Two activity-based probes, a chloromethyl ketone probe and a phosphono bis benzguanidine probe, could be successfully employed in SDS-PAGE and immunoblotting experiments to visualize active matriptase-2. Competition experiments with the serine protease inhibitor aprotinin further emphasized the proposed binding mode of these activity-based probes.

In the last project, a test system for the screening of PROTAC activity was conceptualized and established. For this purpose, firefly luciferase was chosen as the target for induced protein degradation. An attached HaloTag should serve as the ligand for the interaction with the PROTACs. Subsequently, a fusion protein expression vector encoding firefly luciferase equipped with the HaloTag was constructed by PCR and cloning techniques. The luciferase-based assay was established by transfection of cell cultures and a small series of PROTACs was to be evaluated in this system. After determination of suitable application times and concentrations, six PROTACs equipped with a HaloTag ligand and ligands for the E3 ligases cereblon or von-Hippel Lindau were applied in the luciferase assay. Treatment with three of the four designed active PROTACs resulted in a significant reduction of fusion protein activity. Finally, immunoblot experiments were employed for the verification of assay test results. However, these experiments failed to provide suitable conclusions for this approach.

Danksagung

An dieser Stelle möchte ich danken:

Frau Dr. Agata Gitlin-Domagalska vom Institut für Biochemie der Universität Gdansk für die Bereitstellung der SFTI Verbindungen.

Christian Steinebach und Dr. Daniela Häußler für die Bereitstellung der PROTACs und Phosphonatsonden.

Dr. Marit Stirnberg für die sehr gute fachliche und persönliche Betreuung zu Beginn meiner Doktorarbeit.

Dr. Anna-Christina Schulz-Fincke, Dr. Anna-Madeleine Beckmann und Carina Lemke für die gute Zusammenarbeit und Stimmung im Biochemielabor.

Alexandra Hingst, Dr. Anna-Madeleine Beckmann, Dr. Daniela Häußler, Dr. Jan Krönke und Dr. Stefanie Lindner für die gute Zusammenarbeit in gemeinsamen Projekten.

Dr. Christian Breuer, Dr. Janina Schmitz und Jim Küppers für die angenehme Atmosphäre im Büro.

Jiafei Yin und Leyla Kathep für die tatkräftige Mitarbeit.

Allen aktuellen und ehemaligen Kolleginnen und Kollegen des Arbeitskreises für die kollegiale Zusammenarbeit, Freundschaft und schöne gemeinsame Zeit innerhalb und außerhalb des Instituts. In diesem Rahmen außerdem den Mitarbeitern des Arbeitskreises Müller innerhalb und außerhalb der Zellkultur.

Nicht zuletzt meiner Familie und besonders Ruth für die unermüdliche Unterstützung während meines Studiums und während meiner Promotion.

Konferenzen

Mangold, M.; Gütschow, M.; Stirnberg, M. A Short Peptide Inhibitor as an Activity-Based Probe for

Matriptase-2. 3rd International Electronic Conference on Medicinal Chemistry, 2017 (Vortrag).

Mangold, M.; Häußler, D.; Beckmann, A.-M.; Gitlin, A.; Rolka, K.; Gütschow, M.; Stirnberg, M. Activity-Based Probes for Detection of Active Matriptase-2. 2nd International Symposium: Protease World in Health & Disease, 2016, Kiel (Poster).

Mangold, M.; Häußler, D.; Beckmann, A.-M.; Gütschow, M.; Stirnberg, M. Imaging of Matriptase-2 by Activity-Based Probes. European Iron Club Annual Meeting, 2016, Innsbruck (Poster).

Publikationen

Gitlin-Domagalska, A.; Dębowski, D.; Gucwa, K.; Starego, D.; Ptaszyńska, N.; Sieradzan, A.; Karczyńska, A.; Samsonov, S. A.; Mangold, M.; Gütschow, M.; Łęgowska, A.; Rolka, K. Truncation of *Huia versabilis* Bowman-Birk inhibitor Increases its Selectivity, Matriptase-1 Inhibitory Activity and Proteolytic Stability. *Biochimie*. **2020**, *171-172*, 178-186.

Lindner, S.; Steinebach, C.; Kehm, H.; Mangold, M.; Gütschow, M.; Krönke, J. Chemical Inactivation of the E3 Ubiquitin Ligase Cereblon by Pomalidomide-based Homo-PROTACs. *J. Vis. Exp.* **2019**, *147*.

Gitlin-Domagalska, A.; Mangold, M.; Dębowski, D.; Ptaszyńska, N.; Łęgowska, A.; Gütschow, M.; Rolka, K. Matriptase-2: Monitoring and Inhibiting its Proteolytic Activity. *Future Med. Chem.* **2018**, *10*, 2745-2761.

Mangold, M.; Gütschow, M.; Stirnberg, M. A Short Peptide Inhibitor as an Activity-Based Probe for Matriptase-2. *Pharmaceuticals* **2018**, *11*, E49.

Häußler, D.; Schulz-Fincke, A. C.; Beckmann, A.M.; Kelis, A.; Gilberg, E.; Mangold, M.; Bajorath, J.; Stirnberg, M., Steinmetzer, T.; Gütschow, M. A Fluorescent-Labeled Phosphono Bisbenzguanidine As an Activity-Based Probe for Matriptase. *Chemistry* **2017**, *23*, 5205-5209.

Häußler, D.; Mangold, M.; Furtmann, N.; Braune, A.; Blaut, M.; Bajorath, J.; Stirnberg, M.; Gütschow, M. Phosphono Bisbenzguanidines as Irreversible Dipeptidomimetic Inhibitors and Activity-Based Probes of Matriptase-2. *Chemistry* **2016**, *22*, 8525-8535.

Beckmann, A. M.; Glebov, K.; Walter, J.; Merkel, O.; Mangold, M.; Schmidt, F.; Becker-Pauly, C.; Gütschow, M.; Stirnberg, M. The Intact Kunitz Domain Protects the Amyloid Precursor Protein from Being Processed by Matriptase-2. *Biol. Chem.* **2016**, *397*, 777-790.

Jäckle, F.; Schmidt, F.; Wichert, R.; Arnold, P.; Prox, J.; Mangold, M.; Ohler, A.; Pietrzik, C. U.; Koudelka, T.; Tholey, A.; Gütschow, M.; Stirnberg, M.; Becker-Pauly, C. Metalloprotease Meprin β is Activated by Transmembrane Serine Protease Matriptase-2 at the Cell Surface thereby Enhancing APP Shedding. *Biochem. J.* **2015**, *470*, 91-103.